GeoPlanet: Earth and Planetary Sciences

Marek Górski

# Seismic Events in Glaciers

Springer

# GeoPlanet: Earth and Planetary Sciences



For further volumes:
http://www.springer.com/series/8821

Marek Górski

# Seismic Events in Glaciers

Springer

Marek Górski
Institute of Geophysics
Polish Academy of Sciences
Warsaw
Poland

The Geoplanet: Earth and Planatory Sciences Book Series is in part a continuation of Monographic Volumes of Publications of the Institute of Geophysics, Polish Academy of Sciences, the journal published since 1962 (http://pub.igf.edu.pl/index.php).

ISSN 2190-5193 ISSN 2190-5207 (electronic)
ISBN 978-3-642-31850-4 ISBN 978-3-642-31851-1 (eBook)
DOI 10.1007/978-3-642-31851-1
Springer Heidelberg New York Dordrecht London

Library of Congress Control Number: 2013945804



Printed on acid-free paper

Springer is part of Springer Science+Business Media (www.springer.com)

# Series Editors



# Managing Editor

# Advisory Board

# Preface

This book deals with glacier flow and seismic activity depending on the glacier's structure, its thickness, and background. I wish to underline an important finding of Dr. Marek Górski, the author of this book, who clearly distinguished the two types of tremors: icequakes and the so-called icevibrations. The icevibrations present a new fracture element, associated with the glacier's flow and molecular fractures; they bring an additional factor to the typical mechanism of glacier seismic events, similar to the fracturing in rocks.

In this Preface, let me briefly describe and explain why I am involved in the glacial seismology research problems and also put forward some suggestions as to theoretical background related to the glacier flow processes.

My first encounter with glacial seismology dates back to 1962, when Professor Stanisław Siedlecki, leader of the Spitsbergen wintering expeditions of the Polish Academy of Sciences in the framework of International Geophysical Year 1957–1959 (IGY 1957–1959), organized a small expedition to Hornsund Fiord, Spitsbergen. This was an important idea with an interesting research program, including seismic measurements. This small, three-person expedition was the first stage of the further systematic research on the south part of Spitsbergen. Our base at Hornsund Fiord was established during the International Geophysical Year; the continuation of research was initially not planned. The post-IGY expedition of 1962 created circumstances for renewing this basis, which eventually became a permanent research facility.

It is worth mentioning that the research program in the framework of IGY1957–1959 included important expeditions to three regions of the world, namely: the above-mentioned wintering in Spitsbergen, directed by Professor Stanisław Siedlecki; the expedition to North Vietnam, with a broad geophysical research program, and the 1958 short-time expedition to Antarctica, aiming at gravimetric survey in the Bunger Oasis. The organization of these expeditions was headed by Professor Stefan Zbigniew Różycki, an outstanding Polish geologist, with a great support of Alina and Czesław Centkiewicz.

The North Vietnam expedition was the first Polish scientific project carried out in tropical countries on such a large scale. With an important help of local institutions (Vietnamese IGY Committee led by Professor Nguyen Xien) we were able

to establish two geophysical observatories, in Cha-Pa and Phu-Lien; I have been the Leader of this expedition. I had an opportunity to work together with Professor Siedlecki in preparation of both the Spitsbergen expedition and that to North Vietnam; owing to these circumstances, we became close friends.

Few years later, in 1962, Professor Siedlecki proposed me to take part in the above-mentioned next research expedition to Spitsbergen; a third member was a technician help for our geological and geophysical programs. Our program included two tasks: The first was to collect some very specific geological samples from the Sorkappoya, a small island just few kilometers south of Spitsbergen, and the second task included seismological recordings of the fracture events in glaciers. It is worth to emphasize that such recordings related to seismic events in glaciers were unique at that time. We have decided to undertake such recordings on the Hans Glacier, located very near to our base established during the former expeditions in the years 1957–1960.

On the Hans Glacier we have tried to record some glacier fracture events using seismometers placed directly on ice; we expected to record very weak oscillations. However, it appeared that the horizontal seismometers installed directly on glacier became quite useless; due to unexpected quick glacier flow, these seismometers become rapidly blocked. Yet some interesting glacier events have been recorded by the vertical seismometers (the paper by Lewandowska and Teisseyre, entitled "Investigations of the ice microtremors on Spitsbergen in 1962," was published in 1964 in "Biuletyn Informacyjny Komisji Wypraw Geofizycznych PAN"; full reference inside the book). The experience we gained during these pioneering measurements inspired further research efforts in this direction undertaken by Dr. Marek Górski in next years.

The numerous important scientific results obtained due to systematic observations in the course of the IGY 1957–1959, and especially those obtained by our small expedition in 1962, motivated the Institute of Geophysics, Polish Academy of Sciences, to continue the geophysical and geological investigations in this area, and to establish the permanent Polish Polar Station Hornsund, Spitsbergen. Since then, it has become the base for observations and studies carried out by many scientists from Poland and other countries.

As mentioned above, we started to record some seismic events occurring in a glacier over 50 years ago; according to the later studies by Dr. Górski, the seismic events in glaciers can be divided into two groups: The typical seismic events, similar to those appearing in rocks, and another group presenting the oscillations without a sharp beginning but with slowly increasing and decreasing amplitudes.

This second group of seismic events in glaciers, one of the main issues discussed in this book, presents partly a viscous flow. Such phenomena are an important element of the glacier dynamic processes.

I may mention here that in typical seismic fracture processes a narrow area in seismic focus might become melted due to the friction process; such a melting stage inside a fracture process has been discovered in some near-surface events.

Further studies on the theory of glacier seismology, in terms of Asymmetric Continuum Theory and possible molecular transport inside a glacier, are under way. Research concerns also the seismic activity of glaciers with various thermal structures.

Warsaw, May 2013 Roman Teisseyre

# Acknowledgments

Many persons contributed to the final output of this book through long-lasting collaboration in both field expeditions and data analyses. Special thanks are due to Professor Roman Teisseyre, who initated the whole project of glacial seismology, Professor Stanisław Siedlecki, whose actions opened a new chapter in Polish exploration of the Arctic, and to my colleagues, in particular Dr. Maciej Zalewski, many-year head of the Polar and Marine Research Department, and Professor Aleksander Guterch, initiator and leader of the deep seismic sounding projects in Polar regions carried out by the Institute of Geophysics, Polish Academy of Sciences.

The extensive study reported here was possible due to engagement and cooperation of many academic institutions of the Polish Polar community, including the University of Silesia, Nicolaus Copernicus University of Toruń, and the University of Wrocław, with their well-known glaciologists, notably Professor Jacek Jania, Professor Marek Grześ, and the late Dr. Stanisław Baranowski. As concerns research on Spitsbergen, I also acknowledge the strong support from the Norsk Polarinstitutt in Oslo and full understanding from the Norwegian Authorities, as well as the involvement of researchers from other countries, in particular from the ETH in Zurrich, Switzerland, in the framework of cooperation with the University of Silesia.

I am also very grateful to my colleagues from the Editorial Office of the Institute of Geophysics, Anna Dziembowska and Zofia Okrasińska, for their help in preparing the book for publication.

Marek Górski

# Contents

# Chapter 1
# Introduction: Scope of the Book

The occurrence of seismic events in glaciers has been an issue in the scientific literature since the 1950s, following the report about icequakes in Baffin Island (Rothlisberger 1955). Targeted seismological studies were undertaken by the Polish Expedition to Spitsbergen in 1962. Most of research described in this book has been done by the author in the years 1970–2006, but not all the results have been available to international communities of seismologists and polar researchers, since some of them were published in Polish. Recently, the topic gains actuality in relation to intensified studies on climate changes and the observed growing activity of seismic glacial events.

In recent years, the glacier seismicity has been extensively studied in various regions of the globe. Research has been done on Alaska where an automated detection and event sifting routine was implemented (see, for instance, O'Neel et al. 2010; Mikesell et al. 2012). Studies were also made in the Swiss Alps see, for instance, the paper by Faillettaz et al. (2011), reporting monitoring and measuring of icequake activity prior to the Weisshorn Glacier break-off), and in Greenland (see, e.g., the paper by Veitch and Nettles 2012, describing 121 glacial earthquakes occurring in the period 2006–2010), and in Antarctica (e.g., MacAyeal et al. 2008). Possible mechanisms of glacial earthquakes have also been widely discussed (e.g., Tsai et al. 2008).

The book describes an extensive study of seismic events associated with dynamics of the Hans Glacier in South Spitsbergen (see a photo in Fig. 1.1) as well as an analysis of a series of seismic events observed in Alpine glacier and in the Antarctic region. The study on the Hans Glacier is mainly based on the recordings from the Hornsund seismological station and measurements made by the author directly on the glacier. Research in the Antarctic region has been done at the Antarctic Peninsula area, West Antarctica.

The results obtained until the mid-1997 have been summarized in the book: *Seismicity of the Hornsund Region, Spitsbergen: Icequakes and Earthquakes* (Górski 1997), and are briefly repeated here, together with new data and interpretation.

Since the Hornsund station of the Institute of Geophysics PAS has been playing a key role in the study of seismic glacial events, and was the site of the first targeted recordings in 1962 (Lewandowska and Teisseyre 1964), its brief history

M. Górski, *Seismic Events in Glaciers*, GeoPlanet: Earth and Planetary Sciences,
DOI: 10.1007/978-3-642-31851-1_1, © Springer-Verlag Berlin Heidelberg 2014

**Fig. 1.1** View on part of the Hans Glacier, Hornsund Fiord, South Spitsbergen

is described in Chap. 2. The station, along with the whole Hornsund Fiord, was declared in 2002 as one of the European biodiversity flagship sites. The station is used by many scientific institutions for realizing research projects in South Spitsbergen. Another Polish station in Hornsund area, localized in its western part, in the vicinity of Werenskiold Glacier, was established by the University of Wrocław in 1971. In addition to the Hornsund region, Polish academic institutions do systematic studies using the following two stations: the one in the Kaffiøyra, NW Spitsbergen, belonging to the Nicolaus Copernicus University in Toruń, and the other in Bellsund, West Spitsbergen, operated by the Maria Curie-Skłodowska University in Lublin. The area of the first of these stations, in Kaffiøyra (Coffee Plain), has already been the site of the Polish Glaciological Expedition in 1938 (Grześ and Sobota 2005). The results of the first Polish Glaciological Expedition to Oscar II Land in 1938 were so interesting that further complex environment studies were undertaken in 1975. They have been conducted at the already existing station as well as at the Polar Station of the Nicolas Copernicus University. The expeditions to this station were for many years organized and led by Professor Marek Grześ. This station is certainly the most northerly exposed Polish scientific facility. Polish scientists have also been using Norwegian bases and traper huts located in other regions of Spitsbergen, kindly made available to them.

In Chap. 3 it is described how the two categories of seismic events were distinguished and how they are related to dynamic processes within the glacier. These are the icequake- and icevibration-type events (the distinction made by the author). The icequakes are associated with the velocity gradient of the ice flow in the marginal zone of the glacier; an analysis is made of the ice flow velocity changes in time. The icevibration-type events may be related to glaciodynamical processes occurring in the main stream of the glacier. Of importance are also resonant vibrations of large elements of the glacier.

In Chaps. 4–6 the results of a few seasonal recordings of icequakes in the ablation zone of the Hans Glacier are outlined. The measured seismic wave velocities in the studied glacier part are given. Zones of icequake-type activity are

delineated, and focal parameters of these events are calculated using spectral analysis. A comparison was made of focal parameters of icequakes with focal parameters of weak tectonic earthquakes and mining tremors, calculated using the same method. The calculatons were made with the help of original programs developed at the Institute of Geophysics PAS.

In Chap. 7 a comparison is made of icevibration-type events from various-type glaciers. Three-dimensional spectral analysis is presented and a relation of the dominant frequency with the glacier size is demonstrated.

Chapter 8 presents an application of the shear-band model to the determination of focal parameters. An attempt was made to estimate the thickness of foci on the basis of shear-band model (Teisseyre 1996) for icequakes recorded on the Hans Glacier (Chap. 6).

It is worth noting that the activity of Polish explorers of Polar regions, both the Arctic and the Antarctic, has a very long history. As concerns the bibliography of the Spitsbergen region, the reader is referred to two comprehensive volumes: *Bibliography of Polish Research in Spitsbergen Archipelago, Part I, years* 1932–1996 (Zalewski 2000) and *Bibliography of Polish Research in Spitsbergen Archipelago, Part II, years* 1997–2006 (Giżejewski 2010).

In the years following the period covered by the above-mentioned bibliographies, Polish scientists were active in numerous studies of Spitsbergen glaciers, also those carried out on a large scale in the framework of various international programs, notably within the Fourth International Polar Year 2007–2009. At present, the Institute of Geophysics PAS participates, e.g., in the following projects: *SvalGlac* (2010–2013), aiming at the Svalbard glaciers evolution model under climate change conditions, *Ice2sea* (2009–2013) estimating the future contribution of continental ice to sea-level rise, and *SIOS-PP*—Svalbard Integrated Arctic Earth Observing System.

Of great importance in recognizing the Polar regions are also geodynamical surveys. The Laboratory of Experimental Seismology of the Institute of Geophysics has been carrying out numerous studies in these regions. In particular, between 1976 and 2006 there were five seismic expeditions to Svalbard and five expeditions to West Antarctica. In Svalbard, deep crustal seismic refraction and wide-angle reflection surveys were made along several profiles of a total length of about 2,500 km. In West Antarctica, seismic measurements were performed along a number of profiles of a total length of about 4,000 km. During the Fourth International Polar Year 2007–2009, DSS seismic studies of the crust and upper mantle in Arctic and Antarctic regions were done in the framework of the IPY Cluster program 77: Plate Tectonics and Polar Gateways (PLATES and GATES), in a wide international cooperation. Some papers resulting from the Institute's participation in geodynamic surveys in the Arctic and Antarctic are quoted in Chap. 7.

A new large international deep seismic sounding project, based on ocean bottom seismometer (OBS) measurements, is planned to begin in the years 2014–2015 in the region of Svalbard. In later years it will be continued in the Antarctic.

## References

Faillettaz J, Sornette D, Funk M (2011) Icequakes coupled with surface displacements for predicting glacier break-off. J Glaciol 57(203):453–460

Giżejewski J (ed) (2010) Bibliography of Polish research in Spitsbergen archipelago, Part II, 1997–2006. Publs Inst Geoph Pol Acad Sc M-31(407):149

Górski M (1997) Seismicity of the Hornsund region, Spitsbergen: icequakes and earthquakes. Publs Inst Geoph Pol Acad Sc. B-20(308):77

Grześ M, Sobota I (eds) (2005) Kaffioyra. Zarys środowiska geograficznego (Kaffioyra. Outline of Geographic Environment) Instytut Geografii UMK, Oficyna Wyd. Turpress (in Polish)

Lewandowska H, Teisseyre R (1964) Investigations of ice microtremors on Spitsbergen in 1962. Biul Inf Komisji Wypraw Geof PAN 37:1–5

MacAyeal DR, Okal EA, Aster RC, Bassis JN (2008) Seismic and hydroacoustic tremor generated by colliding icebergs. J Geophys Res 113:F03011. doi:10.1029/2008JF001005

Mikesell TD, vanWijk K, Haney MM, Bradford JH, Marshall HP, Harper JT (2012) Monitoring glacier surface seismicity in time and space using Rayleigh waves. J Geophys Res 117:F02020. doi:10.1029/2011JF002259

O'Neel S, Larsen CF, Rupert N, Hansen R (2010) Iceberg calving as a primary source of regional-scale glacier-generated seismicity in the St. Elias Mountains, Alaska. J Geophys Res: Earth Surf 115, 115, F04034, doi:10.1029/2009JF001598

Rothlisberger H (1955) Studies on glacier physics on the Penny Ice Cap, Baffin Island, 1953, Part III: Seismic soundings. J Glaciol 18:539–552

Teisseyre R (1996) Shear band thermodynamical earthquake model. Acta Geophys Pol 44:219–236

Tsai VC, Rice JR, Fahnestock M (2008) Possible mechanisms for glacial earthquakes. J Geophys Res 113:F03014. doi:10.1029/2007JF000944

Veitch SA, Nettles M (2012) Spatial and temporal variations in Greenland glacial-earthquake activity, 1993–2010. J Geophys Res: Earth Surf 117:F04007. doi:10.1029/2012JF002412

Zalewski SM (ed) (2000) Bibliography of Polish research in Spitsbergen Archipelago, Part I, 1930–1996. Publs Inst Geophys Pol Acad Sc M-23(314):194

# Chapter 2
# Polish Polar Station in Hornsund, Spitsbergen

## 2.1 Brief History of the Polish Polar Station

The Polish Polar Station on the northern coast of the Hornsund fiord on the Spitsbergen island, Norwegian archipelago Svalbard, was established in the framework of the International Geophysical Year 1957–1958. The location in the Hornsund fiord was chosen by Professor Stanisław Siedlecki, based on his survey of the region in the 1930s. Professor Siedlecki spent a winter on the Bear Island during the Second Polar Year 1932–1933, and made a geological mapping of the Torell Land in 1934. In 1936, S. Siedlecki, accompanied by two other persons, traversed the West Spitsbergen glaciers from south to north, hundreds kilometers long route. In the summer of 1956, he led a scientific-technical reconnaissance in the Hornsund fiord, and a site for constructing a future station was finally chosen. The station was built and prepared for wintering in the summer of 1957. The works were coordinated by Professor Stefan Manczarski, Scientific Secretary of the Polish Committee of the Third International Geophysical Year 1957–1958. The station's location in the Isbjornhamna bay in the Hornsund fiord turned out to be optimum for a wide range of research in a variety of fields: geology, geophysics, hydrology, geodesy, glaciology, periglaciology, limnology, climatology, geomorphology, meteorology, oceanology (sea studies), biology, and archeology. The first 10-person winter expedition, led by Stanisław Siedlecki, included Maciej Zalewski, who later on became the many-year head of the Polar Research Department of the Institute of Geophysics. After the 1957/1958 wintering, the Isbjornhamna bay base was the site of summer expeditions in the years 1957–1960 and 1962. The studies, in various scales and time spans, have been carried out up to the present. The results obtained in the years 1957–1962 have been summarized in a book edited by Birkenmajer (1968).

Then, until the end of the decade, the research works have been suspended, and the station was used by a trapper. However, in the summer of 1966 it was visited by Professor K. Birkenmajer from the Institute of Geological Sciences, Polish Academy of Sciences, in Cracow. He proposed a wide spectrum of research to

M. Górski, *Seismic Events in Glaciers*, GeoPlanet: Earth and Planetary Sciences,
DOI: 10.1007/978-3-642-31851-1_2, © Springer-Verlag Berlin Heidelberg 2014

be carried out by numerous Polish scientific centers dealing with Polar studies. Systematic research in summer seasons has been resumed in 1970.

The idea of organizing a new series of expeditions was born in the Polish Commission for Geophysical Expeditions in February 1969. The Working Group "Spitsbergen", basing on the glaciological-climatological research project prepared by Dr S. Baranowski, worked out a framework program of a series of summer expeditions to the Hornsund region in the years 1970–1974.

Of great importance for the planned series of expeditions was to get a means of transportation from the country to Spitsbergen. On the initiative of various institutions interested in Polar research, representatives of three institutes affiliated with the Polish Academy of Sciences, namely, Professors S. Manczarski, R. Teisseyre, and S. Szymborski, arranged the agreement with the State Maritime School in Gdynia to plan, since 1970, a series of training cruises to Spitsbergen of the ship "Jan Turlejski", with participation of a group of 6–10 scientific expedition members.

The Commission of Geophysical Expeditions decided to delegate the organization of a new series of expeditions to the Institute of Geography, University of Wrocław, in cooperation with the Institute of Geophysics, Polish Academy of Sciences. Both institutions had played a very important role in the former Spitsbergen expeditions and scientific research during the International Geophysical Year and International Geophysical Cooperation projects, and have been vividly interested in continuing research in this region. The leadership of the series of expeditions was proposed to Dr S. Baranowski from the University of Wrocław, a participant of several earlier expeditions. He was the leader of consecutive five expeditions (1970–1974).

Right away, in the summer of 1970, S. Baranowski, together with M. Zalewski from the Institute of Geophysics PAS, organized the first one of the planned cycle of expeditions. The transportation of scientific groups to Spitsbergen was ensured owing to the few-year agreement with the State Maritime School.

The University of Wrocław has been continuing the former research in glaciology, periglaciology, climatology, geomorphology and meteorology, initiated during the International Geophysical Year. The Institute of Geophysics PAS has been carried out seismological investigations. These were performed by the author according to a program proposed by R. Teisseyre, who had already accomplished pioneering seismological registrations in 1962, while making research on the Hans Glacier jointly with Professor S. Siedlecki. The Maritime Station (presently the Institute of Oceanology) of the Polish Academy of Sciences in Sopot has been realizing many-year cycle of maritime research. The training cruises of the "Jan Turlejski" ship were fully utilized by scientists from many Polish institutions engaged in Polar research.

A series of Polish scientific expeditions to Spitsbergen in the years 1970–1974 occupies a very important place in the rich history of our Polar expeditions. A consistent program of glaciological, climatological, geomorphological and geophysical studies, complemented by biological and paleontological projects, has been designed and diligently carried into effect over the consecutive five years.

The results were summarized in three symposia and gathered in special publications devoted to this series of expeditions (Baranowski 1975, 1977a, b, c).

Like all the former Polish expeditions to Spitsbergen, also the expeditions of this series were receiving support from the Norsk Polarinstitutt in Oslo and its director Dr Tore Gjelsvik, and the full approval of the Norwegian Authorities. Prior to each expedition, its research program was coordinated and approved by the authorities of Norsk Polarinstitutt and the Governor of Svalbard. Representatives of Norwegian government, Norwegian scientists, fishermen and trappers were often visiting Polish expeditions during the field surveys.

It was decided that the last expedition of the series (1975) would be organized by the Institute of Geophysics PAS in Warsaw, and Ryszard Czajkowski from this Institute was assigned to be the leader. The research covered seismology, paleomagnetism, paleontology, geomorphology, climatology, soil sciences and ornitology.

Geophysical projects were realized during the expeditions in 1970, 1971, and 1974, according to the scientific program designed by R. Teisseyre. They were mainly focused on the problems relating to microtremors of the Hans Glacier. In 1970 they were performed by M. Górski, in 1971 by R. Czajkowski, J. Uchman and J. Wehr, and in 1974 by R. Czajkowski and R. Teisseyre, as part of the Polish-American geophysical expedition.

In 1970, the micro-seismic recording was made at two points along the Fugleberget-Fannytoppen profile, about 1 km from the Hans Glacier head. One of the points was located in the central part of the glacier, the other nearby the northern edge of the glacier (Górski 1975). In 1971, the recording was made by three seismographs located 300 m apart in the glacier movement line, near the Fugleberget-Fannytoppen profile. Finally, in 1974 the research covered the recording of microtremors of the Hans Glacier at two segments: perpendicular and parallel to the glacier's motion (nearby the sites from the years 1970 and 1971) and measurements of seismic noise at two profiles, perpendicular and parallel to the coast line near the expedition base in Isbjornhamna (Czajkowski 1974, 1977a, b).

In 1975 R. Czajkowski was doing seismological studies of the Hans Glacier thickness using the so-called hammer method. He executed a series of profiles in the dead ice and fast glacier's movement regions, in strongly developed cracks and in relatively not much cracked regions. The obtained differences in elastic wave velocity are an interesting contribution to the study of glacier's physics.

In the framework of multi-disciplinary geophysical program, the present author also made a series of measurements of the total ozone content in the atmosphere, by measuring the direct solar radiation and zenith scattered radiation. It was possible to make a total number of 405 of such measurements during fair-weather days.

The research works done in the region of Hans Glacier by Professor Teisseyre in 1974 were related to the mechanism of glacier's deformation considered from the point of view of an elastic medium with the dislocaton field (Teisseyre 1977).

In the summer of 1976, there was initiated the many-year project of deep seismic sounding in the Arctic and Antarctic Peninsula, lead by Professor A. Guterch (see Chaps. 1 and 7). In 1976, the survey was made in the central part of Svalbard.

Studies in other regions of Svalbard have been carried out by various Polish academic institutions. The Nicolaus Copernicus University in Toruń has been carrying out systematic research in its Polar Station, which is the northernmost Polish research unit. It is located in the northern part of coastal plain called Kaffiøyra (Coffee Plain), on the northwestern Spitsbergen. The studies of the Maria Skłodowska-Curie University in Lublin have been carried out in the Polar Station in Calypsobyen.

The Hornsund station, as well as other research institutions in the Svalbard region, have also been used by student's expeditions from various universities, providing excellent facilities for training the future Polar researchers.

In 1978 the Hornsund station was thoroughly rebuilt and adapted for year-round work. Starting with the 1978/1979 wintering, ten-person groups of observers have been exchanged every year at the beginning of summer season. In the summer of 1978, a 70-person group of scientists and technical personnel was residing at the station. The construction works, shared by all the participants, were carried out parallel to the realization of scientific projects. A seismological station, consisting of a simple array composed of 6 seismometers positioned at 4 sites was deployed. Two pavilions for magnetic measurements were built.

In the summer of 1979 the reconstruction was continued. A new building was erected, which greatly enlarged the abilities for doing research in the whole area of South Spitsbergen. A photo of the reconstructed station is in Fig. 2.1. The technical works were led by Janusz Jeleński. The architectural design is due to Jan Szumański, who also designed the next reconstruction of the station, which took place at the beginning of XXI century.

In the summer seasons 1978 and 1979, along with heavy construction works, scientific investigations were still under way in the following fields: geophysics, glaciology, periglaciology, geomorphology, geology, hydrology, geodesy, climatology, meteorology, oceanology, and biology; the research groups included scientists and engineers from many Polish academic institutions.[1] At the same time, R. Czajkowski was carrying out the project of radar sounding of the Hans Glacier (Czajkowski 1980).

In the year 2002 the Hornsund Station, along with the whole Hornsund region, was selected as one of the European biodiversity flagship sites. More details relating to permanent and seasonal measurements in the Hornsund region in the field of geophysics and other domains can be found on the station's homepage http://hornsund.igf.edu.pl/.

[1] The institutions involved: the Institute of Geophysics PAS, University of Silesia, Nicolaus Copernicus University in Toruń, University of Wrocław, Adam Mickiewicz University in Poznań, Maria Curie-Skłodowska University in Lublin, University of Gdańsk, AGH University of Science and Technology in Cracow, Institute of Meteorology and Water Management, Research Center in Cracow of the Institute of Geological Sciences PAS.

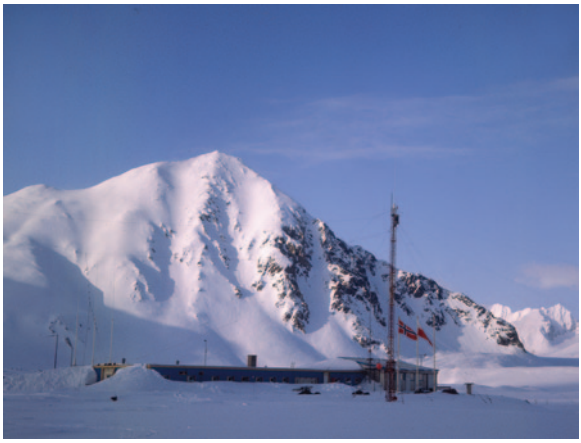

**Fig. 2.1** Polish Polar Station Hornsund, Spitsbergen, after the reconstruction in the years 1978–1979

## 2.2 Hornsund Seismological Station HSP

Polish Polar Station Hornsund began its continuous operation in the fall of 1978; continuous operation of the seismological station also started at that time (Górski and Niewiadomski 1982). In the summer season of 1979, the adjustment of instruments' parameters for the needs of the project was made.

The location of seismological station in the region of Hornsund was chosen taking into account the recording of earthquakes from the Arctic-Atlantic Basin. The Basin, covering the Norwegian Sea and Greenland Sea and the adjacent region of the Arctic Ocean and the shelf-type Barents Sea, is a classical area of application of the theory of lithospheric plates tectonics for reconstructing the evolution of the surface of our globe. The other reason was the possibility of permanent monitoring of the glacier's seismic activity which has been studied since 1962.

In the summer of 1980, as an experiment, two seismometer sites of the HSP station were displaced and, for a period of one month, deployed directly at the Hans Glacier in order to record icequakes and determine their spectral parameters. The experiment was made by Cichowicz (1983).

The station consisted of an array of seismometers deployed at several recording points. The number and location of sites was modified at various measurement periods, depending on the needs of actual research projects. The research projects carried out at the station were based on standard recordings of tectonic earthquakes and monitoring of seismic activity of the Hans Glacier (located few kilometers away of the seismometer array) based on recording of icevibrations. The records of icevibrations generated by the Hans Glacier enabled us to determine the character of these events and to relate them to the glacier's activity. The number of sites ranged from 4 to 8. The vertical components were recorded at all sites, all three components being recorded at one or two sites at least. The array deployed

in the Hornsund region made it possible to locate and monitor a few seismically active areas in the Svalbard region (Górski 1986b), which have previously been localized only during the Norwegian-American expedition in 1979 (Bungum and Kristoffersen 1980) and occasional measurements at stations in three mining centers (Bungum et al. 1982; Chen and Mitchell 1985). The tectonic earthquakes were also visible on seismograms during icequake recording in earlier expeditions of the Institute of Geophysics, but it was not possible to localize them.

At first, the station was equipped in a standard six-channel recording instrument GÓRNIK PDM, replaced in the next years by GÓRNIK PCM (Aleksandrowicz 1982). In 1993, the GÓRNIK instrument was replaced by a computerized local measurement network BJ. In July 1995, we initiated a parallel recording of a standard station MK-2.

The recording instruments at the HSP station were entirely designed and built at the Institute of Geophysics. The GÓRNIK-type instruments (Polish word *górnik* means miner) were in routine use in seismic monitoring of coal and copper mines in Poland.

The objective of the seismological station in Hornsund is to record local earthquakes from the Hornsund region and near tectonic earthquakes. This is accompanied by monitoring of seismic events in the Hans Glacier. Seismological experiments are occasionally organized directly on the Hans Glacier. The seismological station in Hornsund, labelled HSP according to International Seismological Center Code, is a short-period station. Instruments GÓRNIK BJ and MK-2 are connected to seismometers SM-3 of 1.5 s period.

Six seismometers of the basic recording system GÓRNIK were distributed at four sites (Fig. 2.2). All three components of oscillations were recorded in site 2, while in the other sites (1, 3 and 4) only vertical seismometers were placed. The distance between extreme sites (1 and 4) was 2.0 km. The arrangement made it possible to perform preliminary location of epicenters (Górski 1986b).

In 1985 we implemented another recording arrangement of the same type, in sites 5–8, operative from time to time. All three components were recorded in site 6. One of the sites, site 5, was located in the direct vicinity of the glacier. The distance between the extreme sites (1 and 8) was 3.9 km. Directly nearby the seismometers we installed modulators to convert analog amplitude signals into frequency-modulated signals, transmitted by cables into the central recorder. After demodulation, detection and conversion into a digital signal, data are stored on standard tape-recorder cassettes. At the same time, every event noticed by the detection system was recorded by an analog, six-channel pen recorder. These recordings constituted the basic material for preliminary analysis at the Hornsund station, further analyses and publications, mainly within the journal *Publications of the Institute of Geophysics, Polish Academy of Sciences* (Górski 1986a, b, 1987, 1989, 1990, 1993; Górski and Perchuć 1987; Górski and Teisseyre 1991; see also the Appendix). The analog, pen records were also used for an analysis of seismicity of the Hans Glacier, as presented below. The standard velocity of recording of the analog system was 1 cm/s.

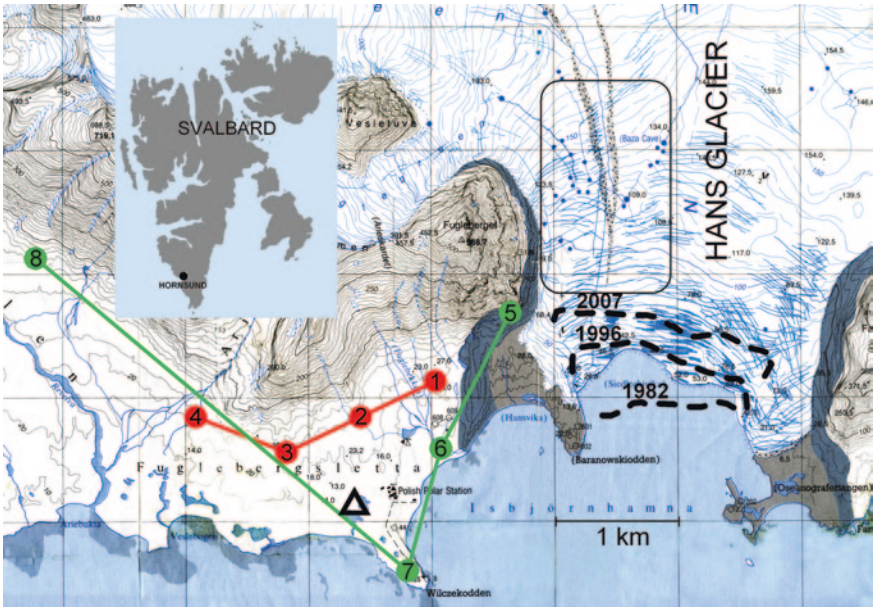


**Fig. 2.2** Seismometer sites in the Polish Station Hornsund (HSP). Sites 1–4 (*red*) operated through the years 1978–1993; in sites 5–8 (*green*) recording has been made over some periods of time since 1985. The *triangle* marks the site of broad-band station HSPD equipped with a STS-2 seismometer (working since 2007). The seismically active Hans Glacier is seen on the right. The *rectangle* marks the area where seismometers for glacial seismic events' recording were seasonally deployed. The heavy *broken lines* delineate the glacier's head in 1982–2007 (Kolondra 2007). The glacier's head shown on the map of the topographic background is related to the year 1990 (Jania et al. 1994)

In 1993, making use of the hitherto experience, we optimized the number and location of the array sites. In the summer of 1993 the GÓRNIK system was replaced by the BJ system, and this was accompanied by a change in location of seismometers (Fig. 2.3). Since then, the seismometers have been placed in five sites. The vertical component has been recorded in all sites, and three components in site 13 (in 1993–1995 it was site 12). In 1995, the location of site 15 was also changed. The frequency-modulated analog signals are sent from seismometers to the recorder via cable. After demodulation and conversion into a digital signal, the data, subject to detection criteria, are processed in a computer-controlled recorder and stored in the mass memory. The digitization frequency is 100 Hz, characteristic band is $0.5 - 25$ Hz. The geographical coordinates of site 12 are: $\varphi = 77.007$ N, $\lambda = 15.545$ E, $h = 26$ m. The coordinates of the other sites are listed in Table 2.1, in the local rectangular system related to site 12. The data recorded in the local network BJ in the years 1993–1994 will be analysed in Chap. 4.

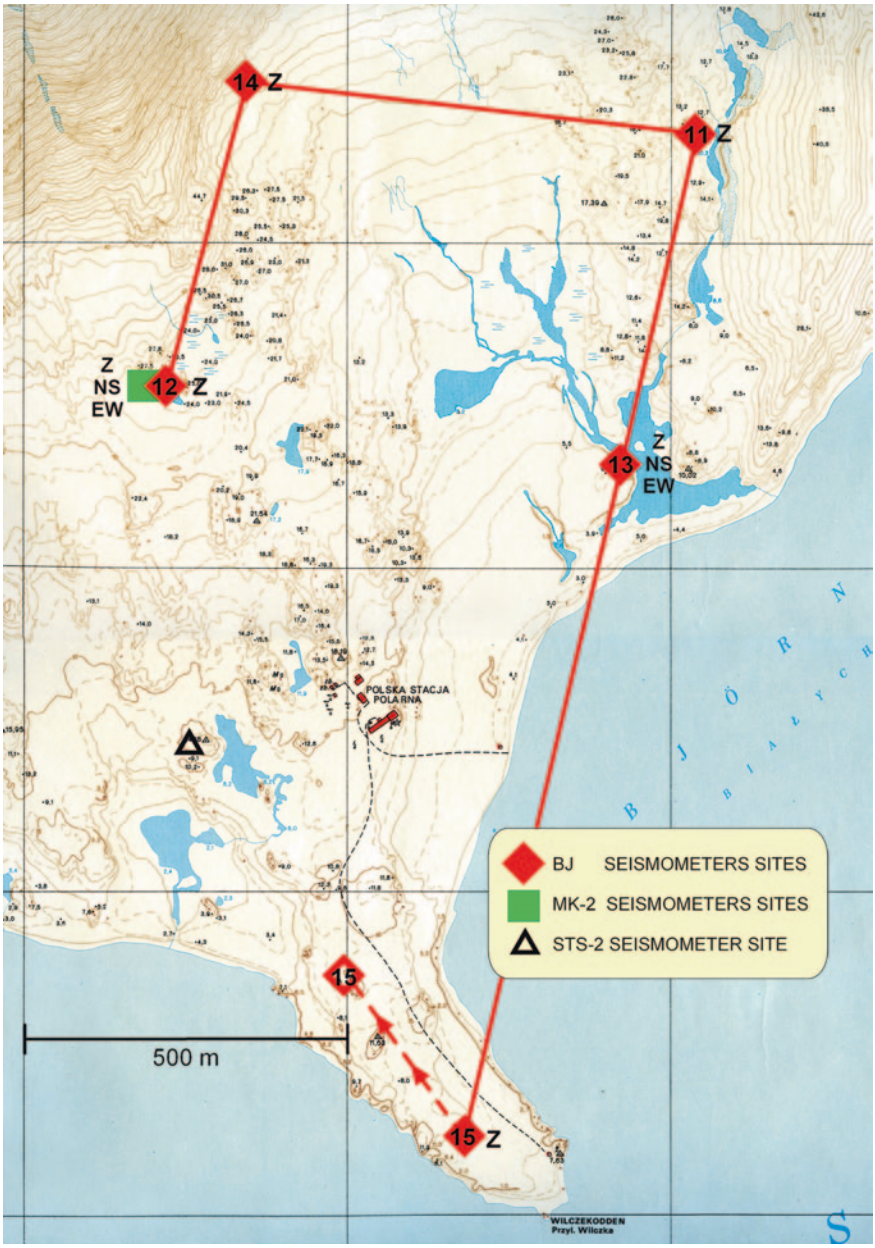


**Fig. 2.3** Distribution of seismometer sites cooperating with the instruments: BJ since 1993 (*red diamonds*), MK-2 since 1995 (*green square*) and broad-band station HSPD with seismometer STS-2 since 2007 (*triangle*). The location of site 15 was later moved (as indicated by the *broken line*). (Topographic background: Spitsbergen… 1984, Polish Polar Station in Hornsund, map 1:5,000)

**Table 2.1** Coordinates of seismometer sites of the BJ system. The *x*-axis is directed to the north, *y*-axis to the east, *h* is the height above sea level

| No | *x* [m] | *y* [m] | *h* [m] |
|---|---|---|---|
| 11 | 395 | 817 | 14 |
| 12 | 0 | 0 | 26 |
| 13 | −120 | 675 | 6 |
| 14 | 475 | 132 | 35 |
| 15 | −1,155 | 473 | 8 |

**Fig. 2.4** Site 13 (BJ) of the HSP station with three *dome-shaped boxes* containing seismographs

The instrument MK-2 installed at HSP in the summer of 1995 is a short-period instrument, routinely used in Polish seismological stations. Seismometers Z, N–S and E–W, and the analog–digital converter, are placed in site 12. The digitization frequency is 100 Hz.

In 1999, multi-channel arrangement was installed at the Hornsund station, enabling a parallel recording from a network of HSP station sites and a network of seismometers located at the Hans Glacier (see Chap. 3, Figs. 3.2 and 3.4).

In 2007, in the framework of cooperation with NORSAR, a broad-band seismometer type STS-2 was installed in the site with coordinates $\varphi = 77.0019$ N, $\lambda = 15.5332$ E, h = 11 m. (Figs. 2.2 and 2.3).

In the present book we analyze the glacial seismic events. The results of many-year recording of seismic events in the Hans Glacier, collected by the author, were the basis for determining the seismic activity of the glacier over a long period of time. Spectral and physical parameters of icequakes were determined on the basis of the series of quakes recorded directly on the Hans Glacier. The recordings were made by a team, led by the author, with participation of M.S. Zalewski and J. Suchcicki.

We should keep in mind that the main purpose for deploying the station was the recording of earthquakes. The HSP station is a member of the world network of seismological stations.

An analysis of tectonic earthquakes based on a series of near earthquakes recorded at Hornsund in the local network with digital multichannel recording at several sites, made it possible to estimate the location of earthquake foci and calculate their spectral and physical parameters. Several seismically active areas in Svalbard have been delineated. An analysis of physical parameters of tectonic earthquakes was supplemented with theoretical results following from the shear-band model proposed by Teisseyre (1996), and Górski (1997). The local array enabled us also to localize and determine the focal parameters of weak earthquakes in the Hornsund fiord region (Górski 2000). Location of earthquakes from the Heer Land region made it possible to relate the P wave phases with the kinematic model of the Earth's crust in this area (Górski 1987).

A serious problem was how to protect the seismometers against polar bear's activity. The model of a dome-shaped box for a seismometer we developed in the year 1985 turned out ideal. The box also proved to be an excellent protection in harsh arctic weather conditions and sustained until now; it was also used in expeditions to other regions. In Fig. 2.4 we show a photo of site 13 with three seismometers placed in the above-mentioned boxes.

## References

Aleksandrowicz D (1982) Automatic Seismic Station PCM 6/10, Acta Geophysica Polonica XXX:381–392

Baranowski S (ed) (1975) Results of investigations of the Polish Scientific Spitsbergen Expeditions. Acta Univ Wr I:251

Baranowski S (ed) (1977a) Results of investigations of the Polish Scientific Spitsbergen Expeditions. Acta Univ Wr II:387

Baranowski S (ed) (1977b) Results of investigations of the Polish Scientific Spitsbergen Expeditions. Acta Univ Wr III:410

Baranowski S (ed) (1977c) Results of investigations of the Polish Scientific Spitsbergen Expeditions. Acta Univ Wr IV:525

Birkenmajer K (ed) (1968) Polish Spitsbergen expeditions 1957–1960, summary of scientific results. Wydawnictwa Geologiczne, Warszawa

Bungum H, Kristoffersen Y (1980) A microearthquake survey of the Svalbard region. Final Report Phase I, NORSAR Tech Rep Kjeller, Norway, p 28

Bungum H, Mitchell BJ, Kristoffersen Y (1982) Concentrated earthquake zones in Svalbard. Tectonophysics 82:175–188

Chen WW, Mitchell BJ (1985) Intraplate earthquakes in northern Svalbard. Tectonophysics 114:181–191

Cichowicz A (1983) Icequakes and glacier motion: the Hans Glacier, Spitsbergen. Pure Appl Geophys 121:27–36

Czajkowski R (1974) Wyniki badań mikrowstrząsów na lodowcu Hansa (Results of a study of microtremors at the Hans Glacier). In: Polskie Wyprawy na Spitsbergen 1970–1971, Materiały z Sympozjum Spitsbergeńskiego, Uniwersytet Wrocławski, 30–34 (in Polish)

Czajkowski R (1977a) The Results of Investigations into Microquakes on the Hand Glacier. Acta Universitatis Wratislaviensis 387:119–138

Czajkowski R (1977b) Próba określenia grubości lodowca i jego ruchu za pomocą pomiarów sejsmicznych prowadzonych w latach 1971–1972 (An attempt to determine a glacier thickness and movement basing on seismic measurements in 1971 and 1972). In: Polska Wyprawa na Spitsbergen in 1974, Materiały z Sympozjum Spitsbergeńskiego, Uniwersytet Wrocławski, 35 (in Polish)

Czajkowski R (1980) Radar measurements of thickness of "warm" glaciers. Pol Pol Res 1–4:21–41

Górski M (1975) Observations of natural ice micro-tremors of the Hans Glacier. Acta Univ Vratisl 251:95–100

Górski M (1986a) Hornsund Polish Station (HSP), 1979–1985. Publs Inst Geophys Pol Acad Sc B-9(193):49–54

Górski M (1986b) Preliminary analysis of seismological data from the Hornsund Polish Station. Publs Inst Geophys Pol Acad Sc B-9(193):79–83

Górski M (1987) Hornsund Polish Station (HSP), 1985–1986. Publs Inst Geophys Pol Acad Sc B-11(208):33–41

Górski M (1989) Hornsund Polish Station (HSP), 1986–1987. Publs Inst Geophys Pol Acad Sc B-12(222):29–38

Górski M (1990) Seismicity of Spitsbergen Platform and its relation to geotectonics of the region. Polish Polar Res 11:277–285

Górski M (1993) Hornsund Polish Station (HSP), 1988–1991. Publs Inst Geophys Pol Acad Sc B-15(258):51–74

Górski M (1997) Seismicity of the Hornsund region, Spitsbergen: icequakes and earthquakes. Publs Inst Geoph Pol Acad Sc B-20(308):77

Górski M (2000) Focal parameters of earthquakes of the Hornsund region. In: Polish Polar Studies. 27th International Polar Symposium, Toruń, 2000, Pracownia Sztuk Plastycznych sp. z o.o., Toruń, pp 159–165

Górski M, Niewiadomski J (1982) Seismological station of the Institute of Geophysics, Polish Academy of Sciences, in the Hornsund Fiord, Spitsbergen. Acta Geophys Pol 30:279–285

Górski M, Perchuć E (1987) An nalysis of P waves of shocks from the Heer Land recorded at the Hornsund Station. Publs Inst Geophys Pol Acad Sc B-18(284):2–16

Górski M, Teisseyre R (1991) Seismic events in Hornsund, Spitsbergen. Polish Polar Res 12:345–352

Jania J, Kolondra L, Schroeder J (eds) (1994) Hans Glacier 1:25,000, Topographic Map. Department of Geomorphology, University of Silesia, Sosnowiec, Poland; Norsk Polarintitutt, Oslo, Norway; Universite du Quebec, Montreal, Canada. Uniwersytet Slaski, Katowice

Kolondra L (2007) Stulecie pomiarów zmian położenia klifu Lodowca Hansa (S Spitsbergen) (The centenaryof Hans glacier front position change measurements (S Spitsbergen)) Archiwum Fotogrametrii, Kartografii i Teledetekcji, vol 17a, ISBN 978-83-920594-9-2

Spitsbergen: Polska Stacja Polarna w Hornsundzie, mapa 1:5000 (1984) (Spitsbergen, Polish Polar Station in Hornsund, map 1:5000). Instytut Geodezji i Kartografii, Warszawa

Teisseyre R (1977) Procesy dyslokacyjne i tworzenie się szczelin rozrywu na lodowcach (Dislocational processes and formation of tensile cracks in glaciers). In: Polska Wyprawa na Spitsbergen in 1974, Materiały z Sympozjum Spitsbergeńskiego, Uniwersytet Wrocławski (in Polish)

Teisseyre R (1996) Shear band thermodynmical earthquake model. Acta Geophys Pol 44:219–236

# Chapter 3
# Seismological Measurements: Icequakes and Icevibrations

## 3.1 Introduction

Most generally speaking, the seismic events in the glacier region can be divided into two categories: icequakes associated with the release of stresses accumulated in ice, and icevibration events (or icevibrations) of a relatively long duration (from few to tens of seconds), in the spectrum of which a relatively low frequency (2–3 Hz) predominates. The latter events are most probably related to large-scale dynamic processes within the glacier, e.g., the displacement of a considerable part of the glacier due to gravity or uplift forces. The observed monochromaticity of the events may be an indication of their resonant character. Examples of an icequake and icevibrations are shown in Fig. 3.1.

The analysis of seismic events in glaciers presented below is mostly based on their recording at the Hans Glacier.

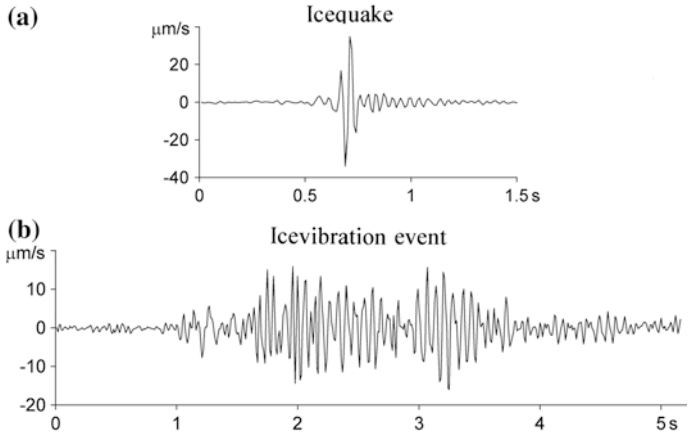


**Fig. 3.1** Examples of seismograms: icequake (**a**) and icevibration event (**b**)

M. Górski, *Seismic Events in Glaciers*, GeoPlanet: Earth and Planetary Sciences,
DOI: 10.1007/978-3-642-31851-1_3, © Springer-Verlag Berlin Heidelberg 2014

The study of seismic events in the Hans Glacier was begun in 1962. Measurements had been made over some periods of time directly on the glacier's surface, and since 1979 a permanent seismic monitoring of the glacier has been performed.

Prior to the implementation of the permanent seismological station in Hornsund, the study of icequakes in the Hans Glacier has been made occasionally, over short (few weeks in duration) periods in summer seasons. The aim was to associate seismic events with the glacier's geometry, to determine the glacier's thickness and the zones of maximum activity, and to look for a relation between the seismicity and movement of the glacier (Lewandowska and Teisseyre 1964; Górski 1975; Czajkowski 1974, 1977a, b). All the recordings were made directly on the glacier, with seismometers placed on the ice surface; the analog recorders used a photo-paper or a tape-recorder's tape. In 1975 and 1978, attempts were made of probing the glacier with a hammer method. When the Polish Polar Station Hornsund began its continuous operation in 1978, a remote, continuous monitoring of the Hans Glacier seismicity has been initiated and lasts up to the present time. The monitoring is made with the use of records at the seismological station HSP. The short (few weeks in duration) seasonal measurements executed directly on the glacier since 1992 provide an additional source of information for the study of seismicity of this glacier (Fig. 3.2). The main purpose of seasonal digital recordings on the glacier is the study of processes taking place in focal areas (see Chaps. 5 and 6).

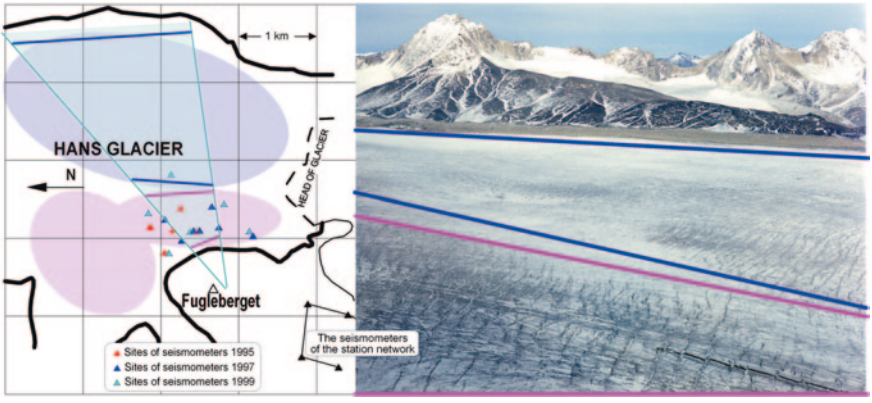


**Fig. 3.2** The Hans Glacier region under study. The *left part* presents a map of the glacier. The *heavy black line* delineates the glacier's edge. Distribution of seismometers in consecutive field experiments: *red triangles* in 1995, *blue triangles* in 1997, *cyan triangles* in 1999, *black triangles* refer to seismometers of the station network. *Ellipses* delineate the areas in which the glacial seismic events have been generated (*blue* refer to the icevibrations, *magenta* to icequakes). The *light blue* area is the region seen on the photo made from the top of Fugleberget (569 m a.s.l.). The photo is shown in the *right panel*. The event generation areas that are visible on both the map and the photo are marked by *heavy straight lines* with the same colors (*magenta* for icequakes and *blue* for icevibrations)

Until the 1970s, the literature devoted to the seismicity in glaciers has been very scanty. The problem was investigated by Neave and Savage (1970), who made measurements on the Athabasca Glacier (British Columbia, Canada), using multi-channel seismic instruments, with geophones distributed over the surface and inside the glacier. They investigated the relationship between the location of foci and the glacier's structure. Strong icequakes (2.0–2.5 in magnitude) were recorded by Van Wormer and Berg (1973) nearby the College Fiord in Alaska. Weaver and Malone (1979), making use of local seismometer networks, analysed icequakes recorded in glaciers nearby volcanoes, studied annual behaviours of glacier seismicity (they calculated the number of seismic events per month) and evaluated the energy of icequakes. It is to be noted, however, that the behaviour of seismicity of glaciers on slopes of volcanoes does not provide a comparative material for the Hans Glacier because of differences in glacier's type and climatic zones. Icequakes were first observed in 1953 by Rothlisberger (1955) on the occasion of seismic soundings on the Baffin Earth. The studies of seismic events in glaciers have become more intensive since the 1980s. Some publications have been quoted in Chap. 1.

The Hans Glacier is a warm glacier, flowing into the sea. Its length reaches 16 km, the average surface slope is 1.7°, the width nearby the head (on the Fugleberget-Fannytoppen profile, 500 m from the head) is about 2.5 km. The substratum in the major part of its main stream is below the sea level (the maximum depression reaches 100 m), the ice thickness in the bottom, ablation zone is 150–200 m, the maximum glacier thickness being 400 m (all parameters after Jania 1992). The head retreats some 17 m per year (the mean value estimated since 1936). Glaciological investigations of the Hans Glacier (measurements of its velocity) were begun in 1938 (Pillewizer 1939). Next glaciological observations were made in the framework of the International Geophysical Year in 1957–1958, in the summer season of 1959, and in several summer seasons up to 1962. Intensified studies in summer seasons have been carried out since 1970 (Baranowski 1977a, b, c). Year-round glaciological observations and measurements were initiated along with the activation of Polish Polar Station Hornsund in 1978, and have been carried out up to now. In the years 1982–1985 the glaciological project of the Silesian University was executed, which included the measurements of velocity of the Hans Glacier (Jania 1992). The glacier has also been subject to systematic glaciological research connected with the project *Mass Balance of Arctic Glaciers* (Jania and Hagen 1996). In the framework of the project *World Glacier Monitoring Service*, the Hans Glacier was selected as one of reference glaciers.

The seismic events in the glacier recordings initiated in 1962 and carried out through the early seventies in ablation zone of the Hans Glacier made it possible to determine the area of the maximum summer seismic activity (Lewandowska and Teisseyre 1964; Górski 1975; Czajkowski 1974, 1977a, b). This area in the ablation zone coincides with the main stream of the glacier.

The seismometers of the HSP station are located rather far away from the most active zone of the glacier, and due to this fact, in association with sharp conditions

imposed on the criterion and threshold of recording activation, weak icequakes have not been recorded at the station. The permanent seismic monitoring of the glacier is mainly based on icevibrations, which are relatively strong events well recorded at the HSP station. The study of icequakes requires that the recording be made by means of a network of seismometers placed directly on glacier surface, in the direct vicinity of seismically active region.

Figure 3.2 shows the studied region of the Hans Glacier and distribution of seismometer sites in consecutive field experiments. The ellipses delineate areas where the glacial seismic events described below are generated. In the right-hand side of the figure we show a view from the Fugleberget top on the studied part of the Hans Glacier. Traces of slip planes along the glacier and shear ice displacements perpendicular to them are clearly seen in the lower part of the photo. As follows from the research described here, this is the region that is responsible for the generation of icequake events, while the central part of the glacier (its main flow) is the source of vibrations.

From spring to autumn 2002, a seismometric array composed of six vertical seismometers, as shown in Fig. 3.3, has been in operation at the Hans Glacier. The array was closely cooperating with the HSP station. This system enabled us to compare eleven channels which recorded glacial seismic events from seismometers placed over a relatively large area. We were able to estimate the location of

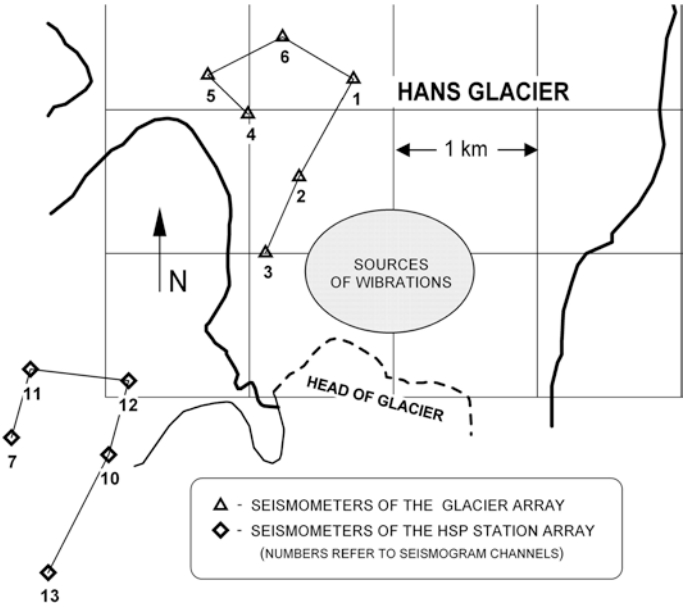


**Fig. 3.3** System for seismic glacial events monitoring in the Hans Glacier region in operation from April through September 2002. The numbers by seismometer sites correspond to channels of icevibration seismograms shown in Fig. 3.4; the *ellipse* marks the location of these events

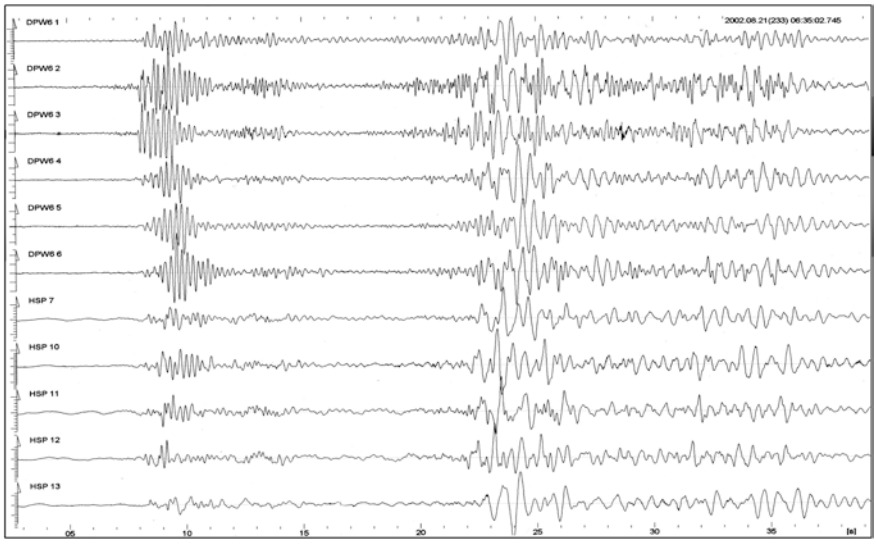


**Fig. 3.4** Icevibration event recorded at the Hans Glacier in August 2002. Channels *1–6* correspond to recordings at six seismometers placed directly on the glacier. Channels *7* and *10–13* show vibrations recorded at respective sites of the HSP station (see Fig. 3.3). The recordings represent vertical components of vibrations and are related to the maximum amplitudes at individual channels

icevibration sources. The location of these events is difficult because of the fact that no characteristic phases to enable determining the time displacements on individual channels were visible on the seismograms. It is only possible to estimate time displacements of the whole wave packets (sequences), and compare the amplitude changes at individual channels. Of importance is also the fact that the size of icevibration-generating regions is relatively large.

An example of icevibration-type event composed of two parts is shown in Fig. 3.4. The event was recorded at the Hans Glacier in August 2002. Recording was made at an array of six seismometers placed directly on ice (channels 1–6) and the HSP station array (channels 7, 10–13) in Fig. 3.3. The recordings show vertical components of vibrations and at individual channels they are scaled to the maximum amplitudes. The recordings enable a description of the mechanism how the icevibrations were formed. Distinctly monochromatic character of the first part of the event is most probably related to the resonance in the release of stresses gathered in this part of the glacier. The later part of the event is not so monochromatic; dominating vibrations can also be observed there, but of much lower frequency than in the first part of the icevibration, which may be related to the growth of the icevibration-generating area. Of similar character are the icevibrations recorded in the same region of the Hans Glacier, which we describe in Chap. 7 (Figs. 7.8 and 7.9).

In what follows, we describe experiments showing how the occurrence of icequakes and icevibrations is related to the kinematic activity of the glacier.

The recordings of icequakes in spring 1995 made it possible to establish their relation with the ice flow velocity gradient. The recordings of icevibrations at the HSP station in the period 1982–1985 made it possible to relate the seismic activity of the glacier with glacier's velocity (Jania et al. 1985). The experiment of 1999 demonstrated the interrelations between icequakes, icevibrations and the increase of flow velocity.

## 3.2 Icequake Location in Relation to Ice Velocity Gradient (Field Experiment 1995)

Measurements were performed from April 4 through 18, 1995. The network was placed in the ablation zone of the glacier, on the western edge of its main stream, some 2 km away from the head (Fig. 3.2). The measuring system consisted of five vertical seismometers; four of them were placed in the vertices of a rectangle, while the fifth one occupied a central position on the intersection of diagonals of the rectangle (the diagonals were 600 m long). The short-period (T = 1.5 s) seismometers SM-3 were located directly on the ice surface in 1–3 m deep wells, dug in snow. The seismometers were connected by cables with a portable computerized recording instrument PDAS-100 (*Portable Data Acquisition System*, TELEDYNE GEOTECH), placed directly nearby the central seismometer. Using the PDAS recorder equipped in electronic memory we must from time to time read-out the data.

The parameters of recording: gain, criterion and threshold of recording activation, and the sampling frequency, were specified in the program. The amplitude detection threshold was fixed taking into account the microseismic noise. The velocity amplification was $3.4 \times 10^{-14}$ m/s/quantum. The band of recording path was 0.7–50 Hz wide.

Preliminary assessment and analysis of data was made at the Polish Polar Station Hornsund. The recorder cooperates with *Data Analysis and Display Software* system (DADISP). Using this program, we evaluated all the recorded icequakes (a total of 600). For further analysis we chose those which were recorded at all five sites in such a way that the recording of the phase of *P* and *S* waves was readable at four sites at least (examples are shown in Fig. 3.5). This requirement is necessary for making the epicenter location. Figure 3.5 shows seismograms of six events (a–f) recorded at five channels; For each event, the gain in channels 1–5 was kept the same.

The outprints of seismograms of events recorded at five sites were an auxiliary material for making further selection of a group of events chosen for calculating the spectral parameters. The events selected were those which had a large ratio of amplitude to microseismal noise. Weak events, with foci nearby one of the seismometers, were very poorly recorded at the rest of the sites and were not suitable for spectral analysis (see Chap. 6). The record of a quake whose focus is located very close to the seismometer was, as a rule, contaminated with a characteristic

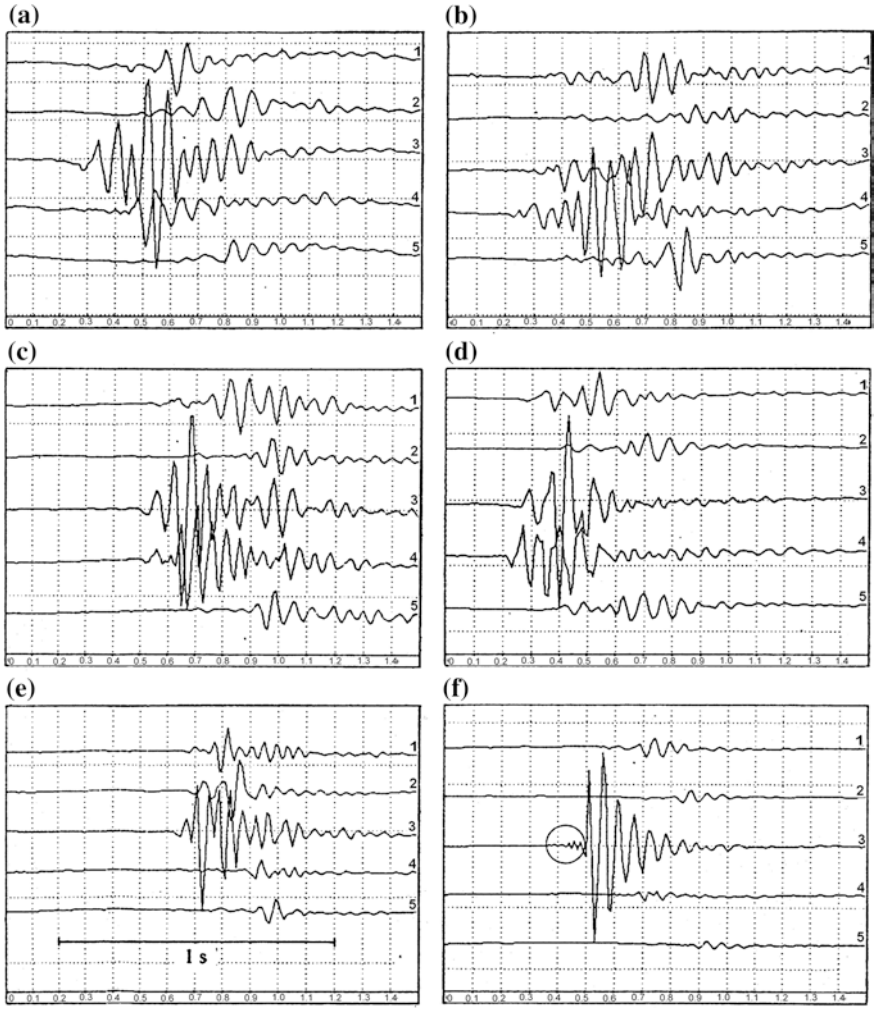


**Fig. 3.5** Examples of seismograms of six events, **a**–**f**, recorded on channels *1*–*5*. The channel numbers correspond to the seismometer site numbers (Fig. 3.2). Amplifications with which the events **a**–**f** are recorded vary, but the amplifications of channels *1*–*5* for one shock are the same. The *circle* indicates the distortion introduced by the instrument (the Finite Impulse Response filter effect). The seismograms are based on outprints obtained with program DADISP

distortion introduced by a digital filter (FIR, *Finite Impulse Response* filter effect) and was not suitable for a direct interpretation (Scherbaum et al. 1994); an example of so disturbed recording is shown in Fig. 3.5f. The characteristic distortion preceding the proper group of waves is marked with a circle. The record at such a channel was disregarded, and in further interpretation the use was made of the remaining four channels, provided that the signal was sufficiently strong in

relation to the level of microseisms. More distant events were not much differentiated in amplitude in all channels and, if the event was strong enough, all channels were suitable for further interpretation (Fig. 3.5a–d). Finally, the group of 58 events selected for spectral analysis (Chap. 6) consisted of stronger near quakes and the majority of distant quakes that have been recorded.

The problem of determining the position of icequake foci is complicated; one can distinguish its two main aspects: (1) the relation between the place the quake occurred and the dimensions of seismometer network, and (2) the model of the medium embracing the glacier with its neighbourhood. The diameter of the area occupied by the seismometers was 600 m; the icequakes that were recorded occurred at a distance from tens of meters to over 2 km. In the case of events whose foci were nearby the seismometer network (hypocentral distances of some hundred meters), we can use the algorithms of mining tremors location; we applied the program LOCAL (Domański 1993). Its algorithm is based on Leighton and Duvall's (1972) method, used for preliminary location. The preliminary location is followed by a minimization of the sum of residua of arrival times at the stations. The residuum is defined here as a difference between the time the wave arrived to the seismometer and the theoretically calculated time value.

At the output, the program gives the coordinates of the focus, time in the focus, and a series of auxiliary data; the number of iterations can be adjusted practically unrestrictedly. In computations we used arrival times of P and S waves. For events at epicentral distances in excess of 1 km, the algorithm has not produced satisfying results. For such events, we preliminarily adopted a two-dimensional model of the glacier and determined the coordinates of the foci on the basis of their distances from seismometers and their azimuths. The latter were determined from the P-wave arrival times at individual sites, under the assumption of the plane wave head. For this purpose, we also often used the program LOCAL, assuming that the focus position produced by this program is contaminated with large error only in the focus depth. The distances of the foci from the seismometers were calculated from the differences in arrival times of P and S waves. In the ablation zone one can assume a seismic wave velocity which is almost invariable with depth. A thin (up to 3 m) snow layer placed on the ice during recording did not play any role; the more so since the seismometers were positioned on the ice surface. In the ablation zone of the glacier, the thick snow layer, gradually passing with depth into denser and denser ice, does not exist. This phenomenon occurs in the accumulation zone of the glacier and is accompanied by large gradient of seismic wave velocities (Kohnen and Bentley 1973). The adopted values are: $V_P = 3{,}150$ m/s, $V_S = 1{,}540$ m/s, and consequently $V_P/V_S = 2.05$. In the glacier's substratum we adopted $V_P = 4{,}600$ m/s and $V_P/V_S = 1.73$. The ice density adopted for computations is $\rho = 850$ kg/m$^3$. In the summer of 1997, measurements were made which verified the velocity values adopted here. The experiment is described in Chap. 4.

The epicenters of localized events are shown in Fig. 3.6 (red circles). The geometry of the glacier model for the area in which the icequakes were recorded was based on the 1:25,000 Hans Glacier Topographic Map (Jania et al. 1994) and radar data determining the location of the Hans Glacier bottom (Glazovsky et al. 1991).

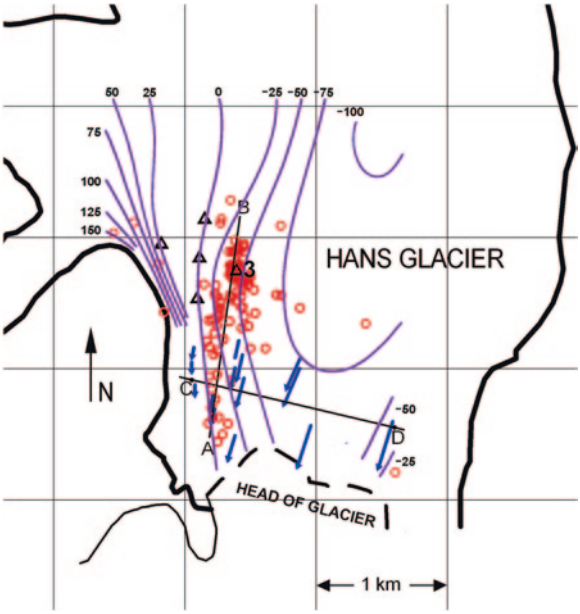


**Fig. 3.6** Epicenters of the localized events. *Red circles* mark the icequake epicenters, *triangles* the seismometer sites. The cross-section on profile A–B, approximated with *straight lines*, is shown in Fig. 3.8. The *violet contour lines*, showing the location of the glacier bottom, are based on radar measurements (Glazovsky et al. 1991). *Arrows* are the vectors of annual glacier motion velocity (Jania 1992). Line C–D is the profile at which the ice velocity gradient was estimated

Fragments of the two maps, overlapping each other, are shown in Fig. 3.6. The thick violet lines are the contour lines on the glacier bottom. Seismometer sites are marked by triangles. Line C–D represents the profile at which the ice velocity gradient was estimated. The behavior of this gradient is shown in Fig. 3.7.

As can be seen in Fig. 3.7, one of the main areas of the glacier in which the relatively strong icequakes occur coincides with the site of maximum values of annual glacier velocity gradient. In this region, the main stream of the glacier meets the marginal zone. This is the region of strong stresses, the release of which in the form of seismic events gives rise to ice dislocations at its surface (see photo in Fig. 3.2). The dislocations occur in mutually perpendicular directions: along the main flow direction of the glacier, and transversely to the glacier's axis.

The glacier in the area of our interest can be approximated by an ice wedge delineated by the mutually inclined planes of the bottom and surface of the glacier. The section across this wedge, along profile A–B, nearby the seismometer site 3, is shown in Fig. 3.8. Changes in the ice thickness through the time that elapsed between the instant of mapping and that of making seismological measurement are so small that they can be neglected.

In Table 3.1 we give the ice thickness values underneath the seismometer sites. They were determined from the measurements of the elevations of the sites made in the course of seismological observations and from radar measurements (Glazowsky et al. 1991).

The vertical cross-section through the seismically active region situated in the marginal zone of the glacier (in the place where the gradient of the glacier velocity in its annual movement is large) is shown in Fig. 3.8. The glacier's bottom is in

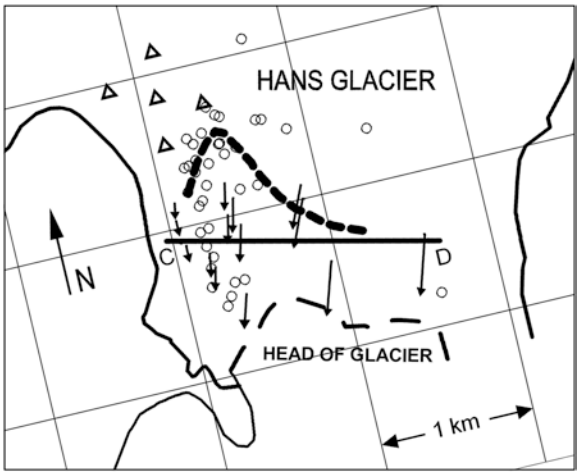


**Fig. 3.7** Glacier velocity gradient estimated at profile C–D (see Fig. 3.4) is shown by a *thick broken line*. *Arrows* are the vectors of annual glacier motion velocity (Jania 1992). *Circles* mark the location of epicenters of events with magnitudes greater than −0.7. After elimination of weak events, grouped mainly around site 3 and associated with vertical water flow (Fig. 3.6), we get a more homogeneous pattern of seismically active area, as indicated by profile A–B. *Triangles* are the seismometer sites

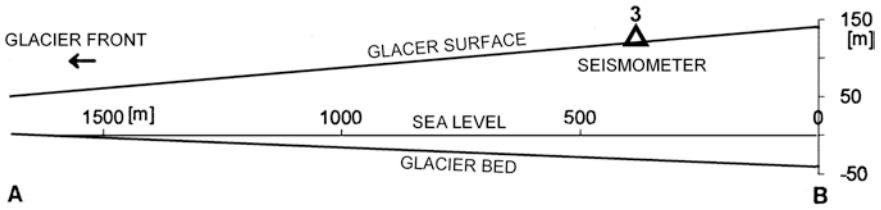


**Fig. 3.8** The Hans Glacier cross-section along profile A–B (see Fig. 3.6), approximated by *straight lines*

**Table 3.1** Glacier thicknesses under seismometer sites

| Seismometer site | 1 | 2 | 3 | 4 | 5 |
|---|---|---|---|---|---|
| Glacier thickness (m) | 130 | 150 | 165 | 115 | 125 |

this area at a depth from 0 to over 50 m below sea level. Profile A–B runs along the western border of the maximally cracked region. The effects of discontinuous dynamical processes occurring in this region, related to the large velocity gradient, are visible as cracks on the glacier's surface (Fig. 3.2).

In Fig. 3.9 we show the depths of foci on the Hans glacier. We selected foci at a distance no greater than 500 m from site 1 (Fig. 3.6). The section through the glacier covers part of profile A–B. The south-north directed horizontal axis in the figure represents the glacier surface; its inclination toward the geodetical vertical direction is not taken into account. The position of site 3 is marked with the triangle. The dashed

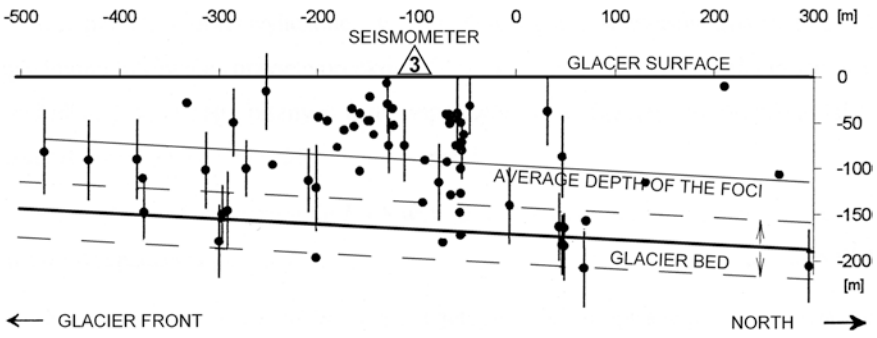


**Fig. 3.9** Depths of shock foci (*circles*) in the Hans Glacier. The section through the glacier was made along profile A–B (Fig. 3.6). The horizontal axis represents the ice surface and does not coincide with the horizontal direction in the terrain. It is directed from south to north. *Triangle*: the location of site 3 (Fig. 3.6). The *broken lines* in the lower part of the figure indicate the depth of the edge of the glacier bottom belt running along the profile; the belt is 500 m wide and dips from west to east. The *vertical bars* show the foci diameters (Chap. 6); the lengths of the bars indicate only the size of the focus; the fault plane position has not been determined

lines at the bottom of the figure delineate the depth of the edge of the glacier bottom belt running along the profile; the belt is 500 m wide and dips from W to E. The vertical bars mark the foci diameters calculated for major events (Chap. 6); they only indicate the size of the foci—their vertical direction has no relation to the fracture plane location, which was undeterminable. The straight line calculated with the least squares method, indicating the course of the average focal depth, runs parallel to the glacier's bottom, The foci diameters are large in comparison to the glacier thickness. The cluster of foci nearby site 3 is most probably due to local hydroglacial processes.

All these observations lead to the conclusion that the recorded seismicity can be related to the release of stresses formed in the marginal zone of the glacier, on the boundary between the two parts of the glacier: the part which is strongly associated with rocky environment and the other which constitutes the glacier's main stream and is subjected to gravity pressure of the ice accumulated in the winter. In addition, there also occur displacements of water masses blocked within the glacier in the winter, which are accompanied by a change in the stress field due to uplift forces. The latter phenomena are probably related to the intense seismic activity nearby site 3. In this region there are many wells, testifying to the occurrence of hydroglacial processes. The structure of the glacier is very complicated, with the occurrence of interglacial caves.

## 3.3 The Relative Energy Flow (Experiments of 1995 and 1999)

Seismic recording of icevibration events made at the HSP station (Fig. 3.2) enables monitoring the Hans Glacier activity over longer time spans (in a continuous manner).

In 1982–1985, the Silesian University realized on the Hans Glacier a glaciological project, which included the measurements of glacier velocity (Fig. 3.10)

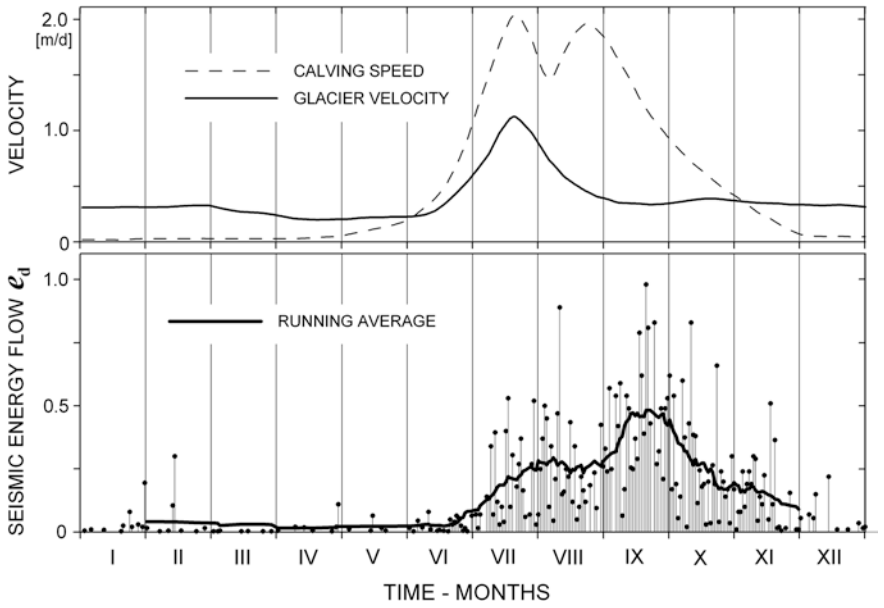


**Fig. 3.10** A comparison of velocity distribution in annual glacier motion (*top*) and relative daily seismic energy flow $e_d$ recorded at the HSP seismic station (*bottom*) (Jania et al. 1985)

the results were compared with the icevibration data obtained in this period by the author by means of the HSP station (Jania et al. 1985).

In this chapter, the velocity distribution in annual glacier motion and the annual velocity of the glacier calving of the Hans Glacier has been compared with the course of daily seismic energy flow recorded at the HSP seismic station. The results are shown in Fig. 3.10 (Jania et al. 1985).

The lower part of Fig. 3.10 shows the annual course of relative daily seismic energy flow $e_d$ recorded at the HSP (Jania et al. 1985). The daily flow is understood to mean the sum of energy flows of seismic events in the glacier, as recorded by the HSP station per day. The relative energy flow $e_d$ is a ratio of the daily seismic energy flow recorded in a given day to the maximum daily flow recorded in the year. The seismic energy flow is directly proportional to the square of the vibrating ground velocity amplitude; this quantity is directly recorded on seismograms. The black points mark the daily flow $e_d$, thick solid line is the running average of the values $e_d$ calculated for a 21-day period. The upper panel of Fig. 3.10 shows the annual course of glacier velocity on a transverse profile, few hundred meters away from the glacier's head (solid line) and the annual velocity of the glacier calving (dashed line). The velocities were determined from fotogrammetric pictures. Plots in Fig. 3.10 are the averaged curves, based on data collected over a few years.

Comparing the plots of seismic activity, glacier's velocity and the calving velocity we see that the seismic activity recorded at the HSP station is closely

related to the motion of the glacier observed on its surface. The delay of the main maximum of seismic activity relative to that of the glacier motion may be associated with the displacement of ice masses in areas that were not subject to photogrammetric observations and the processes occurring at that time in the glacier's interior; one may also take into consideration changes in the distribution of interglacial waters and the associated change in the hydrostatic uplift force field. The changes in the amount of water in the glacier's substratum affect the conditions of bottom slide. This may lead to local hampering of the glacier motion and the accompanying abrupt growth of stresses to be then released in the form of seismic events which do not have to be accompanied by visible ice displacements.

The assessment of the flow velocity of the Hans Glacier on the basis of energy recorded in seismic glacial events was made by Czajkowski (1977b). The author draws the attention to a relationship between characteristic impulse frequencies and the thickness of the glacier. The maximum amplitudes of the recorded events were 1.4–3.3 Hz, which are the characteristic frequencies of icevibrations. The quoted chapter is based on measurements performed on the Hans Glacier in August and September 1971.

A comparison of time course of seismic activity of icevibrations with the activity of icequakes in relation to the violent changes in the glacier's flow velocity was possible owing to measurements of velocity of ice flow made by scientists from the ETH, Zurich.

The determination of seismicity in the 1999 summer campaign is based on two measurement networks: the glacier network and the station network. The glacier network is placed on the glacier surface (Fig. 3.11), while the other one is the network of Hornsund station, located 3–4 km from the main stream of the glacier (Fig. 3.11). In principle, each network records different types of events.

We analyzed series of events recorded from 21 June through 3 July 1999. During this period also measurements of velocity of ice flow on the surface of glacier were made by scientists from the ETH, Zurich.

The glacier network consisted of six short-period (T = 1.5 s) seismometers SM-3 to record vertical oscillations of ice; the sampling frequency was 500 Hz. The seismometers were placed directly on the ice surface, in western part of the glacier's ablation zone. They have been detecting typical short-duration icequakes (Fig. 3.1a), related to the release of stresses accumulated in ice. The instruments were programmed to record icequakes only. Icequakes are too weak to be recorded by the station network. In addition to typical short-duration events, the glacier network recorded also some untypical wave packets. Some of such events had foci located near the glacier's front.

The icequake seismic activity is related to the west edge of the glacier's main stream (though some events were also observed in other places) (Fig. 3.11).

The permanently working station network (Górski 1997) is equipped in seismometers of the same type as the glacier network, and the sampling frequency is 100 Hz. The seismometers are distributed at five sites over the area of 500 m

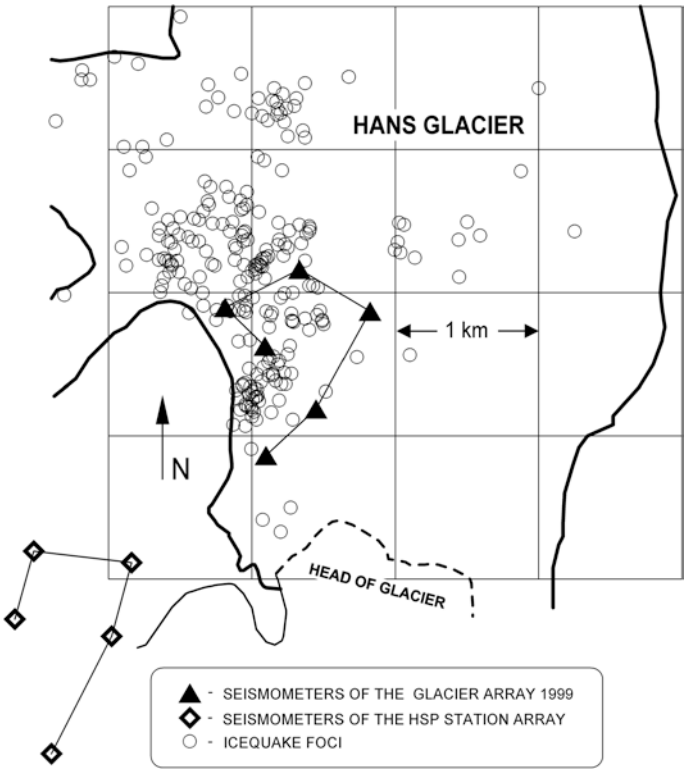


**Fig. 3.11** Location of icequake epicentres. *Circles* denote icequake epicentres, *triangles* the seismometer sites

extent. Vertical vibrations of the ground are recorded at all sites, one of the sites being additionally equipped in seismometers recording the horizontal components. The station network records icevibration events (Fig. 3.1b).

Figure 3.12 shows comparisons of daily numbers of icequakes (recorded by the glacier network) and the relative daily energy flow. The energy flow recorded by the station network is directly related to the intensity of icevibration generation by the Hans Glacier. The relative energy flow is a ratio of the daily seismic energy flow recorded in a given day to the maximum daily flow recorded during the whole registration period. The seismic energy flow is directly proportional to the square of the vibrating ground velocity amplitude. The running average drawn in the figure is taken with a window 5.

A maximum gradient of energy flow can be seen around June 26, which roughly corresponds to the maximum of velocity of ice flow and the minimum of the daily number of icequakes. Information about the ice flow velocity was obtained by the author directly from A. Vieli during the measurements in 1999. These values and detailed description of velocity measurement are contained in the later publication by Vieli et al. (2004). Icequakes associated with the area of

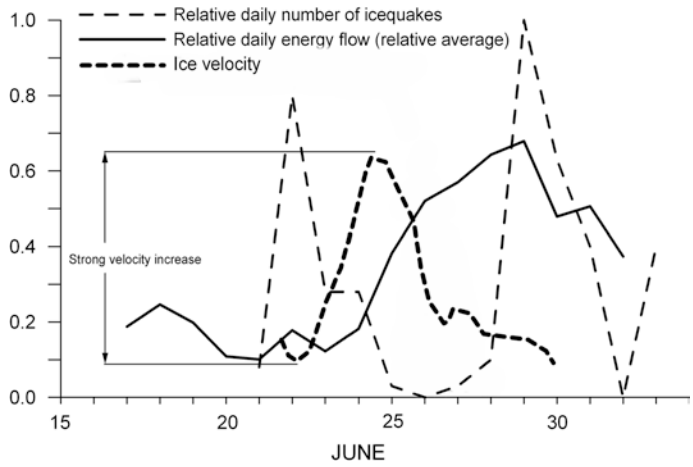


**Fig. 3.12** Comparisons of daily numbers of icequakes (recorded by the glacier network) and the relative daily energy flow (recorded by the station network) in relation to strong increase of flow velocity

large velocity gradient (see Sect. 3.2) are related to changes and time rate of glacier motion. When a glacier starts to move in a large scale, the icequakes occur due to breaking of ice. Icevibration events are related to a more steady phase of motion (flow) and to some friction processes (ice-bedrock contact, for example). These events may be related to glaciodynamical processes occurring in the main stream of the glacier. Of importance are also resonant vibrations of large elements of the glacier. We observe icequakes in association with change of motion velocity and icevibration events for the maximum of velocity.

## References

Baranowski S (ed) (1977a) Results of investigations of the Polish Scientific Spitsbergen Expeditions. Acta Univ Wratisl II(387)

Baranowski S (ed) (1977b) Results of investigations of the Polish Scientific Spitsbergen Expeditions. Acta Univ Wratisl III(410)

Baranowski S (ed) (1977c) Results of investigations of the Polish Scientific Spitsbergen Expeditions. Acta Univ Wratisl IV(525)

Czajkowski R (1974) Wyniki badań mikrowstrząsów na lodowcu Hansa (Results of a study of microtremors at the Hans Glacier), in: Polskie Wyprawy na Spitsbergen 1970 i 1971, Materiały z Sympozjum Spitsbergeńskiego, Uniwersytet Wrocławski, pp 30–34 (in Polish)

Czajkowski R (1977a) The results of investigations into microquakes on the Hans Glacier. Acta Univ Wratisl 387:119–138

Czajkowski R (1977b) Próba określenia grubości lodowca i jego ruchu za pomocą pomiarów sejsmicznych prowadzonych w latach 1971 i 1972 (An attempt to determine a glacier thickness and movement basing on seismic measurements in 1971 and 1972), in Polska Wyprawa na Spitsbergen in 1974, Materiały z Sympozjum Spitsbergeńskiego, Uniwersytet Wrocławski, p 35 (in Polish)

Domański B (1993) Programs SPAG, LOCAL. Department of Seismology, Institute of Geophysics, Polish Academy of Sciences

Glazovsky AF, Macheret YY, Moskalevsky MY, Jania J (1991) Tidewater glaciers of Spitsbergen, vol 208. IAHS Publication, pp 229–239

Górski M (1975) Observations of natural ice-micro-trmors of the Hans Glacier, Acta Univ Wratisl 251:95–100

Górski M (1997) Seismicity of the Hornsund region, Spitsbergen: icequakes and earthquakes. Publs Inst Geophys Pol Acad Sci B-20(308):1–76

Jania J (1992) Some results of glaciological research—Hansbreen. In: Field workshop on glaciological research in Svalbard, University of Silesia, V/19–V/34

Jania J, Kolondra L, Schroeder J (eds) (1994) Hans Glacier 1:25,000 topographic map. Department of Geomorphology, University of Silesia, Sosnowiec, Poland; Norsk Polarintitutt, Oslo, Norway; Universite du Quebec, Montreal, Canada. Uniwersytet Slaski, Katowice

Jania J, Kolondra L, Rudowski S, Górski M (1985) Annual activity of Hans Glacier, Spitsbergen as determined by photogrammetry and microtremors recording. In: Proceedings of symposium on glacier mapping and surveying, Reykyavik, August 1985

Jania J, Hagen JO (1996) Mass balance of Arctic Glaciers, IASC report No 5, 62, p 62

Kohnen H, Bentley CR (1973) Seismic refraction and reflection measurements at "Byrd" station. Antarctica J Glaciol 12:101–111

Leighton F, Duvall WI (1972) Least square method for improving rock noise source location techniques. U.S.BuMines—R.I. 7626, p 19

Lewandowska H, Teisseyre R (1964) Investigations of ice microtremors on Spitsbergen in 1962. Biul Inf Komisji Wypraw Geof PAN 37:1–5

Neave KG, Savage JC (1970) Icequakes on the Athabasca glacier. J Geophys Res 75:1351–1362

Pillewizer W (1939) Die kartographischen und gletscherkundlichen Ergebnisse der deutschen Spitsbergen-Expedition 1938, Petermanns Mitteilungen, Erganzungsheft Nr 238, Gotha

Rothlisberger H (1955) Studies on glacier physics on the penny ice cap, Baffin Island, 1953, part III: seismic soundings. J Glaciol 18:539–552

Scherbaum S, Wielandt E, Steim JM (1994) Removal of the non-causal FIR filter response from digital seismic records, manuscript

Van Wormer D, Berg E (1973) Seismic evidence for glacier motion. J Glaciol 12:259–265

Vieli A, Jania J, Blatter H, Fukk M (2004) Short-term velocity variation on Hansbreen, a tidewater glacier in Spitsbergen. J Glaciol 50(107):389–398

Weaver CS, Malone SD (1979) Seismic evidence for discrete glacier motion in the rock-ice interface. J Glaciol 23:171–184

# Chapter 4
# Seismic Wave Velocities in the Hans Glacier, Spitsbergen

## 4.1 Introduction

The knowledge of seismic wave velocities in a medium is a very important factor in the process of location of seismic events foci and determination of their spectral and physical parameters. In the former studies on earthquakes in the Hans Glacier, Spitsbergen, the P and S wave velocities were determined in the course of foci location process (Cichowicz 1983; Górski 1997). Values obtained in the studies on other Arctic and Antarctic glaciers (Theil and Ostenso 1961; Neave and Savage 1970; Kohnen and Bentley 1973; Rendleman and Levin 1990) were used as input data.

The direct measurements of seismic wave velocities reported in the present chapter have been first presented at the XXVI Polar Symposium in Lublin, Poland (Górski 1999).

## 4.2 The Field Experiment

Here we will describe direct measurements of P and S wave velocities performed on the Hans Glacier in the summer of 1997 in a special array of seismometers deployed near the Polish Polar Station Hornsund, Spitsbergen. The location of measurement sites is shown in Fig. 4.1. Artificial quakes were generated three times at the point of central location between the seismometer sites (point 1 in the figure). The source was situated in a narrow crack at a depth of about 5 m, as schematically drawn in Fig. 4.2. The width of the crack was narrowing with depth, and the artificial icequakes were generated at its bottom. We tried to keep identical conditions of seismic wave generation in all the three cases. The measurements of seismic wave velocity in ice were a supplement to the research on icequakes; the shortage of time and difficult field conditions made it impossible to implement a special network of profiles targeted at velocity measurements over a larger area.

M. Górski, *Seismic Events in Glaciers*, GeoPlanet: Earth and Planetary Sciences,
DOI: 10.1007/978-3-642-31851-1_4, © Springer-Verlag Berlin Heidelberg 2014

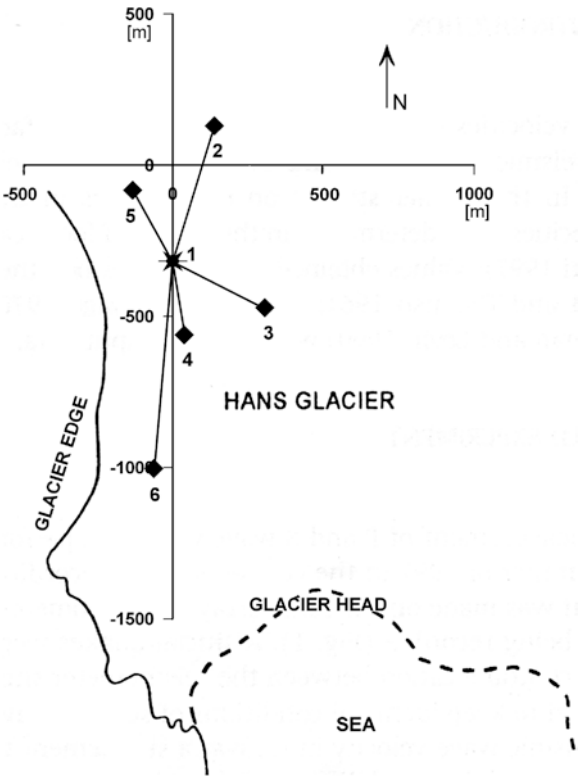


**Fig. 4.1** Location of seismometer sites (*black diamonds*) on the Hans Glacier. The artificial quakes were located at site 1

The network was located in the ablation part of the glacier, on the western margin of its main stream; the most distant seismometers were from 200 to 1,200 m away from the glacier head, as seen in Fig. 4.1. The photo in Fig. 4.3 is an illustration how the glacier surface looked like in the region of site 6; the photo was taken from the 560 m high top of a nearby mountain.

The measurement array consisted of five vertical seismometers. Short-period (T = 1.5 s) seismometers SM-3 were placed directly on the ice surface, in holes dug in snow. The snow layer in the studied region was from zero to some tens centimeters thick. The seismometers were connected by cables with Portable Data Acquisition System Teledyne Geotech; the sampling frequency was 500 Hz.

## 4.3 Results of Measurements

In Fig. 4.4 we show averaged seismograms of the three quakes generated. On the vertical axis is the distance from site 1, at which the quake was generated, to the consecutive seismometer sites. The moment of quake generation at site 1 is

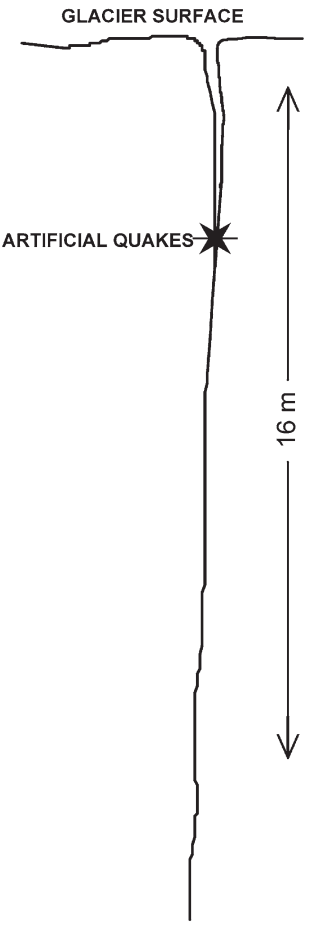


**Fig. 4.2** Vertical cross-section through the crack in the Hans Glacier. The *asterisk* marks the place in which the artificial quakes were generated

marked in the figure by an asterisk. As can be seen, at the three sites that are the closest to the source (4, 5 and 3), the first wave observed is the P wave propagating in ice (line *a*). At the two farthest sites (2 and 6), it is the refracted wave that arrives first (line *b*). As the next arrival, a group of S waves together with surface waves is observed (line *c*) in all the seismograms. The intersection of lines *a* and *b* corresponds to the distance from the source at which the direct P wave and the refracted wave arrive simultaneously; this distance is 420 m. The P and S wave velocities were calculated under the assumption that the glacier is a plane-parallel layer. In reality, the glacier's top and bottom are surfaces of varying mutual dip (Fig. 4.4). However, in our case the upgrade dip between the source and the rest of the sites differs from the downgrade dip. Owing to this fact, the averaging of results calculated for various dips is reasonably well fitted to the assumption of a plane-parallel layer. The dips were evaluated on the basis of the glacier's surface map (*Hans Glacier*, *Topographic Map* 1:25,000; Jania et al. 1994) and radar

**Fig. 4.3** A general view on the Hans Glacier surface around site 6, as seen from top of a 560 m high mountain

measurements of glacier's thickness (Glazovsky et al. 1991). The velocities calculated from lines *a*, *b* and *c* (Fig. 4.4) are: Vp = 3,620 m/s, Vs = 1,780 m/s. The apparent velocity of refracted wave is 5,260 m/s. The velocity measurement error is estimated at ~50 m/s.

On the basis of the traveltimes shown in Fig. 4.4 we estimated the thickness of the glacier under the source at h = 90 m. This value is lower than the value of 130 m derived from radar measurements and shown in Fig. 4.5. Though the absolute value of glacier thickness during the measurements reported here might have differed from that shown in Fig. 4.5 on account of considerable ablation in this part of the glacier, still the observed discrepancy is too large and should be verified through additional measurements.

The P-wave velocity calculated here is greater than that used in calculation of spectral parameters of icequakes recorded in April 1995 (Górski 1997). The velocity Vp = 3,150 m/s adopted in that work was determined through optimization of earthquake foci location. The value Vp = 3,400 m/s obtained by Cichowicz (1983) in his study of icequakes on the Hans Glacier in the summer of 1980 was calculated from the measured traveltimes between the sites. Neave and Savage (1970) obtained the velocities of P, S and Rayleigh waves of 3,650 m/s, 1,820 m/s and 1,700 m/s, respectively, as determined from traveltimes over measured distances. During summer, in the ablation zone of the Hans Glacier we are dealing with solid ice, intersected by snow-free cracks. The situation on ice in the Antarctic is different. The values obtained at the base Little America V on the Ross Ice Shelf (Thiel and Ostenso 1961) are the following: Vp = 3,839 m/s, Vs = 1,978 m/s. Similar results were obtained at the Byrd station, Antarctica (Kohnen and Bentley 1973).

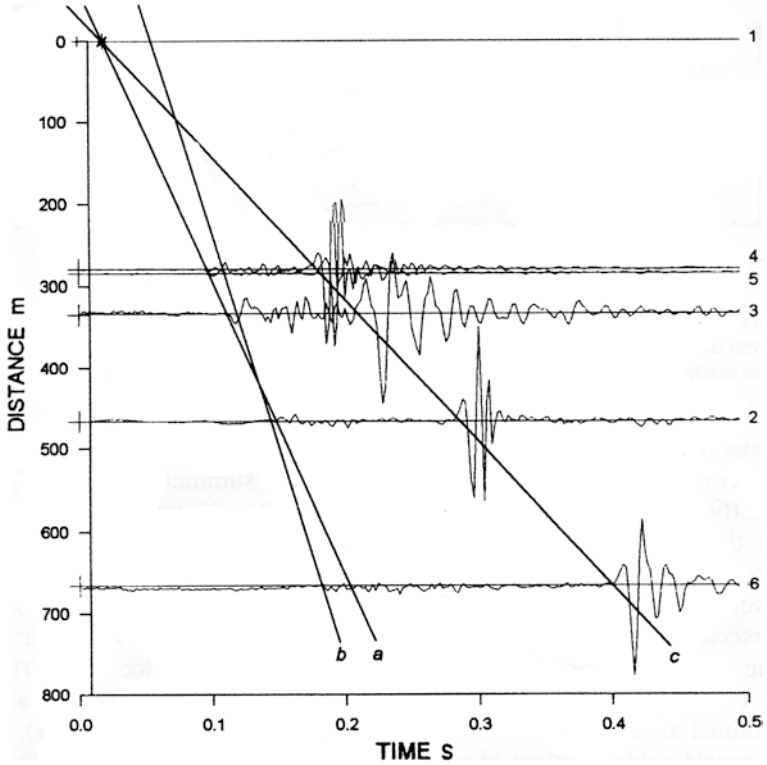


**Fig. 4.4** Averaged seismograms of an artificial quake recorded at sites *2–6* (see Fig. 4.1). Line *a* (P wave) was recorded at sites *3–5*; line *b* (refracted wave) was recorded at sites *2* and *6*; line *c* (S wave together with surface waves) was recorded at all sites. On the *vertical axis*, the distances of seismometer sites to the quake generation place are marked with *crosses*, and the moment of quake emission by an *asterisk*. The time the quake was generated was recorded at site *1* at the top of the crack

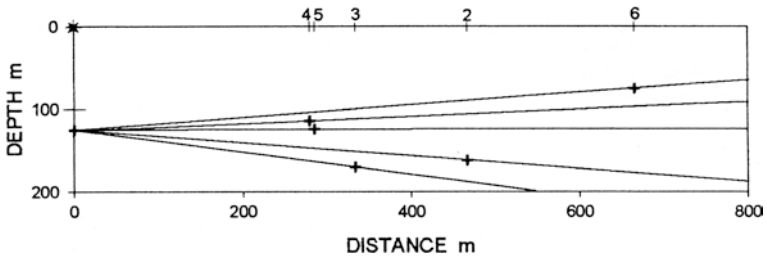


**Fig. 4.5** Dip of the glacier's bottom. The lines marked with *crosses* show the dip of glacier's bottom in the directions from the artificial quake site toward the seismometer sites. The sites on the glacier surface are marked with *numerals*; the cross directly *below* the numeral indicates the respective *straight line*

In both cases, a considerable gradient of velocity with depth was observed when ice was covered with a snow layer: in the downward direction, as snow has been changing its crystalline structure through a gradual transformation into ice, the velocity of seismic waves was growing.

It is to be noted that the artificial quakes described in this chapter were used not only for velocity determination. We also calculated their focal parameters, as will be discussed in detail in Chap. 5.

## References

Cichowicz A (1983) Icequakes and glacier motion: the hans glacier, spitsbergen. Pure Appl Geophys 121:27–36

Glazovsky AF, Macheret YY, Moskalevsky MY, Jania J (1991) Tidewater glaciers of Spitsbergen, vol 208. IAHS Publication, pp 229–239

Górski M (1997) Seismicity of the Hornsund region, Spitsbergen: icequakes and earthquakes. Publs Inst Geophys Pol Acad Sci B-20(308):1–76

Górski M (1999) Seismic wave velocities in the Hans Glacier. In: Repelewska-Pękalowa J (ed) Polish Polar Studies. 26-th International Polar Symposium, Maria Curie-Skłodowska University Press, Lublin, pp 77–81

Jania J, Kolondra L, Schroeder J (eds) (1994) Hans glacier 1:25 000, topographic map. Department of Geomorphology, University of Silesia, Sosnowiec, Poland, Norsk Polarintitutt, Oslo, Norway, Universite du Quebec, Montreal, Canada. Uniwersytet Slaski, Katowice

Kohnen H, Bentley CR (1973) Seismic refraction and reflection measurements at “Byrd” Station. Antarctica J Glaciol 12:101–111

Neave KG, Savage JC (1970) Icequakes on the Athabasca glacier. J Geophys Res 75:1351–1362

Rendleman CA, Levin FK (1990) Seismic exploration on a floating ice sheet. Geophysics 55:402–409

Thiel E, Ostenso NA (1961) Seismic studies on Antarctic ice shelves. Geophysics 26:706–715

# Chapter 5
# Spatial Distribution of Icequakes in the Hans Glacier

## 5.1 Introduction

The analysis presented here (see also Górski 2003) was made for icequakes located in Hans Glacier. Once the three-dimensional coordinates of icequakes have been determined, it turned out that the majority of quakes occur in the upper or lower part of the glacier, only a few of them being located in intermediate depths. The quakes were divided into three groups: those localized nearby the glacier's bottom, localized at its surface, and at intermediate depths. Such a grouping enabled us to make a clear graphic illustration. The analysis covers the following three recording periods: from 4 through 18 April 1995, from 19 through 27 June 1997, and from 14 April through 3 July 1999. All the measurement series were obtained using the same instruments and six seismometers of the same type. It is only the location of seismometers sites that has varied, but the area covered by the recording has been the same. The glacier networks consisted of six short-period ($T = 1.5$ s) seismometers SM-3 to record vertical oscillations of ice. The seismometers were placed directly on the ice surface, in western part of the glacier's ablation zone. The network has been detecting typical icequakes related to the release of stresses accumulated in ice. While designing the seismometric recording systems at the Hans Glacier, the use was made of the experience gained in mining seismicity research in the Upper Silesian region in Poland. Unfortunately, the three-dimensional distribution of seismometers, typical for mining seismic networks, was not possible in the Hans Glacier study. The seismometers were placed at the glacier's surface. Spatial distribution of seismometers would involve deep drillings in ice, which was not possible for technical reasons at that time. The hypocentral distance of the focus was determined by the difference ($t_S - t_P$). In the analysis presented here we do not take into account the icevibrations, which are described in other chapters.

M. Górski, *Seismic Events in Glaciers*, GeoPlanet: Earth and Planetary Sciences,
DOI: 10.1007/978-3-642-31851-1_5, © Springer-Verlag Berlin Heidelberg 2014

## 5.2 Location of Icequake Epicentres

The location of icequakes is based on arrival times of P and S waves with the help of software packet called LOCAL (Domański 1993) developed for the needs of seismological network in Polish mines. The adopted mean P-wave velocity is 3,620 m/s, the ratio of P over S wave velocity is 2, as described in greater detail in Chap. 4 (see also Górski 1999).

In Figs. 5.1, 5.2 and 5.3 we show the location of icequakes for the studied series. The blue-coloured wireframe represents the glacier basement determined from radar measurements (Glazovsky et al. 1991) with the account of some details observed during radar profiling made by Moor et al. (1999). The glacier surface is red-coloured (*Hans Glacier Topographic Map* 1:25000, Jania et al. 1994). The broken line marks the line along which the two networks meet, i.e., the glacier's edge. From the south, i.e., from the direction of the sea, the glacier is limited by its head, roughly delineated in the figure. The foci of quakes associated with the glacier surface are marked with red circles, while those located in the lower part of the glacier are marked with blue circles. The green circles represent the medium-depth foci. Black triangles joined by a solid line represent the location of seismometer sites placed at the ice surface. To facilitate the comparison of icequake location in individual measurement series, only the network of seismometers used

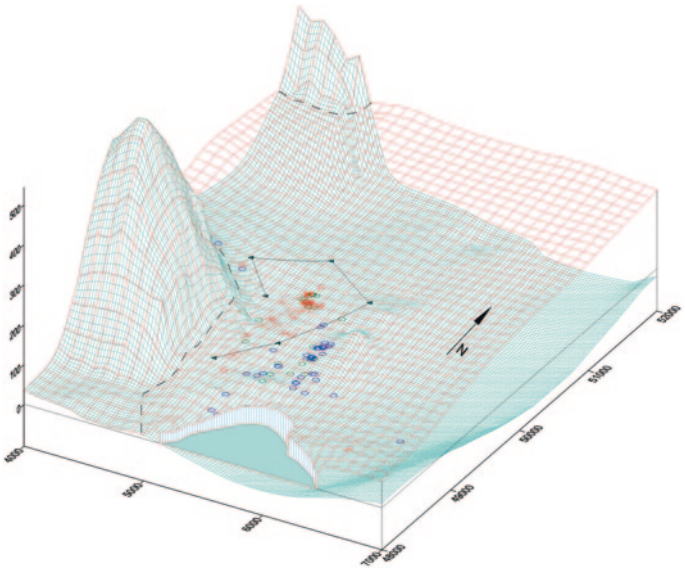


**Fig. 5.1** Spatial distribution of foci of icequakes recorded from 4 through 18 April 1995. The wireframe of glacier bottom and foci in the bottom zone are marked in *blue*. The wireframe of glacier surface and foci in the surface zone are marked in *red*. The *green* colouring refers to the middle-depth foci. The glacier's edge is indicated by a *broken line*. *Black triangles* connected by a *solid line* indicate the sites of seismometers at the ice surface (measurements in 1999)

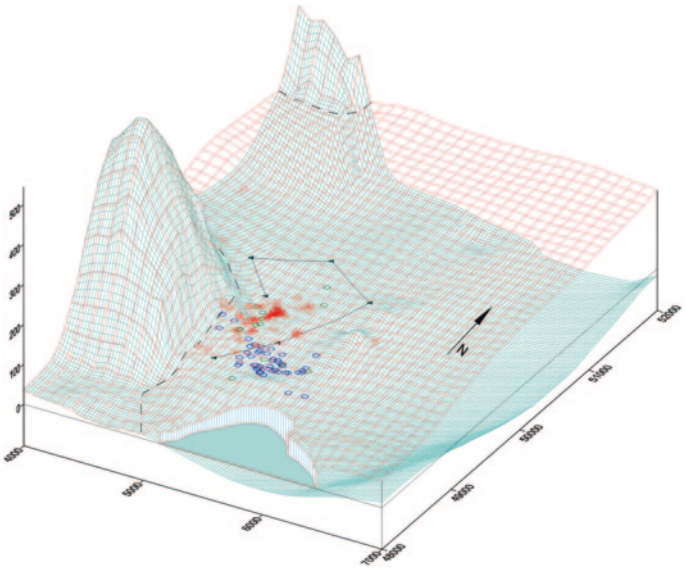

**Fig. 5.2** Spatial distribution of foci of icequakes recorded from 19 through 27 June 1997. Explanations as in Fig. 5.1

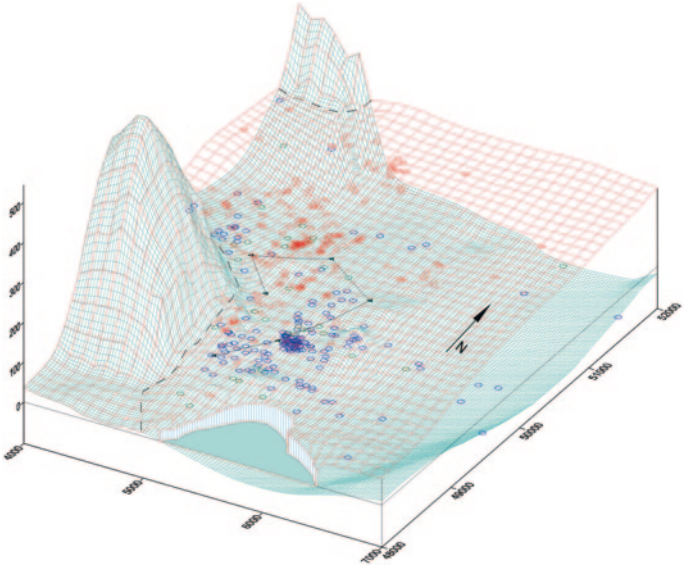

**Fig. 5.3** Spatial distribution of foci of icequakes recorded from 4 April through 3 July 1999. Explanations as in Fig. 5.1

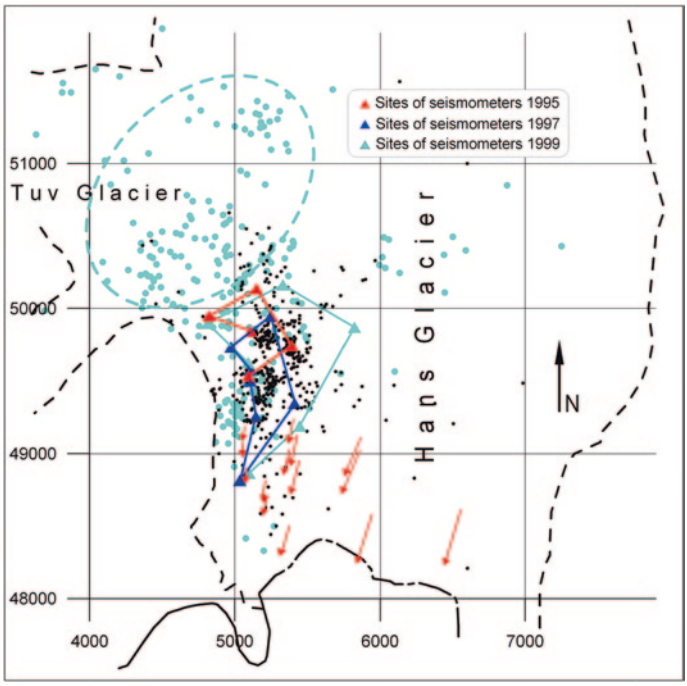


**Fig. 5.4** Location of icequake epicentres of measurement series 1995, 1997 and 1999 at the Hans Glacier—*black* and *cyan dots*. *Cyan-color dots* refer to the icequake series recorded from 15 June through 3 July 1999, *black dots* to the remaining series. Seismometer sites of measurement series are marked by *triangles*: 1995 in *red*, 1997 in *blue*, 1999 *cyan*. *Arrows* are the vectors of annual glacier motions velocity (Jania, 1992) The glacier's margin is marked by a *broken line*. The ellipse drawn by *cyan-color broken line* indicates the area where the Hans Glacier and Tuv Glacier merge. Coordinates on the axes are in meters

in the measurements of 1999 is marked on the figures. Seismometer sites in the other series are shown in Fig. 5.4.

In Fig. 5.1 we show the icequake series recorded from 4 to 18 April 1995. In Fig. 5.2 there is a series recorded in the summer of 1997, from 19 to 27 June. Both series give evidence of a large activity of the glacier in its eastern margin. The glacier is active in this region both during its spring start and in the summer season. It is almost equally active in its surface and bottom zones. The events marked in blue, located in the lower part, are related to the basement unevenness.

Figure 5.3 presents the icequakes recorded and localized from 14 April through 3 June 1999. The seismic activity is related to the west edge of the glacier's main stream (although some events were also observed in the middle of the glacier). These foci occur mainly in the lower part of the glacier and are related to unevenness of its basement, likewise those in Figs. 5.1 and 5.2. The thickest cluster of foci in the glacier's lower part is most probably associated with displacement of intra-glacial waters. This is a confirmation of the previously observed hydroglacial

processes (Górski 1997). In the region where the Tuv Glacier and Hans Glacier meet, the seismicity is probably related to the glacier surface and, as shown in Fig. 5.4, the glacier was active in this region in the second half of June.

Observing the ice flow velocity (red arrows in Fig. 5.4) we see numerous occurrences of icequakes due to stress release, which indicates that the icequakes are associated with places of large velocity gradient (i.e., the edges of the main stream), rather than with a large velocity value (see Chap. 3 and Górski 1997).

Observing the location of icequakes recorded in the second half of June (cyan-colored points in Fig. 5.4) we see that in this period it is the zone of Hans Glacier and Tuv Glacier junction that gets activated (as marked by the ellipse drawn by a broken line of cyan color). Strong.shearing stressess, accompanied by dislocations, occur there. The release of these stressess generates numerous icequakes located in the near-surface layer of ice.

## 5.3 Conclusions

The icequakes accompanying the dynamic activation of the area where the Hans Glacier and the Tuv Glacier merge are recorded mainly in the upper layer of ice. The glacier's seismic activity related to the release of stress accumulated in ice (icequakes) is the greatest in the marginal zone of the glacier, in the area of large velocity gradient. This zone is active both in spring, when the glacier starts, as well as in the summer. In this area, the icequakes occur in the vicinity of the glacier's bottom as well as around its surface. Local seismically active zones are associated with irregularities in the glacier basement.

## References

Abercrombie R, Leary P (1993) Source parameters of small earthquakes recorded at 2.5 km depth, Cajon Pass, Southern California: implication for earthquake scaling. Geophys Res Lett 20:1511–1514

Cichowicz A (1983) Icequakes and glacier motion: the Hans Glacier, Spitsbergen. Pure Appl Geophys 121:27–36

Domański B (1993) Programs SPAG, LOCAL, Department of Seismology, Institute of Geophysics, Polish Academy of Sciences

Gibowicz SJ (2002) Apparent stress and stress drop from seismic events induced by mining. Acta Geophys Pol 50:35–49

Glazovsky AF, Macheret YY, Moskalevsky MY, Jania J (1991) Tidewater glaciers of Spitsbergen, vol 208. IAHS Publication, pp 229–239

Górski M (1997) Seismicity of the Hornsund region, Spitsbergen: icequakes and earthquakes. Publs Ins Geophys Pol Acad Sci B-20(308): 1–77

Górski M (1999) Seismic wave velocities in the Hans glacier. In: Repelewska-Pękalowa J (ed) Polish polar studies, 26th international polar symposium. UMCS Press, Lublin, pp 77–81

Górski M (2003) Icequakes in Hans Glacier, Spitsbergen: Source parameters of icequake series. Acta Geophys Pol 51:399–407

Jania J (1992) Some results of glaciological research—Hansbreen. In: Field workshop on glaciological research in Svalbard, University of Silesia, pp V/19–V/34

Jania J, Kolondra L, Schroeder J (eds) (1994) Hans Glacier 1:25 000, topographic map. Department of Geomorphology, University of Silesia, Sosnowiec, Poland; Norsk Polarintitutt, Oslo, Norway; Universite du Quebec, Montreal, Canada. Uniwersytet Slaski, Katowice

Moore JC, Palli A, Ludwig F, Blatter H, Jania J, Gadek B, Głowacki P, Mochnacki D, Isaksson E (1999) High-resolution hydrothermal structure of Hansbreen, Spitsbergen, mapped by ground-penetrating radar. J Glaciol 45:524–532

# Chapter 6
# Spectral Analysis and Source Parameters of Icequakes

## 6.1 Spectral Analysis: Method and Assumptions

The calculation of focal parameters was based on Brune's (1970) model. The geometry of distribution of seismometer sites and foci location made it impossible to determine the fracture mechanism model. Adopting in the calculations of spectral parameters the shear model with a double pair of forces we consequently assumed that the source is a circular fault of radius $r_0$, and the time of stress release in the focus is short as compared to the time the seismic waves travel through the seismically active area of the focus. Brune's model was also used by Osten-Woldenburg (1990) while studying the focal parameters in the Antarctic shelf glacier and by Cichowicz (1983) in his study of the Hans Glacier.

The computations were made using the SPAG program (Domański 1993). The input data in the case of icequakes are the records of quakes, parameters of measurement and the calculated coordinates of foci (see Sect. 3.2). We also took into account the adopted P and S wave velocities, density and rigidity modulus of the medium, and a series of coefficients described below. We assumed that the attenuation of P and S waves in ice can be neglected, $Q = 5000$ (Rendleman and Levin 1990).

For the selected P and S wave sequences we calculated displacement spectra, which were the basis for calculating the spectral parameters. The latter was done on the basis of FFT.

The displacement spectrum for the adopted model is described by two independent parameters: spectral level $\Omega_0$ and corner frequency $f_0$. The third parameter we calculated is the seismic energy $E_0$ emitted from the source. Subsequently, on the basis of the spectral level $\Omega_0$ and corner frequency $f_0$ we calculated the seismic moment $M_0$, focus radius $r_0$, stress drop $\Delta\sigma$, apparent stresses $\sigma_a$ and the magnitude $M$. The parameters were determined for P and S waves under the assumption that the measurements were made in the far field of radiation. The definitions and relations used in program SPAG (Domański 1993), based on the book by Gibowicz and Kijko (1994), are outlined below.

M. Górski, *Seismic Events in Glaciers*, GeoPlanet: Earth and Planetary Sciences,
DOI: 10.1007/978-3-642-31851-1_6, © Springer-Verlag Berlin Heidelberg 2014

The spectral level and corner frequency can be determined on the basis of two integrals calculated directly from the recorded spectra

$$J = 2\int_0^\infty |V(\omega)|^2\, df = 2\int_0^\infty |\omega U(\omega)|^2\, df \tag{6.1}$$

$$K = 2\int_0^\infty |U(\omega)|^2\, df \tag{6.2}$$

where $V(\omega)$ and $U(\omega)$ are the velocity and displacement of the medium in the recording place, respectively.

The spectral level $\Omega_0$ and corner frequency $f_0$ are related to integrals $J$ and $K$ as follows (Andrews 1986; Snoke 1987):

$$\Omega_0 = 2\left(\frac{K^3}{J}\right)^{\frac{1}{4}} \tag{6.3}$$

$$f_0 = \frac{1}{2\pi}\left(\frac{J}{K}\right)^{\frac{1}{2}} \tag{6.4}$$

It was assumed here that the displacement field as a function of time is described by the equation (Snoke 1987)

$$u(t) = \Omega_0 \frac{1}{\tau^2} H(t) \exp(-t/\tau) \tag{6.5}$$

where $H(t)$ is Heaviside's function, $\tau$ is the rise time of the pulse. Correspondingly, the displacement amplitude as a function of frequency is

$$|U(\omega)| = \frac{\Omega_0}{1 + (\omega/\omega_0)^2} \tag{6.6}$$

where $\omega_0 = 2\pi f_0$ and $\omega_0 = 1/\tau$.

The seismic moment is defined as (Aki and Richards 1980):

$$M_0 = \mu \bar{u} A \tag{6.7}$$

where $\mu$ is the rigidity modulus in the focal area, $\bar{u}$ is the mean displacement in the focus, $A$ is the fault area (in the considered case $A = \pi\, r_0^2$). Moment $M_0$ related to the spectral level $\Omega_0$ is determined from the formula

$$M_0 = \frac{4\pi\rho_0 c_0^3 R \Omega_0}{F_c R_c S_c} \tag{6.8}$$

Index $c$ indicates the type of wave (P or S), $\rho_0$ is the medium density, $c_0$ the P or S wave velocity, and $R$ is the distance from seismometer to the source. Coefficients

$F_C$, $R_C$, $S_C$ relate to the radiation energy distribution model. For coefficient $F_C$ we assumed the values averaged over the whole sphere: $F_P = 0.52$ and $F_S = 0.63$ (Boore and Boatwright 1984). Coefficient $R_C$ accounts for the effect of free surface (in calculations we adopted $R_C = 2$). Coefficient $S_C$ is a correction related to the place of measurement (the adopted value is $S_C = 1$).

The seismic energy $E_C$ emitted from the source in the form of seismic waves is directly related to the integral $J$ (Boatwright and Fletcher 1984)

$$E_c = 4\pi\rho_0 c_0 \langle F_c \rangle^2 \left(\frac{R}{F_c R_c}\right)^2 J_c \tag{6.9}$$

where $\rho_0$ is the density of the medium, $R$ is the distance between the measurement point and the source, and $c_0$ is the P or S wave velocity. Coefficients $F_C$ and $R_C$ are related to the radiation energy distribution model in the medium. The mean square radiation pattern coefficient $\langle F_C^2 \rangle$ takes the value as in the case of Eq. (6.8).

The total seismic energy radiated from the source is the sum of energies $E_P$ and $E_S$ radiated in the form of P and S waves.

Magnitude $M$ is a quantity directly related to the seismic moment $M_0$ ($M_0$ is expressed in N·m) according to the definition given by Hanks and Kanamori (1979):

$$M = \frac{2}{3}\log M_0 - 6.0 \tag{6.10}$$

The focus radius $r_0$ is determined by the corner frequency of the spectrum $f_C$ according to the formula

$$r_0 = \frac{K_c \beta_0}{2\pi f_c} \tag{6.11}$$

where $K_C$ is a coefficient depending on the adopted source model. For our calculations we took the values given by Madariaga (1976), which are as follows: $K_P = 2.01$, $K_S = 1.32$. Symbol $\beta_0$ denotes the S wave velocity in the source area.

The stress drop $\Delta\sigma$ was calculated on the basis of the relation given by Brune (1970, 1971):

$$\Delta\sigma = \frac{7}{16}\frac{M_0}{r_0^3} \tag{6.12}$$

The apparent stresses were calculated as:

$$\sigma_a = \frac{\mu E_0}{M_0} \tag{6.13}$$

where $\mu$ is the shear modulus of the medium, $E_0$ is the energy radiated from the source, and $M_0$ is the seismic moment.

Parameters of icequakes recorded in 1995 are shown in the following Sect. 6.2. In Sect. 6.3 we compare parameters determined for measurement series in the years 1995, 1997 and 1999.

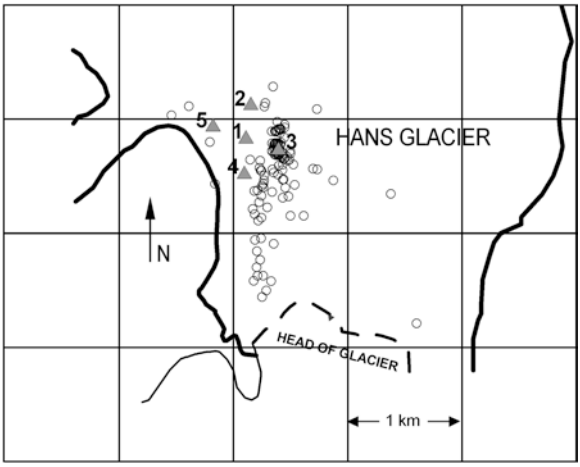


**Fig. 6.1** Measurement arrangement on the Hans Glacier (April 1995). Sites of five seismometers SM-3 are marked with *triangles*, icequakes are indicated by *circles*. The seismometers, placed directly on ice, recorded vertical vibrations

In Fig. 6.1 we show the location of seismometers sites (April 1995) and icequakes, whose parameters are listed in Table 6.1.

Figure 6.2 contains seismograms of two icequakes. Consecutive channels, counting from the top, correspond to seismometer sites 1–5 (see Fig. 6.1). The seismograms are examples of recordings from which we selected P and S

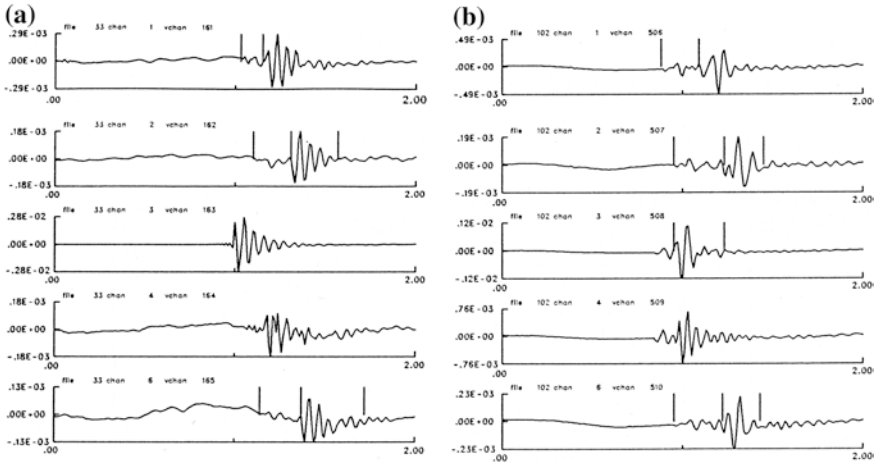


**Fig. 6.2** Velocity seismograms for two icequakes (**a** and **b**); consecutive channels from the top correspond to seismometers sites 1–5 (Fig. 6.1). *Horizontal axis*: time [s]; *vertical axis*: ice velocity [m/s]. *Vertical bars* indicate consecutive sequences of P and S waves selected for spectral analysis. The spectrum corresponding to the selected P wave packet on channel 2 in (**a**) is shown in Fig. 6.3a

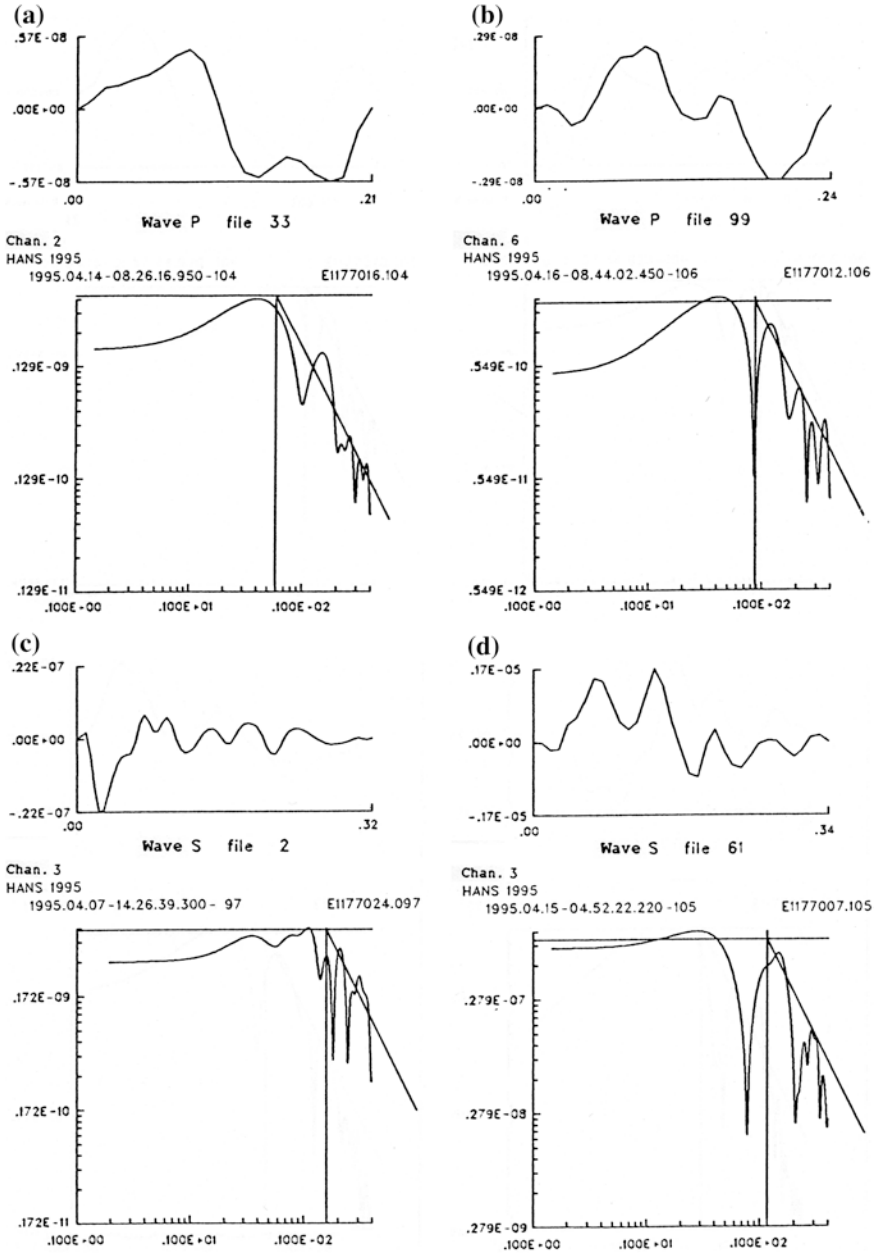


**Fig. 6.3** Examples of displacement spectra for icequakes. Examples **a** and **b** show the P-wave spectra, **c** and **d** the S-wave spectra. In the upper part of each example there is the respective segment of displacement seismogram (*horizontal axis*) time [s]; *vertical axis* ice displacement [m]). Spectra (*horizontal axis* in Hz) are shown in the lower parts. Straight lines: spectral level (*horizontal line*), corner frequency (*vertical line*), and high-frequency asymptote of the spectrum for an impulse in Brune's model (*slant line*)

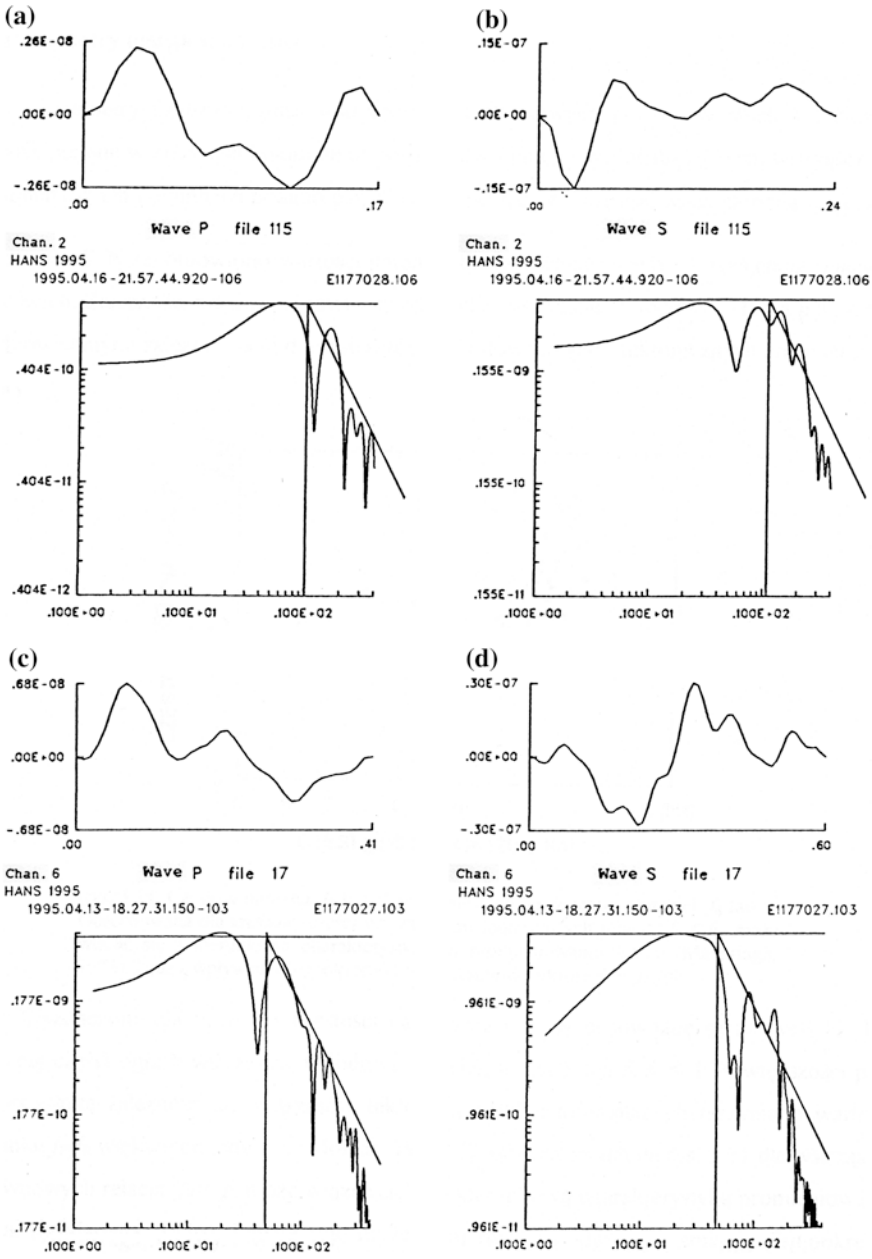


**Fig. 6.4** Examples of displacement spectra for icequakes. Description same as in Fig. 6.3

wave fragments to be further used for spectrum calculation. The selected segments are marked with vertical bars. The spectrum corresponding to the P wave packet,

marked in channel 2 of Fig. 6.2a, is displayed in Fig. 6.3a. For the rest of examples of spectra in Figs. 6.3 and 6.4 we do not show the input seismograms,

In Figs. 6.3 and 6.4 we give examples of records containing velocity seismograms and displacement spectra of icequakes. These are raw recordings; information that is not included in the diagrams has been supplemented in the captions. In the upper part of each diagram we show the respective fragment of the calculated displacement seismogram. The lower parts of the figures display the spectra. The spectral level and corner frequency are marked by the horizontal and vertical lines, respectively. The slant line indicates the high-frequency asymptote of the spectrum for an impulse in Brune's model. In Fig. 6.3 we show examples of spectra of the P wave (a and b) and the S wave (c and d). The spectra shown in Fig. 6.3 are related to different quakes. The spectra of selected P and S wave seismograms for the same recording channel are illustrated by examples for two quakes (Fig. 6.4); parts a and b pertain to the first quake, parts c and d to the other).

The calculated focal parameters are presented in the form of tables and diagrams in the next section.

## 6.2 Parameters of Icequake Foci

On the basis of the assumptions and mathematical procedures outlined above we calculated spectral parameters for icequakes recorded in the period 4–18 April 1995. The manner of recording has been described in Chap. 3. A series of relations for spectral parameters is presented and compared to respective relations for weak tectonic earthquakes, mining tremors and icequakes that have previously been recorded at Hans Glacier and Antarctic shelf glacier.

The physical parameters of icequakes are listed in Table 6.1. The numbering in the first column relates to the consecutive events localized. In the last two columns we give the spectral parameters: the corner frequency calculated for P and S waves. Below we will discuss the values of the parameters and illustrate their mutual relationships in diagrams. The relationships between the focal parameters in the Hans Glacier have been compared with those for icequakes and earthquakes available in the literature.

The P and S-wave corner frequencies, $f_P$ and $f_S$, are compared in Fig. 6.5. For the majority of icequakes in the Hans Glacier we have $f_P/f_S < 1$. In most papers examining this relation for tectonic earthquakes and mining tremors, the obtained values of the ratio $f_P/f_S$ were greater than unity (Molnar et al. 1973). The values $f_P/f_S < 1$ observed for icequakes in the Hans Glacier may be related to a directional characteristic of the source radiation (Madariaga 1976). Some role may be also played by the presence of long-period seismic noise, enhancing the low-frequency part of the spectrum. Since the recorded S-waves are stronger than the P-waves, the effect of long-period microseisms on the P waves will be stronger, which in turn may change the ratio $f_P/f_S$.

The mean values of corner frequencies $f_P$ and $f_S$ are 11.6 Hz and 13.9 Hz, respectively. The corner frequency $f_S$ estimated for icequakes recorded in the Antarctic shelf glacier is not much lower and amounts to 11 Hz (Osten-Woldenburg 1990).

**Table 6.1** Focus parameters of selected icequakes calculated from the P and S wave spectra

| Event No. | Magnitude $M$ | Seismic Moment $M_0$ [$10^8$Nm] | Total Seismic Energy $E_0$ [J] | $P$-Wave Energy $E_P$ [J] | $S$-Wave Energy $E_S$ [J] | Ratio $E_S$ to $E_P$ $E_S/E_P$ | Source Radius $r_0$ [m] | Stress Drop $\Delta\sigma$ [kPa] | Apparent Stress $\sigma_a$ [kPa] | $P$-Wawe Corner Frequency $f_P$ [Hz] | $S$-Wawe Corner Frequency $f_S$ [Hz] |
|---|---|---|---|---|---|---|---|---|---|---|---|
| 1 | −1.0 | 0.35 | 0.45 | 0.01 | 0.43 | 29.2 | 35.9 | 0.334 | 0.036 | 12.2 | 16.1 |
| 2 | −1.1 | 0.34 | 0.18 | 0.03 | 0.15 | 4.9 | 35.5 | 0.329 | 0.015 | 13.7 | 15.7 |
| 4 | −0.6 | 1.31 | 3.59 | 0.34 | 3.25 | 9.4 | 35.9 | 1.242 | 0.077 | 13.1 | 14.4 |
| 5 | −1.4 | 0.09 | 0.07 | 0.00 | 0.06 | 29.2 | 28.8 | 0.174 | 0.020 | 17.6 | 21.2 |
| 6 | −1.1 | 0.27 | 0.20 | 0.03 | 0.16 | 4.8 | 29.5 | 0.461 | 0.021 | 14.3 | 22.1 |
| 7 | −1.0 | 0.34 | 0.47 | 0.02 | 0.45 | 22.4 | 31.9 | 0.452 | 0.039 | 14.5 | 17.2 |
| 8 | −0.3 | 4.63 | 12.10 | 2.44 | 9.65 | 3.9 | 50.9 | 1.539 | 0.073 | 8.9 | 12.3 |
| 9 | 0.2 | 20.86 | 310.26 | 40.26 | 270.00 | 6.7 | 52.6 | 6.262 | 0.418 | 9.3 | 9.4 |
| 10 | −1.3 | 0.14 | 0.03 | 0.00 | 0.02 | 9.6 | 41.1 | 0.086 | 0.005 | 10.1 | 15.8 |
| 11 | −1.2 | 0.15 | 0.06 | 0.01 | 0.05 | 6.4 | 31.1 | 0.216 | 0.011 | 15.0 | 18.7 |
| 12 | −0.8 | 0.89 | 1.10 | 0.12 | 0.98 | 8.1 | 39.2 | 0.643 | 0.035 | 12.1 | 13.4 |
| 13 | −1.2 | 0.18 | 0.07 | 0.01 | 0.06 | 9.3 | 33.9 | 0.198 | 0.011 | 16.1 | 12.5 |
| 14 | −1.1 | 0.21 | 0.12 | 0.02 | 0.10 | 5.9 | 29.6 | 0.352 | 0.016 | 16.8 | 15.5 |
| 16 | −1.3 | 0.13 | 0.02 | 0.01 | 0.01 | 5.2 | 38.0 | 0.100 | 0.004 | 12.1 | 14.1 |
| 17 | −0.7 | 1.03 | 1.50 | 0.16 | 1.34 | 8.5 | 39.1 | 0.752 | 0.041 | 11.8 | 14.2 |
| 18 | −0.6 | 1.35 | 4.98 | 0.27 | 4.71 | 17.3 | 38.4 | 1.046 | 0.104 | 11.6 | 15.6 |
| 19 | −1.0 | 0.34 | 0.31 | 0.03 | 0.28 | 9.8 | 35.7 | 0.324 | 0.026 | 12.4 | 17.9 |
| 20 | −0.9 | 0.59 | 0.32 | 0.06 | 0.26 | 4.7 | 41.8 | 0.354 | 0.015 | 12.3 | 11.2 |
| 23 | −0.1 | 7.96 | 34.65 | 1.48 | 33.18 | 22.4 | 64.7 | 1.283 | 0.122 | 6.7 | 10.6 |
| 24 | −0.8 | 0.60 | 1.13 | 0.12 | 1.01 | 8.4 | 30.8 | 0.891 | 0.053 | 16.2 | 15.1 |
| 26 | −1.1 | 0.24 | 0.07 | 0.01 | 0.07 | 7.3 | 43.1 | 0.133 | 0.009 | 11.0 | 13.9 |
| 27 | −0.2 | 6.19 | 19.77 | 6.11 | 13.66 | 2.2 | 48.1 | 2.438 | 0.090 | 11.0 | 9.6 |
| 33 | −0.8 | 0.75 | 0.30 | 0.05 | 0.24 | 4.4 | 48.6 | 0.287 | 0.011 | 9.4 | 11.0 |
| 38 | −0.1 | 8.84 | 15.80 | 2.28 | 13.52 | 5.9 | 74.3 | 0.943 | 0.050 | 6.0 | 8.4 |

(continued)

**Table 6.1** (continued)

| Event No. | Magnitude $M$ | Seismic Moment $M_0$ [$10^8$Nm] | Total Seismic Energy $E_0$ [J] | $P$-Wave Energy $E_P$ [J] | $S$-Wave Energy $E_S$ [J] | Ratio $E_S$ to $E_P$ $E_S/E_P$ | Source Radius $r_0$ [m] | Stress Drop $\Delta\sigma$ [kPa] | Apparent Stress $\sigma_a$ [kPa] | $P$-Wawe Corner Frequency $f_P$ [Hz] | $S$-Wawe Corner Frequency $f_S$ [Hz] |
|---|---|---|---|---|---|---|---|---|---|---|---|
| 47 | −0.3 | 3.91 | 5.89 | 0.89 | 5.00 | 5.6 | 58.5 | 0.855 | 0.042 | 7.3 | 11.3 |
| 48 | −0.3 | 3.85 | 19.10 | 3.82 | 15.29 | 4.0 | 39.5 | 2.732 | 0.140 | 13.0 | 12.1 |
| 54 | −0.8 | 0.76 | 0.71 | 0.04 | 0.67 | 18.6 | 45.7 | 0.348 | 0.026 | 10.8 | 13.4 |
| 55 | −0.5 | 1.63 | 3.20 | 0.28 | 2.92 | 10.4 | 43.9 | 0.845 | 0.055 | 9.9 | 13.8 |
| 56 | −0.3 | 2.97 | 18.84 | 1.31 | 17.53 | 13.3 | 36.5 | 2.671 | 0.179 | 12.7 | 14.4 |
| 57 | −0.8 | 0.61 | 0.62 | 0.08 | 0.54 | 6.6 | 41.0 | 0.389 | 0.029 | 11.1 | 14.3 |
| 58 | −0.4 | 3.62 | 22.05 | 2.64 | 19.41 | 7.4 | 36.3 | 3.297 | 0.171 | 13.0 | 13.7 |
| 65 | −0.3 | 4.12 | 25.11 | 1.95 | 23.16 | 11.9 | 43.0 | 2.273 | 0.171 | 10.0 | 14.5 |
| 69 | 0.1 | 14.58 | 312.88 | 51.55 | 261.33 | 5.1 | 37.5 | 12.125 | 0.603 | 12.6 | 13.6 |
| 70 | −0.6 | 1.81 | 3.88 | 0.58 | 3.30 | 5.7 | 40.3 | 1.209 | 0.060 | 10.9 | 14.6 |
| 71 | −1.0 | 0.36 | 0.35 | 0.02 | 0.33 | 21.4 | 37.1 | 0.311 | 0.027 | 117 | 17.9 |
| 72 | −0.2 | 4.74 | 18.81 | 2.84 | 15.97 | 5.6 | 45.6 | 2.188 | 0.111 | 10.5 | 12.1 |
| 82 | −0.4 | 3.36 | 43.05 | 1.53 | 41.52 | 27.1 | 31.2 | 4.818 | 0.361 | 14.9 | 15.2 |
| 84 | −0.7 | 1.01 | 1.76 | 0.26 | 1.51 | 5.8 | 35.7 | 0.975 | 0.049 | 13.0 | 14.5 |
| 86 | −1.1 | 0.27 | 0.09 | 0.01 | 0.08 | 7.3 | 41.0 | 0.174 | 0.009 | 11.2 | 14.0 |
| 87 | −0.4 | 2.48 | 4.78 | 0.90 | 3.88 | 4.3 | 45.0 | 1.195 | 0.054 | 10.4 | 11.8 |
| 88 | −0.8 | 0.77 | 2.18 | 0.11 | 2.07 | 18.6 | 32.8 | 0.960 | 0.079 | 13.7 | 18.1 |
| 107 | −0.9 | 0.44 | 1.14 | 0.03 | 1.10 | 31.8 | 32.0 | 0.583 | 0.073 | 13.5 | 19.2 |
| 108 | −0.8 | 0.88 | 0.75 | 0.08 | 0.67 | 8.4 | 43.6 | 0.466 | 0.024 | 9.9 | 14.3 |
| 111 | −0.5 | 1.94 | 6.68 | 0.95 | 5.74 | 6.1 | 34.2 | 2.111 | 0.097 | 13.7 | 14.9 |
| 115 | 0.3 | 35.56 | 346.08 | 45.81 | 300.26 | 6.6 | 67.5 | 5.069 | 0.274 | 6.9 | 7.8 |
| 116 | −0.3 | 3.96 | 13.66 | 2.19 | 11.47 | 5.2 | 42.8 | 2.205 | 0.097 | 11.6 | 11.0 |
| 117 | −0.2 | 5.78 | 32.14 | 1.49 | 30.65 | 20.6 | 53.7 | 1.632 | 0.156 | 8.1 | 10.8 |
| 118 | −0.5 | 1.63 | 8.28 | 0.39 | 7.89 | 20.2 | 34.2 | 1.785 | 0.143 | 14.4 | 13.8 |

(continued)

**Table 6.1** (continued)

| Event No. | Magnitude $M$ | Seismic Moment $M_0$ [$10^8$Nm] | Total Seismic Energy $E_0$ [J] | $P$-Wave Energy $E_P$ [J] | $S$-Wave Energy $E_S$ [J] | Ratio $E_S$ to $E_P$ $E_S/E_P$ | Source Radius $r_0$ [m] | Stress Drop $\Delta\sigma$ [kPa] | Apparent Stress $\sigma_a$ [kPa] | $P$-Wawe Corner Frequency $f_P$ [Hz] | $S$-Wawe Corner Frequency $f_S$ [Hz] |
|---|---|---|---|---|---|---|---|---|---|---|---|
| 120 | −0.8 | 0.75 | 0.61 | 0.03 | 0.58 | 18.7 | 49.4 | 0.273 | 0.023 | 10.0 | 10.0 |
| 123 | −0.5 | 1.72 | 7.85 | 0.33 | 7.52 | 22.9 | 40.1 | 1.170 | 0.128 | 11.7 | 12.8 |
| 126 | −0.2 | 7.02 | 59.40 | 6.99 | 52.41 | 7.5 | 42.9 | 3.889 | 0.238 | 10.6 | 13.1 |
| 129 | 0.3 | 34.84 | 330.52 | 36.35 | 294.17 | 8.1 | 71.1 | 4.240 | 0.267 | 6.1 | 8.5 |
| 133 | −0.6 | 1.29 | 1.60 | 0.17 | 1.43 | 8.2 | 43.3 | 0.692 | 0.035 | 10.0 | 14.0 |
| 134 | −1.0 | 0.44 | 0.23 | 0.03 | 0.20 | 5.9 | 37.7 | 0.358 | 0.015 | 11.6 | 15.3 |
| 136 | −1.0 | 0.44 | 0.33 | 0.02 | 0.31 | 19.5 | 43.2 | 0.240 | 0.021 | 10.1 | 13.5 |
| 142 | −1.1 | 0.23 | 0.14 | 0.02 | 0.12 | 7.7 | 31.0 | 0.334 | 0.017 | 16.3 | 14.5 |
| 144 | −0.9 | 0.63 | 1.03 | 0.03 | 1.00 | 33.5 | 42.3 | 0.367 | 0.046 | 9.5 | 16.6 |
| 155 | 0.0 | 12.90 | 651.11 | 10.81 | 640.30 | 59.2 | 45.2 | 6.122 | 1.419 | 9.3 | 14.2 |

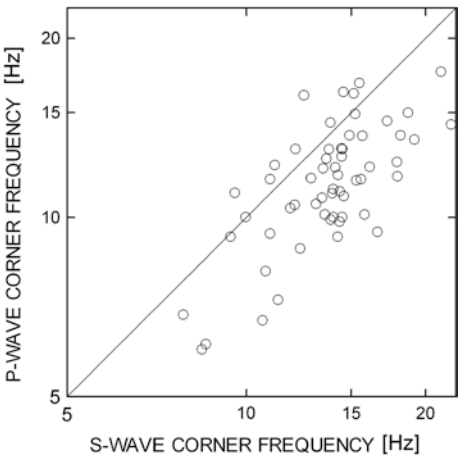


**Fig. 6.5** The P-wave corner frequency $f_P$ versus the S-wave corner frequency $f_S$. The relation $f_P < f_S$, observed for most icequakes, may be associated with directional characteristic of source radiation (Madariaga 1976), or the influence of long-period microseismic noise

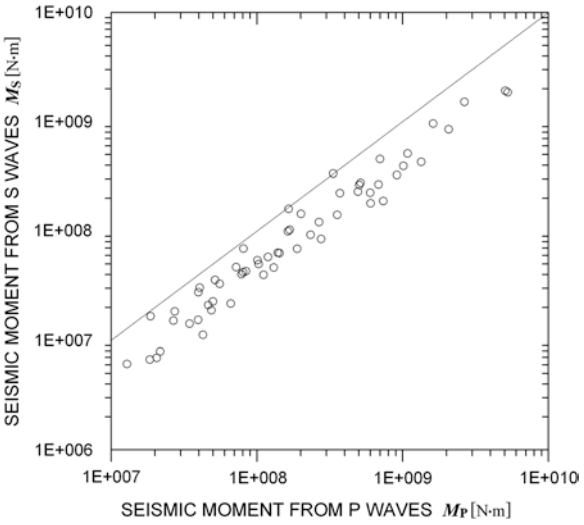


**Fig. 6.6** Comparison of seismic moment $M_S$, calculated on the basis of S-wave spectrum, and seismic moment $M_P$ of the P wave

The seismic moments $M_P$ and $M_S$ calculated on the basis of spectral level $\Omega_0$ (Eq. 6.8) are compared in Fig. 6.6. The moment $M_P$ ranges from $10^7$ to $6 \times 10^9$ N·m, while moment $M_S$ takes somewhat lower values, ranging from $6 \times 10^6$ through $2 \times 10^9$ N·m. The mean moment $M_0$ is in the range from $9 \times 10^6$ to $3.6 \times 10^9$ N·m (Table 6.1).

The knowledge of seismic moment $M_0$ made it possible to determine magnitude $M$, which is directly related to it via Eq. (6.10). The magnitudes calculated for the studied series of icequakes are listed in Table 6.2.

To estimate the magnitudes of the rest of the localized quakes (of unknown seismic moment) we assumed that the magnitude of the $i$-th event is linearly related to the logarithm of the amplitude of maximum ground (in our case ice) velocity $A_i$ and the logarithm of the hypocentral distance $R_i$

**Table 6.2** The magnitudes of the events. $M$ are the magnitudes calculated directly ($M = 2/3 \log M_0 - 6.0$), while $M(A)$ are the magnitudes calculated indirectly on the basis of the formula $M(A) = 1.42 + \log A + 1.34 \log R$

| Event No. | Magnitude $M$ | Magnitude $M(A)$ | Event No. | Magnitude $M$ | Magnitude $M(A)$ | Event No. | Magnitude $M$ | Magnitude $M(A)$ | Event No. | Magnitude $M$ | Magnitude $M(A)$ |
|---|---|---|---|---|---|---|---|---|---|---|---|
| 1 | −1.0 | −1.0 | 40 | – | −1.4 | 79 | – | −1.3 | 118 | −0.5 | −0.2 |
| 2 | −1.1 | −1.1 | 41 | – | −1.3 | 80 | – | −0.6 | 119 | – | −2.1 |
| 3 | – | −1.0 | 42 | – | −1.5 | 81 | – | −1.1 | 120 | −0.8 | −0.7 |
| 4 | −0.6 | −0.5 | 43 | – | −1.6 | 82 | −0.4 | −0.2 | 121 | – | −1.3 |
| 5 | −1.4 | −1.5 | 44 | – | −1.4 | 83 | – | −0.9 | 122 | – | −0.9 |
| 6 | −1.1 | −1.2 | 45 | – | −1.1 | 84 | −0.7 | −0.8 | 123 | −0.5 | −0.5 |
| 7 | −1.0 | −0.9 | 46 | – | −1.5 | 85 | – | −0.4 | 124 | – | −1.6 |
| 8 | −0.3 | −0.4 | 47 | −0.3 | −0.5 | 86 | −1.1 | −1.2 | 125 | – | −1.9 |
| 9 | 0.2 | 0.4 | 48 | −0.3 | −0.2 | 87 | −0.4 | −0.6 | 126 | −0.1 | 0.1 |
| 10 | −1.3 | −1.3 | 49 | – | −1.5 | 88 | −0.8 | −0.8 | 127 | – | −0.8 |
| 11 | −1,2 | −1.1 | 50 | – | −1.1 | 89 | – | −0.9 | 128 | – | −1.2 |
| 12 | −0.8 | −0.9 | 51 | – | −1.7 | 90 | – | −1.3 | 129 | 0.3 | 0.4 |
| 13 | −1.2 | −1.1 | 52 | – | −2.1 | 91 | – | −1.2 | 130 | – | −0.9 |
| 14 | −1.1 | −1.3 | 53 | – | −1.3 | 92 | – | −1.6 | 131 | – | −0.9 |
| 15 | – | −1.0 | 54 | −0.8 | −0.8 | 93 | – | −1.3 | 132 | – | −1.5 |
| 16 | −1.3 | −1.4 | 55 | −0.5 | −0.6 | 94 | – | −1.1 | 133 | −0.6 | −0.9 |
| 17 | −0.7 | −0.8 | 56 | −0.3 | −0.2 | 95 | – | −1.5 | 134 | −1.0 | −1.1 |
| 18 | −0.6 | −0.5 | 57 | −0.8 | −0.9 | 96 | – | −1.2 | 135 | – | −1.4 |
| 19 | −1.0 | −1.0 | 58 | −0.4 | −0.4 | 97 | – | −1.6 | 136 | −1.0 | −1.1 |
| 20 | −0.9 | −1.0 | 59 | – | −0.9 | 98 | – | −1.2 | 137 | – | −1.5 |
| 21 | – | −1.5 | 60 | – | −0.6 | 99 | – | −0.3 | 138 | – | −1.4 |
| 22 | – | −0.8 | 61 | – | −0.6 | 100 | – | −1.5 | 139 | – | −1.3 |
| 23 | −0.1 | −0.2 | 62 | – | −0.4 | 101 | – | −1.4 | 140 | – | −0.9 |
| 24 | −0.8 | −0.9 | 63 | – | −0.7 | 102 | – | −1.0 | 141 | – | −1.9 |
| 25 | – | −1.2 | 64 | – | −1.1 | 103 | – | −1.3 | 142 | −1.1 | −1.0 |

(continued)

**Table 6.2** (continued)

| Event No. | Magnitude $M$ | Magnitude $M(A)$ | Event No. | Magnitude $M$ | Magnitude $M(A)$ | Event No. | Magnitude $M$ | Magnitude $M(A)$ | Event No. | Magnitude $M$ | Magnitude $M(A)$ |
|---|---|---|---|---|---|---|---|---|---|---|---|
| 26 | −1.1 | −1.3 | 65 | −0.3 | −0.2 | 104 | – | −1.3 | 143 | – | −0.6 |
| 27 | −0.2 | −0.2 | 66 | – | −1.0 | 105 | – | −1.2 | 144 | −0.9 | −0.7 |
| 28 | – | −0.9 | 67 | – | −1.4 | 106 | – | −0.4 | 145 | – | −1.3 |
| 29 | – | −1.4 | 68 | – | −1.4 | 107 | −0.9 | −0.8 | 146 | – | −1.9 |
| 30 | – | −1.0 | 69 | 0.1 | 0.3 | 108 | −0.8 | −0.9 | 147 | – | −0.9 |
| 31 | – | −0.5 | 70 | −0.6 | −0.5 | 109 | – | −1.1 | 148 | – | −1.9 |
| 32 | – | −0.3 | 71 | −1.0 | −1.0 | 110 | – | −1.6 | 149 | – | −1.2 |
| 33 | −0.8 | −0.7 | 72 | −0.2 | −0.2 | 111 | −0.5 | −0.4 | 150 | – | −1.0 |
| 34 | – | −1.3 | 73 | – | −1.4 | 112 | – | −1.5 | 151 | – | −1.2 |
| 35 | – | −1.1 | 74 | – | −1.2 | 113 | – | −1.7 | 152 | – | −0.9 |
| 36 | – | −1.4 | 75 | – | −1.7 | 114 | – | −1.0 | 153 | – | −1.6 |
| 37 | – | −1.3 | 76 | – | −0.8 | 115 | 0.3 | 0.3 | 154 | – | −1.0 |
| 38 | −0.1 | −0.2 | 77 | – | −0.8 | 116 | −0.3 | −0.2 | 155 | 0.0 | 0.2 |
| 39 | – | −0.6 | 78 | – | −1.5 | 117 | −0.2 | −0.1 | 156 | – | −1.3 |

$$M\,(A)_{\mathrm{i}} = a_1 + \log A_{\mathrm{i}} + a_2 \log R_{\mathrm{i}} \tag{6.14}$$

The value of coefficients $a_1$ and $a_2$ were determined by solving this equation with the least-squares method for a series of quakes whose seismic moments have been known. The hypocentral distances $R_{\mathrm{i}}$ have been determined earlier, when making the location of foci. The maximum amplitudes $A_{\mathrm{i}}$ were read off in the process of numerical data treatment with program SPAG (Domański 1993). The final result is

$$M\,(A) = 1.42 + \log A + 1.34 \log R \tag{6.15}$$

This relation was used to calculate magnitudes $M(A)$ for all events of known hypocentral distances $R$; the results are in Table 6.2. The calculated magnitudes range from –2.1 to +4.0. Figure 6.7 shows a comparison of magnitudes $M$ and magnitudes $M(A)$ calculated for the same events according to formula (6.15).

Figure 6.8 shows the dependence between the seismic moment and the focus radius. The radii in all diagrams were calculated according to Madariaga's coefficients (Madariaga 1976). The icequakes of the series are marked with triangles. The elipses delineate the regions which contain points corresponding to quake series studied by different authors. The elipses are oriented in accordance with trends in the occurrence of points in measurement series. The rectangle marks the area where we know only the range over which the focus radius and seismic moment vary. The regions are marked with Roman numerals: **I**—quakes recorded in the Antarctic shelf glacier (Osten-Woldenburg 1990); **II**—extremely weak tremors induced in granite rocks in the Underground Research Laboratory in Manitoba, Canada (Gibowicz et al. 1991); **III**—group of various tectonic earthquakes and mining tremors in South African gold mines (Abercrombie and Leary 1993, the ellipse shows only part of events for $M_0 < 10^{13}$ N·m; **IV**—tremors connected

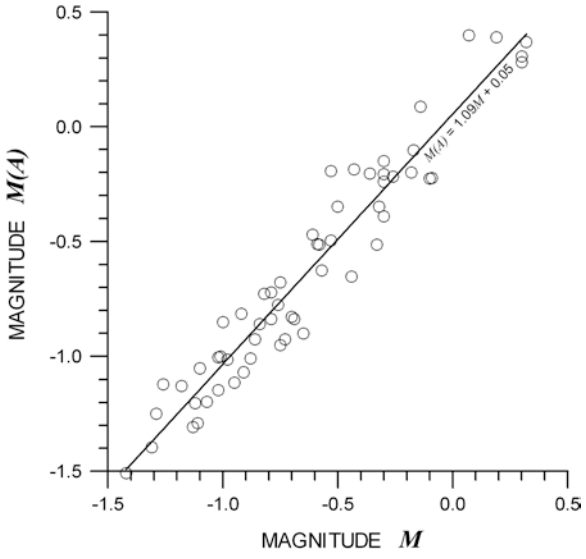


**Fig. 6.7** Comparison of the magnitudes $M$ with magnitudes $M(A)$ calculated for the same events on the basis of Eq. (6.15)

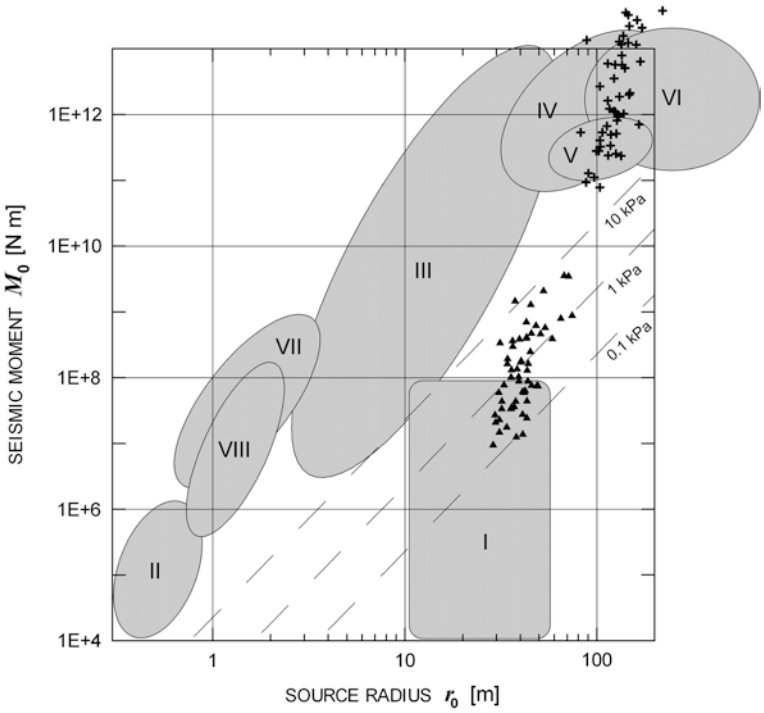


**Fig. 6.8** Dependence between the seismic moment $M_0$ and focus size $r_0$. *Triangles*: tremors recorded on the Hans Glacier. *Crosses*: tectonic earthquakes from the Hornsund fiord region. **I** through **VIII**: areas indicating comparative series of shocks, as described in the text. Labels 0.1; 1; 10 kPa on the lines refer to the values of constant stress drop

with coal mining in Upper Silesia (Gibowicz et al. 1977); **V**—mining tremors in the Ruhr Basin (Gibowicz et al. 1990); **VI**—tremors in the Lubin Copper Basin (Gibowicz 1985), **VII** and **VIII**—mining tremors of negative magnitudes in granite rocks (Urbancic et al. 1992; Urbancic and Young 1993). The crosses mark the series of tectonic earthquakes in the Hornsund fiord (Górski 1997). The lines correspond to constant stress drops (of 0.1, 1, and 10 kPa).

As we see from the figure, the icequake series recorded on the Hans Glacier (triangles) well fits to region **I** (quakes on Antarctic shelf glacier); these regions partially overlap. The range of seismic moments estimated for the Antarctic quakes is by two orders of magnitude lower as compared to that of the Hans Glacier events.

The extremely weak quakes induced in granite rocks in the Underground Research Laboratory (elipse **II**) have, as compared to icequakes (triangles), the sizes of the foci by two orders lower, seismic moments by four orders lower, and stress drops by two orders greater. The foci radii in the Hans Glacier range from 29 to 74 m, the mean radius $r_0$ being 42 m. The icequakes have foci of greater size as compared to those of the regions **III**, **IV** and **V** of the same seismic moment.

Large differences in the foci of icequakes and quakes in other rocks (granite) are observed for small seismic moment values. The sizes of foci of quakes recorded in the Antarctic shelf glacier (region **I**) range from 10 to 60 m, very close to the respective range of $r_0$ values for the Hans Glacier icequakes. Major part of region **I** lies below the $\Delta\sigma = 0.1$ kPa line, so we can expect the stress drops for icequakes in the Antarctic shelf glacier to be very small. In extreme cases, the value of $\Delta\sigma$ might for these icequakes be by three orders of magnitude lower than the mean stress drops in the Hans Glacier.

The plot of stress drops versus seismic moments is shown in Fig. 6.9. In addition to the series of icequakes (triangles), the diagram shows the group of extremely weak quakes induced in granite rocks (elipse **II**), in hard coal mines in Upper Silesia (rectangle **IV**) and Ruhr Basin (rectangle **V**). The crosses mark tectonic earthquakes in the Hornsund fiord. The broken straight lines correspond to the constant focus radii $r_0$ of 1, 10 and 100 m.

For the icequake series, the relationship between the stress drop and seismic moment is clearly visible (line ***a***) and runs in the vicinity of $r_0 = 40$ m. The stress drop $\Delta\sigma$ for events recorded in the ice is markedly small, its absolute value being by two orders of magnitude smaller than the stress drops induced in the granite

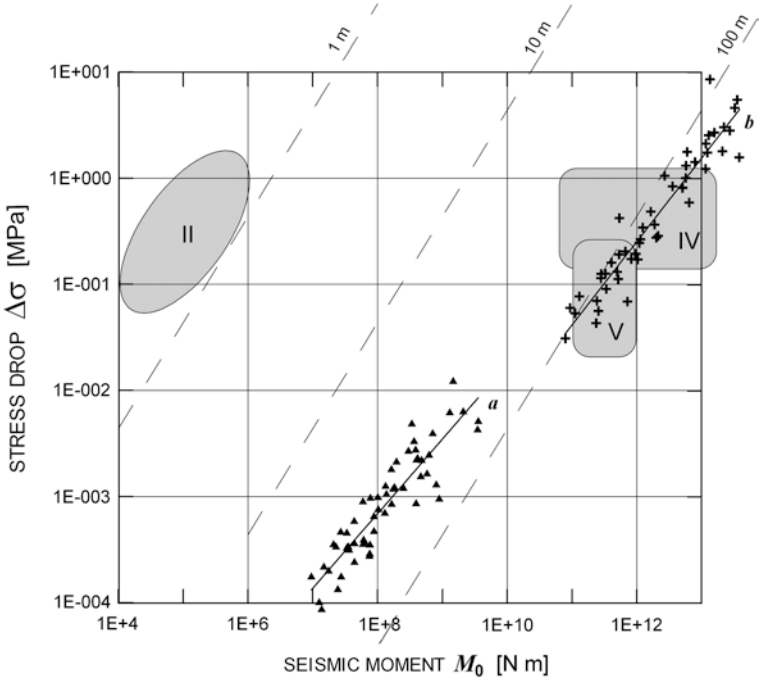


**Fig. 6.9** Stress drop $\Delta\sigma$ versus seismic moment $M_0$. *Triangles* tremors recorded on the Hans Glacier. *Crosses* tectonic quakes from the Hornsund region; ***a*** and ***b***: lines resulting from the least-square fit. **II**, **IV** and **V**: regions indicating comparative quake series, as described in the text. The *broken lines* correspond to the constant focus radii ($r_0$ of 1, 10 and 100 m)

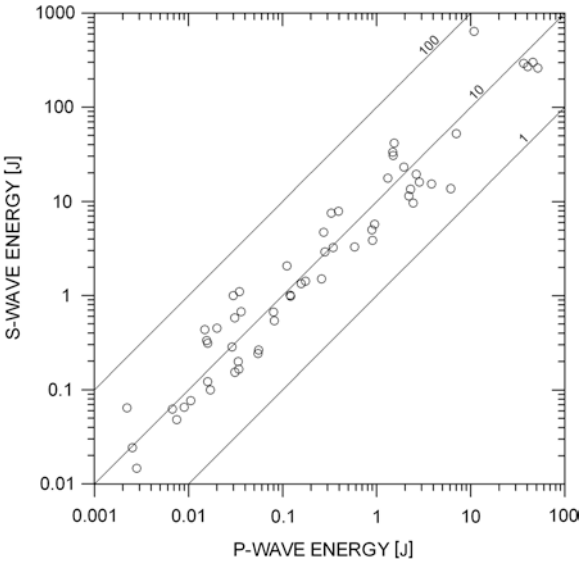


**Fig. 6.10** Comparison of seismic energy $E_S$ emitted from the source in the form of the S wave with the seismic energy $E_P$ of the P wave

(region **II**) and related to hard coal mining (**IV** and **V**). The slope of line *a* approximating the relationship between $\Delta\sigma$ and $M_0$ is 0.7 (according to the straight line equation $\log \Delta\sigma = 0.7 \log M_0 - 20.2$).

The seismic energy emitted from the source was determined from Eq. (6.9). The values are listed in Table 6.1. The values of energy $E_P$ emitted as P waves range in the interval 0.005 J < $E_P$ < 50 J; for the S wave the energy $E_S$ ranges from 0.01 to 300 J (Fig. 6.10). The total energy $E_0 = E_P + E_S$ ranges from 0.03 to 346 J. The ratio of $E_S$ to $E_P$ ranges from 2 to 60, for 60 % of cases being less than 10. The total seismic energies $E_0$ emitted from the source are comparable to $E_0$ values for extremely weak tremors induced in granite rocks in the Underground Research Laboratory in Manitoba, Canada (Gibowicz et al. 1991). Also the values of $E_S/E_P$ do not substantially differ either from the values calculated in the Underground Research Laboratory or from those in hard coal mines (Gibowicz et al. 1990).

The plot of the total seismic energy as a function of seismic moment for the icequakes (marked with triangles) is shown in Fig. 6.11. The regions labelled with Roman numerals **II**, **IV**, **V**, **VI**, **VIII** correspond to series of events studied by different authors and are included here for comparison. Region **IX** relates to the icequake series recorded on the Hans Glacier by Cichowicz (1983). This region exactly coincides with part of the region containing the events recorded by the author (for small energy and seismic moment values). The ranges of energies $E_0$ and seismic moments $M_0$ for the quakes recorded by Cichowicz in the summer season are, respectively, by two and one order of magnitude lower than those for icequake series recorded in April 1995 by the author. Comparing the icequakes with quakes induced in granite (region **II**) we see that, while the seismic moments of these two series differ substantially, their total energies are in the same range. Mining tremors (**IV**, **V** and **VI**) and the group of

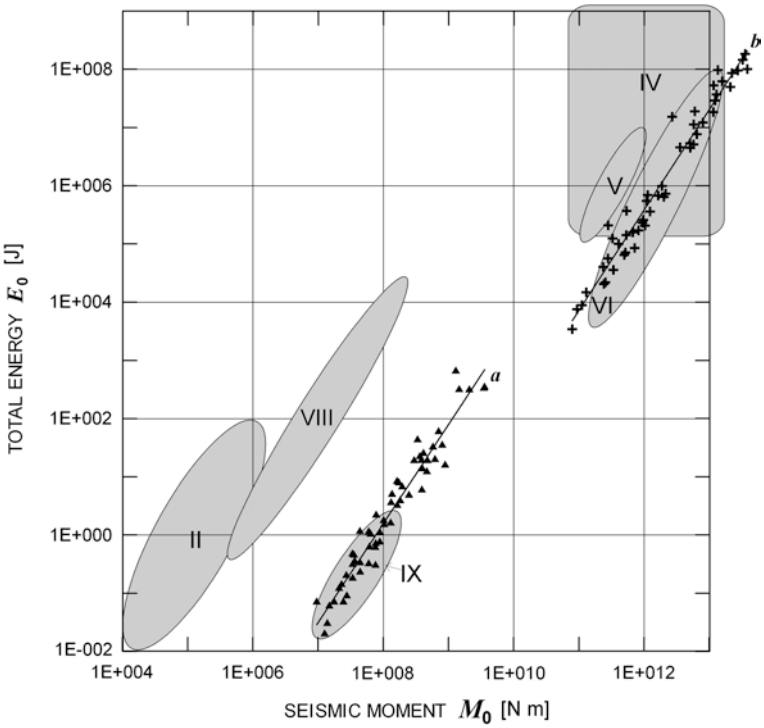


**Fig. 6.11** The total energy $E_0$ versus seismic moment $M_0$. *Triangles*: icequakes recorded on the Hans Glacier. *Crosses*: tectonic quakes from the Hornsund fiord region, ***a*** and ***b***: lines resulting from the least-square fit. **II**, **IV**, **V**, **VI** and **VIII**: regions showing comparative tremor series, as described in the text. **IX**: the series recorded on the Hans Glacier by Cichowicz (1983)

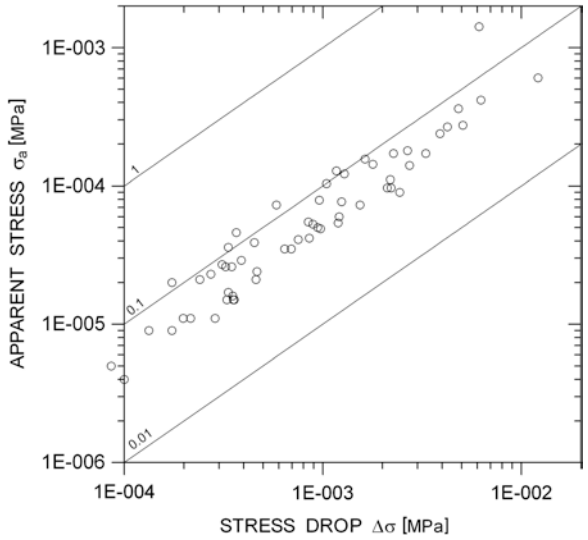


**Fig. 6.12** Apparent stresses $\sigma_a$ versus stress drops $\Delta\sigma$. The *straight lines* represent the ratio $\sigma_a/\Delta\sigma$

earthquakes from the region of Hornsund (crosses, line ***b***) occupy the area at the extension of line ***a*** representing the icequakes. The slope of the straight line ***a*** is 1.7 (according to the equation $\log E_0 = 1.7 \log M_0 - 13.42$).

The relationship between apparent stresses (Table 6.1) and stress drops is shown in Fig. 6.12. The straight lines in the diagram represent the ratio of these quantities. We can estimate the stress drop to be, on the average, 10–20 times greater than the apparent stresses. Both quantities are very small. The apparent stresses range from $4 \times 10^{-3}$ to 1 kPa.

## 6.3 Source Parameters of Spring and Summer Icequake Series

For further analysis, the events recorded in 1999 were divided into two groups: spring series from 14 April through 14 June, and summer series from 15 June through 3 July. In what follows, we considered two spring series and two summer series. In Figs. 6.13, 6.14, 6.15, 6.16 and 6.17 the events are marked as follows:

1995, from 4 through 18 April—red
1997, from 19 through 27 June—green

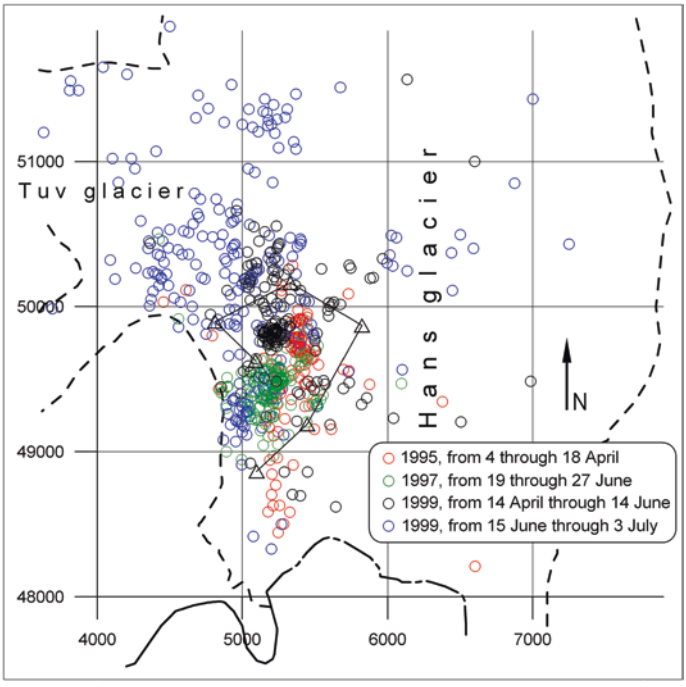


**Fig. 6.13** Location of icequake epicentres of four series at the Hans Glacier (*circles*) and seismometer sites –1999 measurements (*triangles*). The glacier's margin is marked by a *broken line*. The earthquake epicentres of individual series are indicated as follows: from 4 through 18 April 1995 in *red*, from 19 through 27 June 1997 in *green*, from 14 April through 14 June 1999 in *black*, and from 15 June through 3 July 1999 in *blue*

1999, from 14 April through 14 June—black
1999, from 15 June through 3 July—blue

Figure 6.13 shows the icequake epicentre location of four series on Hans Glacier (circles) and location of seismometers (triangles).

Figure 6.14 shows, in a logarithmic scale, seismic moment as a function of source radius: lines of constant stress drop are marked. For comparison, we also marked in this

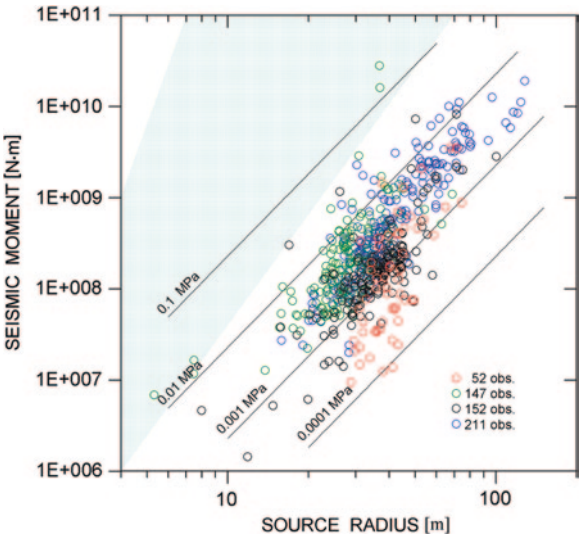


**Fig. 6.14** Seismic moment versus source radius. The coloring marks icequake series recorded in the Hans Glacier. The *lines* labeled 0.0001, 0.001 and 0.1 MPa represent the respective constant stress drops. The *blue-coloured* area represents the location of groups of various earthquakes and mining tremors in South Africa gold mines

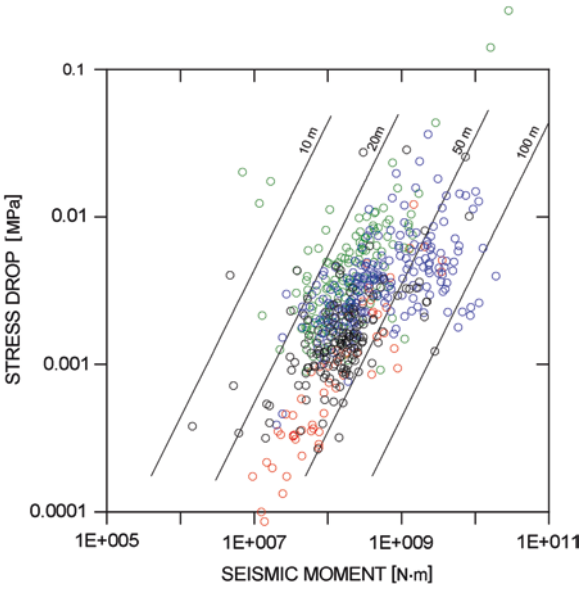


**Fig. 6.15** Stress drop versus seismic moment. The colouring marks icequake series recorded in the Hans Glacier. The *straight lines* correspond to the source radius values: 10, 20, 50 and 100 m

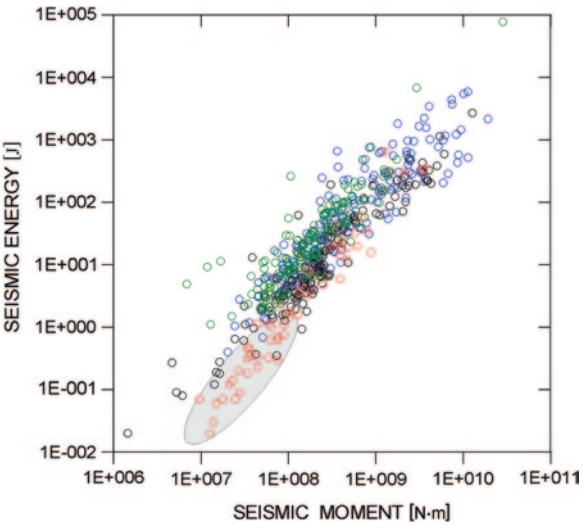


**Fig. 6.16** Seismic energy versus seismic moment. The colouring marks icequake series recorded in the Hans Glacier. The area delineated by an ellipse relates to the icequake series recorded on the Hans Glacier by Cichowicz (1983)

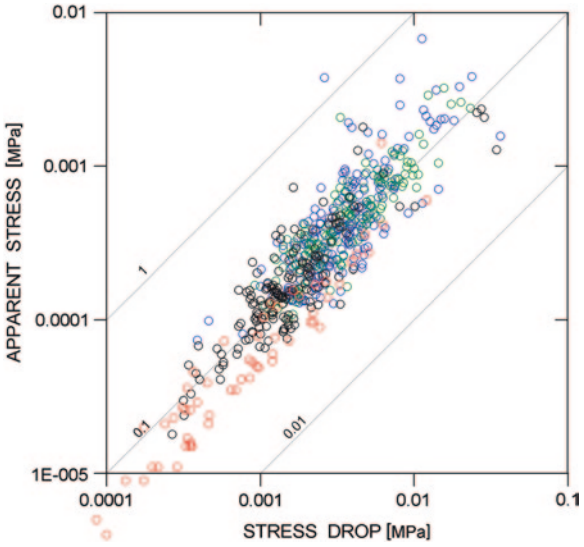


**Fig. 6.17** Apparent stress versus stress drop. The coloring marks icequakes series recorded on the Hans Glacier. The *straight lines* mark the ratios apparent stress/stress drop amounting to 1, 0.1 and 0.01

figure, as a light-blue color area, the area corresponding to the groups of various earthquakes and mining tremors in South Africa gold mines (Abercrombie and Leary 1993). We observe that summer series of icequakes (green and blue circles) are slightly displaced to the left relative to the spring series (red and black). Hence, the summer and spring foci of events of the same seismic moment will have different radii; the spring focus will be somewhat greater. This is most probably due to seasonal changes in physical properties of ice or focus structure.

In Fig. 6.15 we observe a relationship between stress drop and seismic moment for earthquake series recorded in 1995, 1997 and in the spring of 1999; in spite of large scattering, the relationship is distinct. For the 1999 summer series (blue) the

scatter is particularly large; this may be associated with location of earthquakes of large-size foci in another part of the glacier (Fig. 6.13).

The plot of seismic energy in relation to seismic moment for icequake series is shown in Fig. 6.16. The area marked by an ellipse relates to icequake series recorded on the Hans Glacier by Cichowicz (1983). For all four series, a least-squares linear regression was calculated and the straight lines are plotted. The slope coefficient for the three series recorded in 1997 and 1999 (both spring and summer) is 1.3, while that for 1995 series is 1.7. We observed certain displacement of summer series towards lower values of seismic moment as compared to spring series.

Figure 6.17 presents the plot of apparent stress versus stress drop. All four series are located in the vicinity of the line representing the situation in which the apparent stress is ten times less than the stress drop. A similar distribution has been observed in the case of seismic events recorded in South African gold mines (Gibowicz 2002). Some deviation toward lower values of the ratio of apparent stress over stress drop is only displayed by a series recorded in 1995.

Summarizing the above considerations we can state that the glacier's seismic activity related to the release of stress accumulated in ice (icequakes) is the greatest in the marginal zone of the glacier, in the area of large velocity gradient. This zone is active both in spring, when the glacier starts, as well as in the summer. In this area the icequakes occur in the vicinity of the glacier's bottom as well as around its surface. In the second half of the year, the icequake-type events appear also in the main stream of the glacier, and their source radii and seismic moments are much greater than in the first half-year. Local seismically active zones are irregularities in the glacier basement. A comparison of the seismic moment–focal radius and seismic moment–seismic energy relationships for spring and summer seasons point to seasonal changes of physical parameters of ice or focus structure.

## 6.4 Source Parameters of Artificial Icequakes

In June 1997 an experiment was made aiming at the determination of seismic wave velocity in ice (studied in the Hans Glacier region), as described in Chap. 4. The measurement was made in the area which has been a site of icequake observations since 1962. Three artificial earthquakes were generated, for which, in addition to the seismic wave velocities, the following parameters were calculated: seismic moment, focus radius, seismic energy, stress drop and apparent stress.

In the measurements the use was made of the seismometer network deployed for icequake recording in June 19–27, 1997. Artificial quakes were generated in the central part of the region covered by the recording, in a narrowing crack perpendicular to the glacier's axis (see Chap. 5). An additional seismometer to record the moment the earthquake was generated was located at the crack's edge the glacier's surface.

The parameters of the three quakes generated were determined by the same method as for natural quakes, assuming Brune's model. A comparison of parameters of artificial and natural icequakes is shown in consecutive figures.

On the figures, the artificial icequakes are marked by crosses. Dots represent the icequakes. The recordings were made in the years 1995, 1997, and 1999. In Fig. 6.18 the broken line delineates the region containing the records from the Atlantic shelf glacier (Osten-Woldenburg 1990). The grey-color rectangle on the left-hand side of the diagram corresponds to the group of tremors in the South African gold mines (Abercrombie and Leary 1993). The slant lines correspond to constant values of the stress drop. It can be seen that the values of seismic moment and focus radius are lower than the respective values corresponding to the main part of the region occupied by icequakes. The source radius values correspond to mean values for quakes recorded in the Antarctic shelf glacier (Osten-Woldenburg 1990).

Comparing the location of crosses representing artificial earthquakes in the plots of Figs. 6.18, 6.19, and 6.20 one can see that in all the cases analysed it is shifted from the cluster of points representing icequakes towards the regions corresponding to quakes originating in the granite rock material. This effect is most

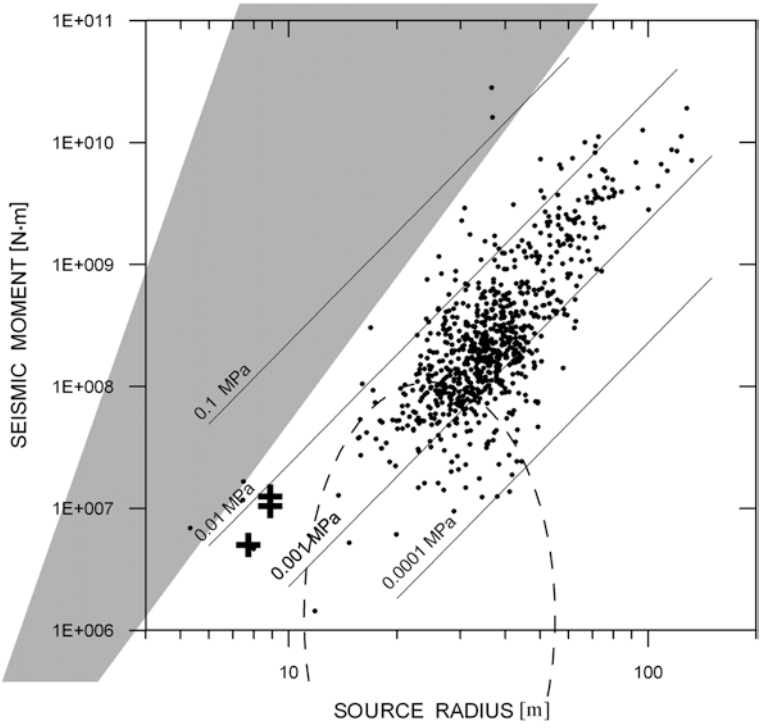


**Fig. 6.18** Dependence between the seismic moment and source radius. *Points*: icequakes recorded on the Hans Glacier in the years 1995, 1997 and 1999. *Crosses*: artificial icequakes. The *grey-color* area corresponds to a group of tremors in South African gold mines (Abercrombie and Leary 1993). The area marked by the ellipse refers to quakes recorded in the Antarctic shelf glacier (Osten-Woldenburg 1990). Labels 0.0001–0.1 MPa on the lines refer to the values of constant stress drop

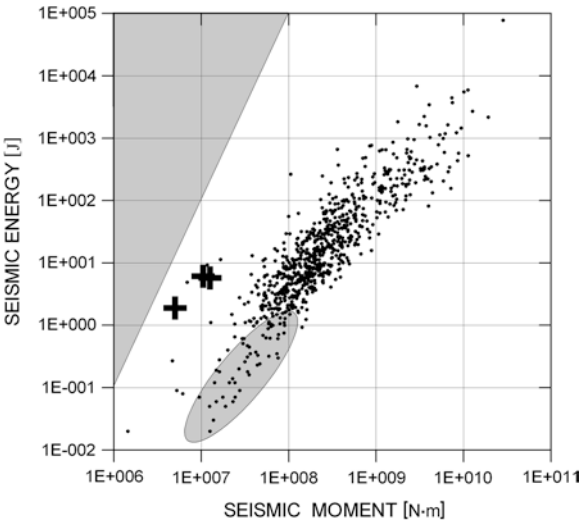


**Fig. 6.19** The seismic energy versus seismic moment. *Points*: icequakes recorded on the Hans Glacier. *Crosses*: artificial quakes. The *grey-color* ellipse marks the series recorded on the Hans Glacier by Cichowicz (1983). The *grey-color triangle* in the *upper left corner* refers to extremely weak tremors induced in granite rocks in the Underground Research Laboratory in Manitoba, Canada (Gibowicz et al. 1991) and mining tremors in granite rocks (Urbancic et al. 1992; Urbancic and Young 1993)

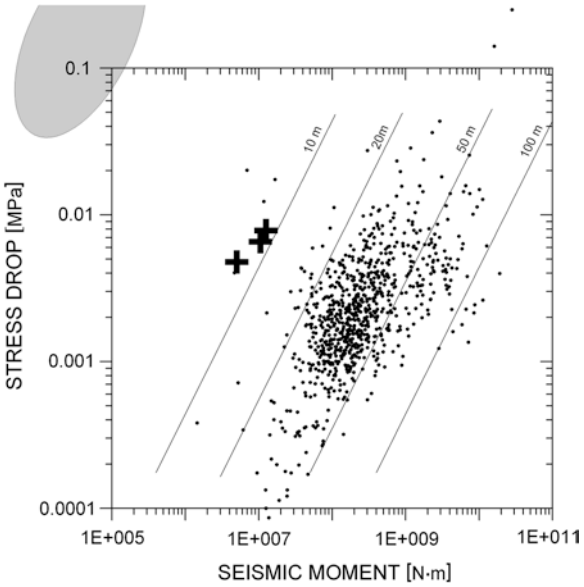


**Fig. 6.20** Stress drop $\Delta\sigma$ versus seismic moment $M_0$. *Points*: icequakes recorded on the Hans Glacier. The *lines* correspond to the constant focus radii $r_0$ of 10, 20, 50 and 100 m. The *ellipse* refers to the extremely weak tremors induced in granite rocks in the Underground Research Laboratory in Manitoba, Canada (Gibowicz et al. 1991)

probably associated with differences in real models of foci of the two types of quakes. The models differ to some extent from the Brune's model adopted in the computations.

The plot of apparent stress in relation to the stress drop for artificial quakes on the Hans Glacier is shown in Fig. 6.21.

The location of the site at which artificial quakes were generated was selected to be placed in the region of strong seismic activity of the glacier (Fig. 6.22). In the chosen area there is a considerable gradient of ice flow velocity on a profile

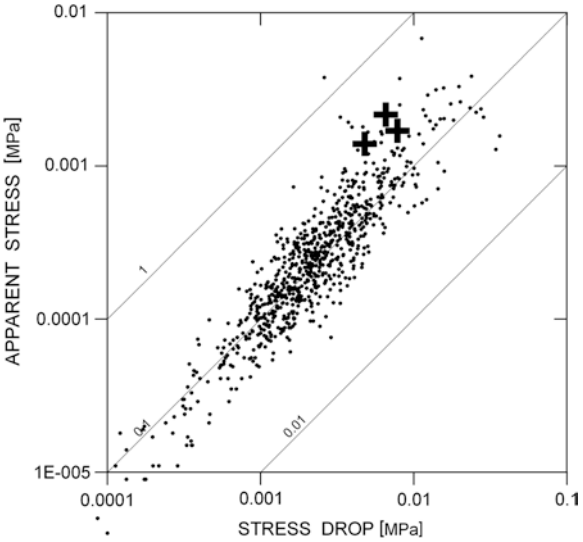


**Fig. 6.21** Apparent stresses versus stress drops. *Points*: icequakes recorded on the Hans Glacier. *Crosses*: artificial quakes. The *straight lines* represent the ratio of apparent stresses to the stress drops

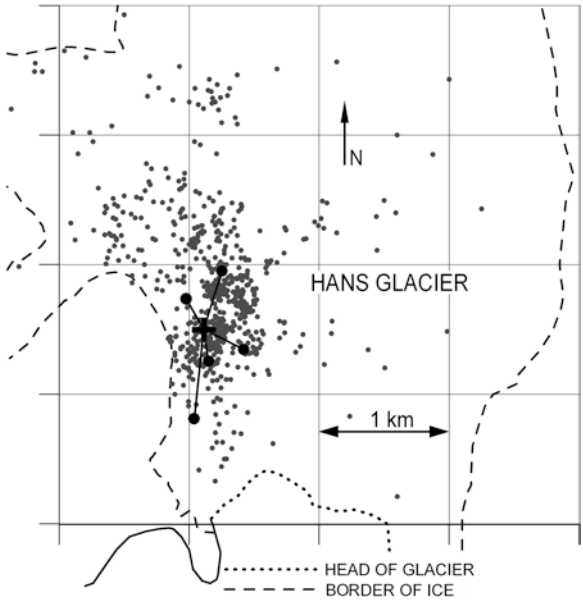


**Fig. 6.22** Artificial icequakes at the Hans Glacier. *Cross*: location of the artificial icequakes generated in June 1997. *Black circles*: location of seismometers which recorded the artificial quakes. *Grey dots*: natural icequakes recorded in the measurement seasons 1995, 1997, and 1999

across the ice flow direction (Fig. 3.7). In this region we also observe numerous discontinuities in the ice displacement, as seen in the photo in Fig. 3.2. The discontinuities are directed along as well as across the main flow. Most probably, the discontinuities, at the time they have originated or later on, when the accumulated stresses have been released, are the source of icequakes.

## References

Abercrombie R, Leary P (1993) Source parameters of small earthquakes recorded at 2.5 km depth, Cajon Pass, Southern California: Implication for earthquake scaling. Geophys Res Lett 20:1511–1514

Aki K, Richards PG (1980) Quantitative seismology. Freeman, San Francisco

Andrews DJ (1986) Objective determination of source parameters and similarity of earthquakes of different size. In: Das S, Boatwright J, Scholz CH (eds) 6. American Geophysics Union, Washington, D.C., pp 259–267

Boatwright J, Fletcher JB (1984) The partition of radiated energy between P and S waves. Bull Seism Soc Am 74:361–376

Boore DM, Boatwright J (1984) Average body-wave radiation coefficients. Bull Seism Soc Am 74:1615–1621

Brune JN (1970) Tectonic stress and spectra of seismic shear waves from earthquake. J Geophys Res 75:4997–5009

Brune NJ (1971) Correction. J Geophys Res 76:5002

Cichowicz A (1983) Icequakes and glacier motion: the Hans Glacier, Spitsbergen, Pure Appl Geophys 121, 27–36

Domański B (1993) Programs SPAG, LOCAL, department of seismology, Institute of geophysics, Polish Academy of Sciences

Gibowicz SJ (1985) Seismic moment and seismic energy of mining tremors in the Lubin Copper Basin in Poland. Acta Geophys Pol 33:243–257

Gibowicz SJ (2002) Apparent stress and stress drop from seismic events induced by mining. Acta Geophys Pol 50:35–49

Gibowicz SJ, Cichowicz A, Dybel T (1977) Seismic moment and source size of mining tremors in Upper Silesia, Poland. Acta Geophys Pol 25:201–218

Gibowicz SJ, Harjes H-P, Schafer M (1990) Source parameters of seismic events at Heinrich Robert Mine, Ruhr Basin, Federal Republic of Germany: Evidence of nondouble-couple events. Bull Seism Soc Am 80:88–109

Gibowicz SJ, Young RP, Talebi S, Rawlence DJ (1991) Source parameters of seismic events at the Underground Research Laboratory in Manitoba, Canada: scaling relations for the events with moment magnitude smaller than -2. Bull Seism Soc Am 81:1157–1182

Gibowicz SJ, Kijko A (1994) An introduction to mining seismology. Academic Press, San Diego

Górski M (1997) Seismicity of the Hornsund region, Spitsbergen: Icequakes and Earthquakes. Publs Inst Geophys Pol Acad Sc B-20(308):1–76

Hanks TC, Kanamori H (1979) A moment magnitude scale. J Geophys Res 84:2348–2350

Madariaga R (1976) Dynamics of an expanding circular fault. Bull Seism Soc Am 66:639–666

Molnar P, Tucker BE, Brune JN (1973) Corner frequencies of P and S waves and models of earthquakes sources. Bull Seism Soc Am 63:2091–2104 (Cytowane chyba jako tylko Molnar)

Osten-Woldenburg H (1990) Icequakes on Ekstrom ice shelf near Atka bay, Antarctica. J Glaciol 36:31–36

Rendleman CA, Levin FK (1990) Seismic exploration on a floating ice sheet. Geophysics 55:402–409

Snoke JA (1987) Stable determination of (Brune) stress drops. Bull Seism Soc Am 77:530–538

Urbancic TI, Young RP (1993) Space-time variations in source parameters of mining-induced seismic events with $M < 0$. Bull Seism Soc Am 83:378–397

Urbancic TI, Feignier B, Young RP (1992) Influence of source region properties on scaling relations for $M < 0$ events. Pure Appl Geophys 139:721–739

# Chapter 7
# Predominant Frequencies in Spectra of Icevibration Events

## 7.1 Introduction

We present here a comparison of selected seismic events of icevibration type recorded at the Hans Glacier in Spitsbergen, Pasterze Glacier in the Alps (see also Górski 2004), and Huron Glacier in Antarctic Peninsula. The glaciers differ considerably as to their location and climatic conditions.

The study of seismic events in the Hans Glacier was begun in 1962 (Lewandowska and Teisseyre 1964). When the HSP station was put into operation in the late 1970s, seismic measurements have been carried out in a continuous manner (see Chaps. 2 and 3). The network of seismometers has been upgraded every few years; it consisted of 4–8 sites with short-period seismometers. The vertical component of vibrations was recorded at all the sites. Three components were recorded at 1–2 sites. The site with a broad-band seismometer was deployed in 2007 (in the framework of cooperation with NORSAR). Also seasonal measurement campaigns have been organized, in which seismometers were placed at the glacier's surface. The icevibrations in the Hans Glacier analyzed here were recorded in August 2002 by both the stationary seismometers and the seismometers placed directly on ice (see Chap. 3).

The recording on Pasterze Glacier was part of a broad project of the study of rotation waves. The recording was made from September 30 through October 2, 2003.

The recording of icevibrations on Huron Glacier were made in January 1991. The recording was carried out on the occasion of deep seismic sounding expedition in the Antarctic region, which was part of the large deep seismic sounding project in Polar regions, carried out by the Institute of Geophysics, Polish Academy of Sciences.

It is to be noted that the above-mentioned large-scale deep seismic sounding project in Polar regions was begun in 1976 in Spitsbergen, and continued in the same region in 1978 and 1985. For more details and the description of results the reader is referred, e.g., to the publications by Czuba et al. (1999) or Sellevoll et al. (1991). Deep seismic sounding in this region has been carried out in later years

M. Górski, *Seismic Events in Glaciers*, GeoPlanet: Earth and Planetary Sciences,
DOI: 10.1007/978-3-642-31851-1_7, © Springer-Verlag Berlin Heidelberg 2014

and are planned for the future. The latest results and an overview on the seismicity of the passive Svalbard continental margin following from the 1985–2008 projects have been published by Czuba (2013). The other region in which the deep seismic soundings were performed was the Antarctic peninsula. The measurements were made in 1979/80, 1984/85, 1987/88, 1991, and are continued to the present. For more details and the description of results, the reader is referred to, e.g., Grad et al. (1997), Guterch et. al. (1998), Środa (2001), Majdański et al. (2008), Yegorova et al. (2011). In some seasons, the deep seismic soundings were accompanied by temporary recording of local seismicity. These were made by short-period seismometers (SM3; T = 1.5 s) and pen recorders of PORTACORDER type. The seismometers, often located nearby the local glaciers, have been recording the glacier events as well. The data thus produced are used in the present study.

## 7.2 Icevibrations Observed in the Studied Glaciers

A typical example of a icevibration-type seismic event recorded at the Hans Glacier by a network of HSP station seismometers in the summer season of 1985 is reproduced in Fig. 7.1. This event was already discussed by Górski and Teisseyre (1991) and later by Górski (1997).

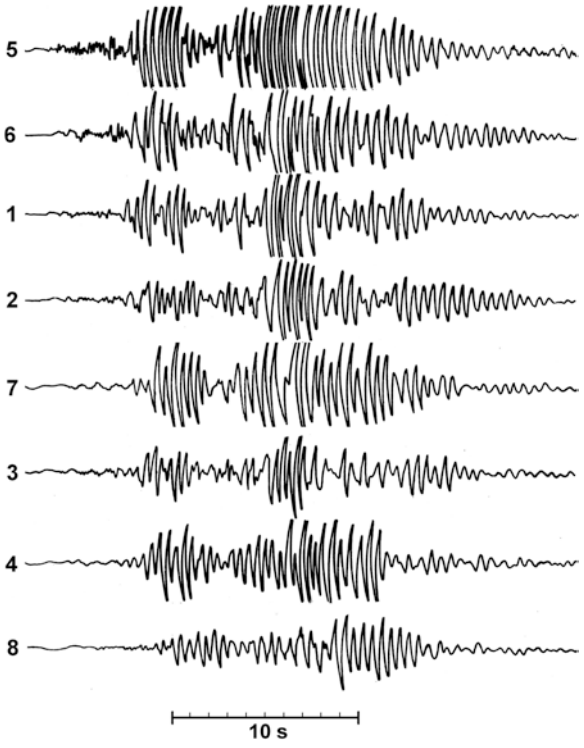


**Fig. 7.1** Seismograms of waves generated in Hans Glacier recorded on eight seismometer sites of the Polish Polar Station Hornsund in the summer season of 1985 (the channel numbers correspond to seismometer sites of Fig. 7.2)

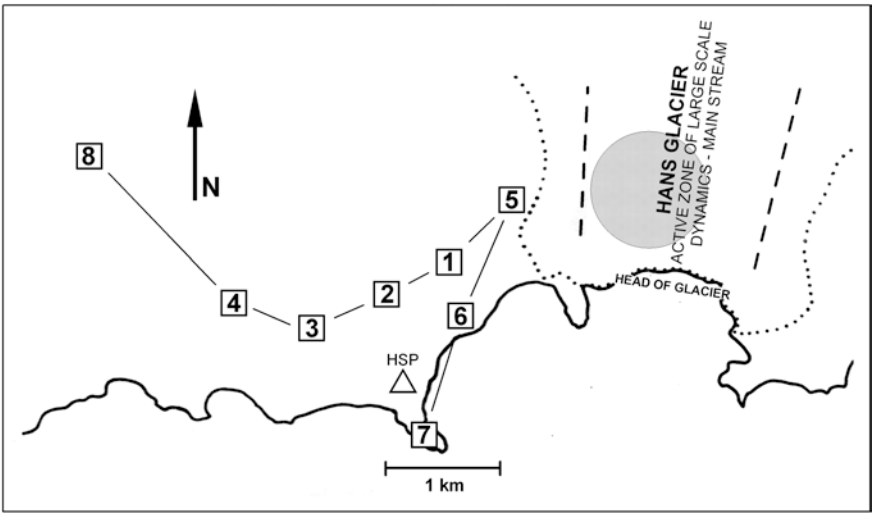


**Fig. 7.2** Location of seismometers sites (*squares*) and main stream of Hans Glacier (*dashed line*). The *gray circle* indicates the source region of icevibrations. The *dotted line* shows the boundary of ice. *Triangle* stands for the Polish Station Hornsund

The presented seismograms come from HSP seismometer network; we show only vertical components recorded at eight sites. The location of the sites is shown in Fig. 7.2.

The magnifications and characteristics of the system are the same at all the channels. The maximally active region of the glacier is related to the main stream (see Chap. 3) and is marked by the dashed line. The icevibration-generating area of the glacier is relatively large (the gray circle). The characteristic sequence of waves, with a period of about 0.5 s, lasts for some 20 s, regardless of the site. Meaningful differences can be observed mainly in the amplitudes recorded at individual sites. The seismograms shown in Fig. 7.1 are arranged according to the distance of the site from the suspected location of the source. The distance of the farthest site is about 5 km, that of the closest being 1–2 km. A decrease in the amplitude of vibrations recorded at consecutive sites is not directly dependent on distance.

The waves travel in the surface layer, whose structure (permafrost, sea bottom), and consequently the attenuation, varies from site to site. Worth noticing is the sequence of vibrations of relatively high frequency recorded in the first phase (at the beginning of the seismogram) at sites 5, 6 and 1. These vibrations were generated in the stress release process in the period preceding the large-scale dynamic processes within the glacier, and are recorded for strong icevibrations by seismometers localized nearby the generated event.

An example of analog recording in the site situated directly on the glacier is shown in Fig. 7.3.

The parameters and frequency characteristics of the measuring arrangement (vertical seismometer SM-3 and pen recorder PORTACORDER) were similar to those of the HSP station. The recording was made in the summer of 1992. In Fig. 7.3a we see a series of near icequakes (examples labelled by letter A) and two records of glacier vibrations: the first lasting for over a minute (labelled B) and the other lasting about 17 s (labelled C). The vibrations B were most probably generated by a dynamic process, tens of seconds in duration, e.g., the glacier displacement; vibrations C may be attributed to a similar process, but shorter in duration. Similar in character are vibrations D of Fig. 7.3b and a series of events E of Fig. 7.3c. The event labelled F (Fig. 7.3b) has a characteristic, nearly constant period of vibrations, most probably due to resonance of a fragment of the glacier. Icequakes A are related to the stress release.

Examples of vibration events recorded on the Huron Glacier, Livingston Island, Antarctic Peninsula on January 15, 1991 are shown in Fig. 7.4 (vertical seismometer SM-3 and pen recorder PORTACORDER). The recording was made by instruments placed at the Half Moon isle, at a distance of 5 km from the glacier's head.

An example of seismogram (vertical component) recorded at the Pasterze Glacier in the Alps is shown in Fig. 7.5.

The Pasterze Glacier photo during the research in 2003 is presented in Fig. 7.6. The next photos, Fig. 7.7, show the view of the glacier three years later (in 2006, left panel) and six years later (in 2009, right panel). The areas of large-scale

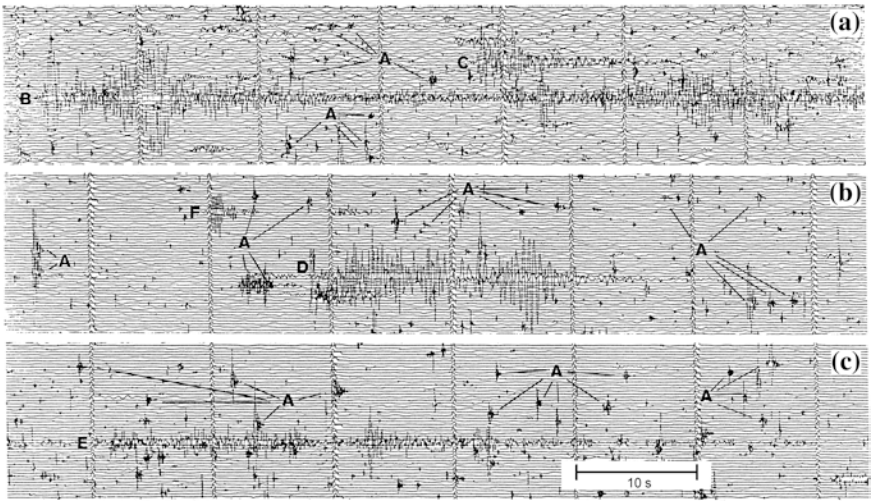


**Fig. 7.3** Examples of seismic events recorded in the Hans Glacier in the period of maximum seismic activity (July 1992). A: icequakes; B, C, D, E, F: seismic events associated with large-scale dynamic processes in the glacier (the observed monochromaticity of the events may indicate their resonant nature). The recordings were made by a seismometer placed directly on the glacier (vertical seismometer SM-3, T = 1.5 s, pen recorder PORTACORDER, velocity recording)

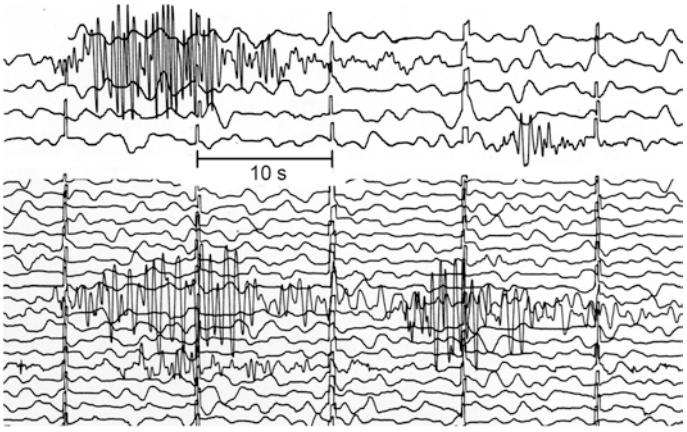


**Fig. 7.4** Icevibration events recorded on the Huron Glacier, Livingston Island, Antarctic Peninsula on January 15, 1991 (vertical seismometer SM-3 and pen recorder PORTACORDER)

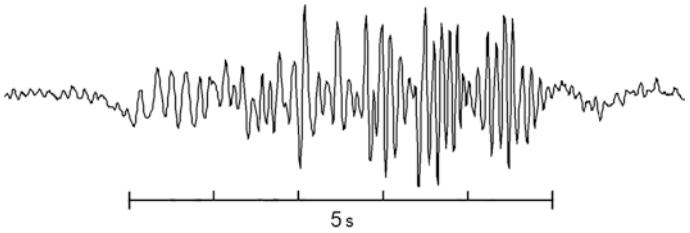


**Fig. 7.5** Icevibration event recorded on the Pasterze Glacier at 9:49 on September 30, 2003 (digital recording)

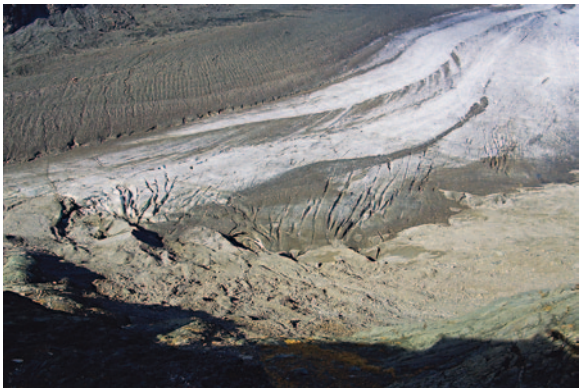

**Fig. 7.6** Photo of the Pasterze Glacier in 2003

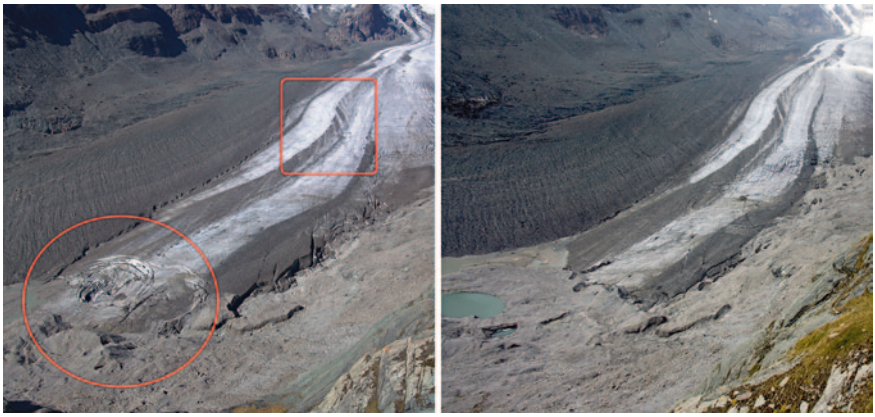

**Fig. 7.7** Photos of the Pasterze Glacier in 2006 (*left*) and 2009 (*right*). The areas of large-scale changes are highlighed: those related to the glacier's retreat by an *ellipse* and to *horizontal* displacements by a *square*

changes in the glacier's structure are highlighted. In the lower part (marked by the ellipse) there are changes related to the glacier's retreat. This region is a site of deep vertical displacements. In this part of the glacier one sees how a characteristic funnel, with features of depression exhibiting rotational elements, is being formed. In the central part of the glacier (marked by the square) there occur horizontal displacements of ice. The displacements, transverse in relation to the main flow, are associated with a change of its direction. These displacements have a character of large-scale transverse dislocations. Such phenomena, in association with violent motions of ice masses in the main flow, often enhanced by resonance, can be a source of the vibrations we recorded. These events are probably accompanied by the generation of infrasounds.

The Pasterze Glacier, unlike the Hans and Huron ones, is an intracontinental glacier, so it does not have a head ending in the sea.

## 7.3 Predominant Frequencies of Icevibrations

For more detailed analysis we chose two events from the Hans Glacier, two from Pasterze, and one from Huron. The displacement seismograms of icevibrations recorded at the Hans Glacier are shown in Figs. 7.8 and 7.9; the figures present also three-dimensional spectra. On both seismograms, the main phase of the event is denoted by letter **a,** and the precursory vibrations by **b**. The icevibrations were recorded by 11-channel seismometer network, which enabled localizing the event-generating area of the glacier (see Chap. 3, Fig. 3.4). As follows from an analysis of seismograms recorded at all 11 recording sites, the precursory vibrations **b** were generated in the same source as vibrations **a**.

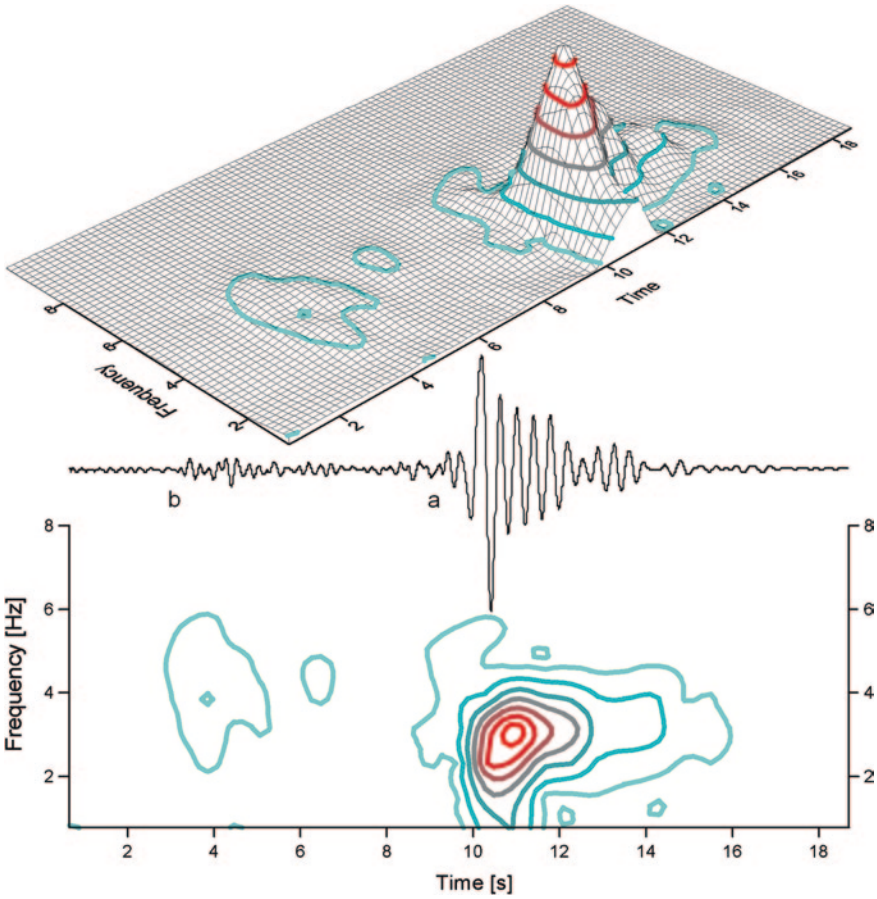


**Fig. 7.8** Icevibration event recorded on the Hans Glacier at 6:27 on August 21, 2002. The displacement seismogram recorded on the glacier is shown in the *middle* the diagram. The *upper* and *lower* diagrams present three-dimensional spectra as seen from different directions. The main phase is marked by letter *a*, and the precursory vibrations by *b*

The events shown in Figs. 7.8 and 7.9 have durations of about 18 and 30 s, respectively. In the region of the main stream of the Hans Glacier, icevibrations whose duration was even in excess of 1 min have been recorded in the past (see Fig. 7.3). An analysis of recordings at sites nearby the source and those far away of the source leads to the conclusion that the time span through which the vibrations are generated in the source is comparable to the time of recording. This property has already been observed previously, when the recordings of vibrations at near and very distant sources have been compared (Fig. 7.1). The three-dimensional pattern of the spectrum reveals a distinct maximum around 3 Hz frequency. This frequency occurs throughout the whole recording of the event and is characteristic for both events analysed.

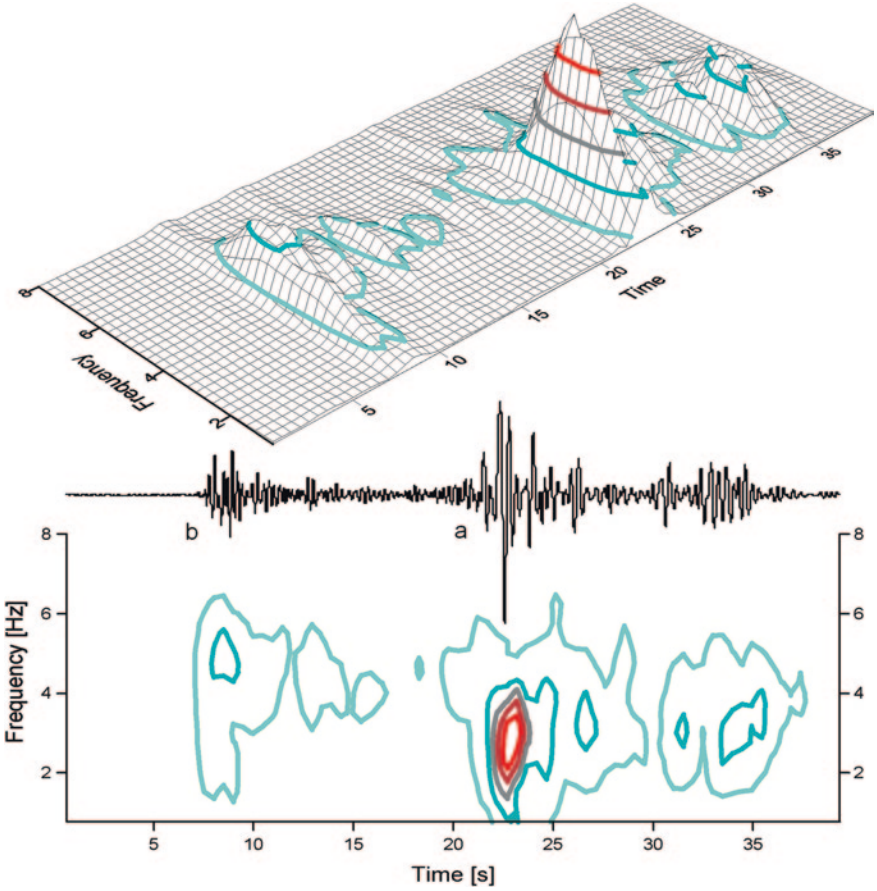


**Fig. 7.9** Icevibration event recorded on the Hans Glacier at 6:35 on August 21, 2002 (description in Fig. 7.8)

The seismograms recorded at 11 sites (Fig. 7.10) made it possible to estimate the location of both events. The seismograms of vertical vibrations were recorded in parallel by five seismometers of the HSP station and a network of six seismometers placed directly on ice. Short-period SM-3 seismometers (digital recording) were used at both the HSP station and the six seismometers placed on ice. An exact location of icevibrations is difficult, since these events do not display distinct phases whose time could be determined with sufficient accuracy. Attempts at determining the time shift of the whole event on recording channels corresponding to various sites enabled only a rough assessment of the location. It is to be pointed out that in the case of icevibrations the wave-generation region is relatively large.

The sources of both vibration events (Figs. 7.8 and 7.9) are located within the main stream of the glacier (Fig. 7.10); the event of Fig. 7.8 is situated at the eastern side and that of Fig. 7.9 at the western side of the main stream, both being at a

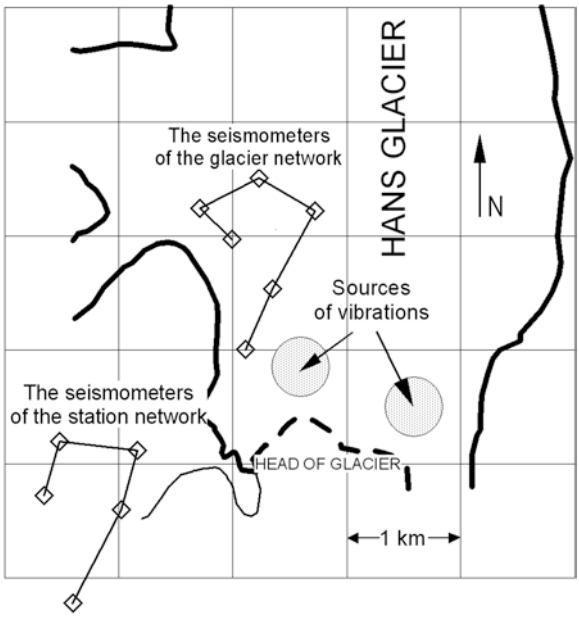


**Fig. 7.10** Location of sources of icevibrations on the Hans Glacier. The *gray circles* indicate sources of icevibrations, *squares* are sites of seismometers. The *heavy line* marks the glacier margin

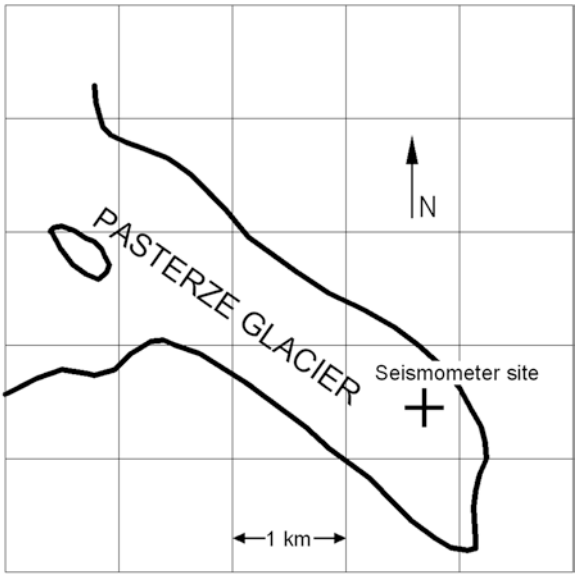


**Fig. 7.11** Location of measurement area on the Pasterze Glacier (Austrian Alps). The *cross* indicates the seismometer site, the *heavy line* marks the glacier margin

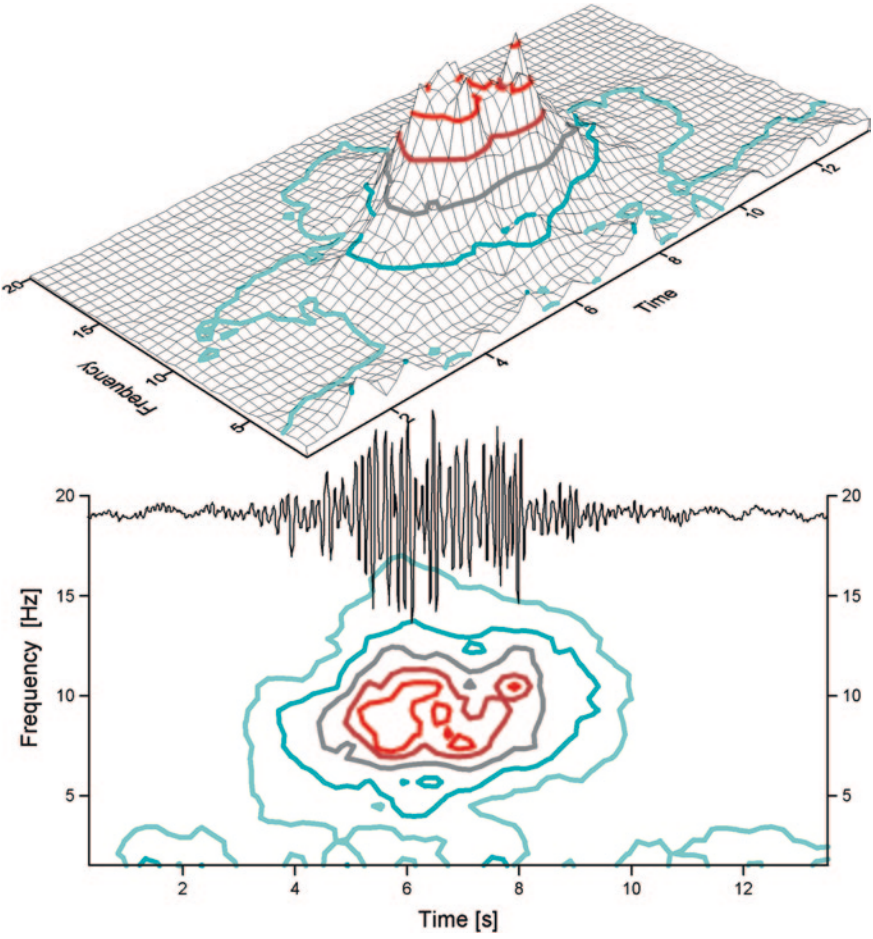


**Fig. 7.12** The icevibration event recorded on the Pasterze Glacier at 00:53 UTC on September 30, 2003 (description in Fig. 7.8)

distance of few hundred meters from the glacier head. In both regions, the glacier bottom is at a depth of 50 meters below sea level, and the average ice layer thickness is 120 m. In both regions, large-scale displacements of ice toward the glacier head take place in the summer, leading to glacier calving. The calving phenomena occur when part of ice in the glacier head whose junction with the rest of the glacier body has been broken slips into the sea, producing short-lived, weak seismic effects. In August, the intraglacial waters have already flown away, and, as a consequence, there do not occur changes in glacier vertical hydrostatic forces related to the displacement and run-off of these waters.

The recordings of glacial seismic events at the Pasterze Glacier were made in the framework of a broader project of studying the rotational wave generation process, led by Professor Roman Teisseyre. The special seismometers applied in these

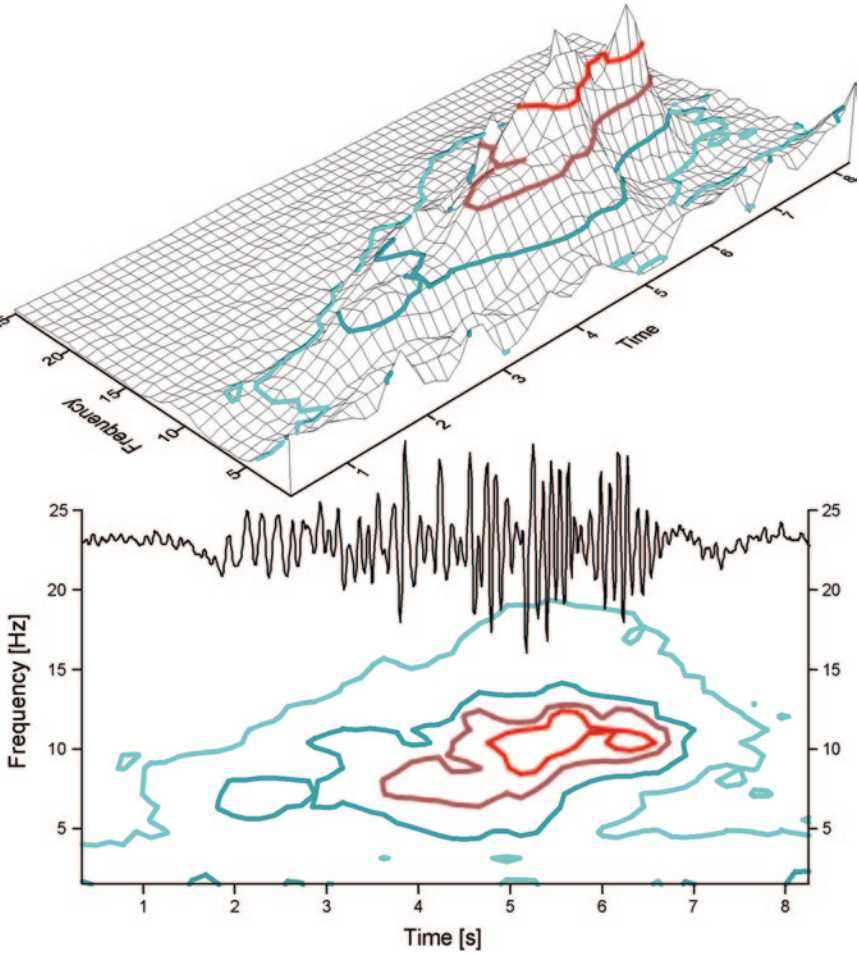


**Fig. 7.13** The icevibration event recorded on the Pasterze Glacier at 9:49 UTC on September 30, 2003 (description in Fig. 7.8)

measurements have the same parameters as the short-period seismometers SM-3 used in the measurements described above.

The displacement seismograms and spectra recorded in the ablation zone of the Pasterze Glacier (Fig. 7.11) which in this region is several tens meters thick and about 1 km wide, are shown in Figs. 7.12 and 7.13. In the time of measurements (turn of September and October), the Alpine glaciers experience down-going motions. Likewise the Hans Glacier, the Pasterze Glacier at the time of measurement was deprived of intraglacial waters, regardless, of course, of free streams flowing down. In spite of the previously mentioned large differences in climatic zones of the two glaciers, similar dynamic processes took place in them during

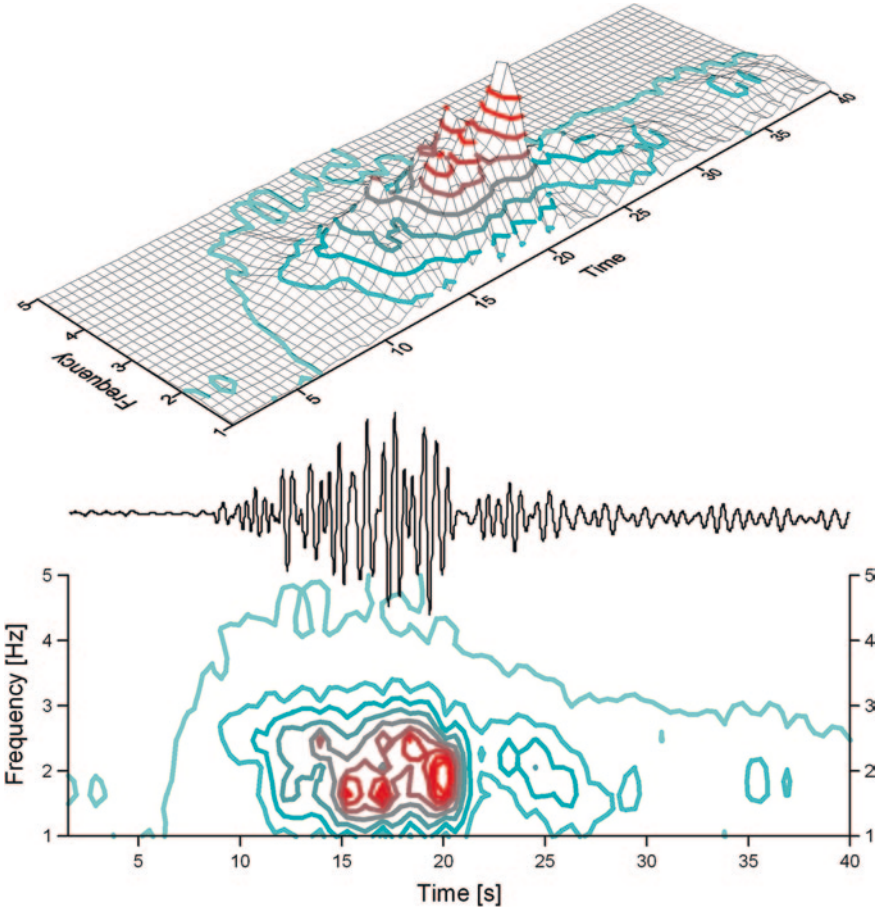


**Fig. 7.14** The icevibration event recorded on the Huron Glacier at 3:15 UTC on January 15, 1991. The displacement seismogram recorded on the glacier is shown in the *middle* diagram. The *upper* and *lower* diagrams present three-dimensional spectra as seen from different directions

measurements: the displacement of large ice masses in the direction of glacier flow.

In the three-dimensional spectra presented in the figures we observe maxima for frequencies of 9 Hz (Fig. 7.12) and 10 Hz (Fig. 7.13); they are three times greater than those observed in the Hans Glacier. This difference may be related to a smaller scale of glacial-dynamic processes in the Pasterze Glacier. The icevibrations recorded in this glacier had no precursory phase and were of shorter duration, 5 and 8 s, respectively. It is to be noted that the precursory-phase vibrations are slightly shifted towards higher frequencies relative to the main-phase vibrations, which is probably associated with the growing source area of vibrations in the main phase.

Two examples of three-dimensional spectra of events recorded at the Huron Glacier are shown in Figs. 7.14 and 7.15.

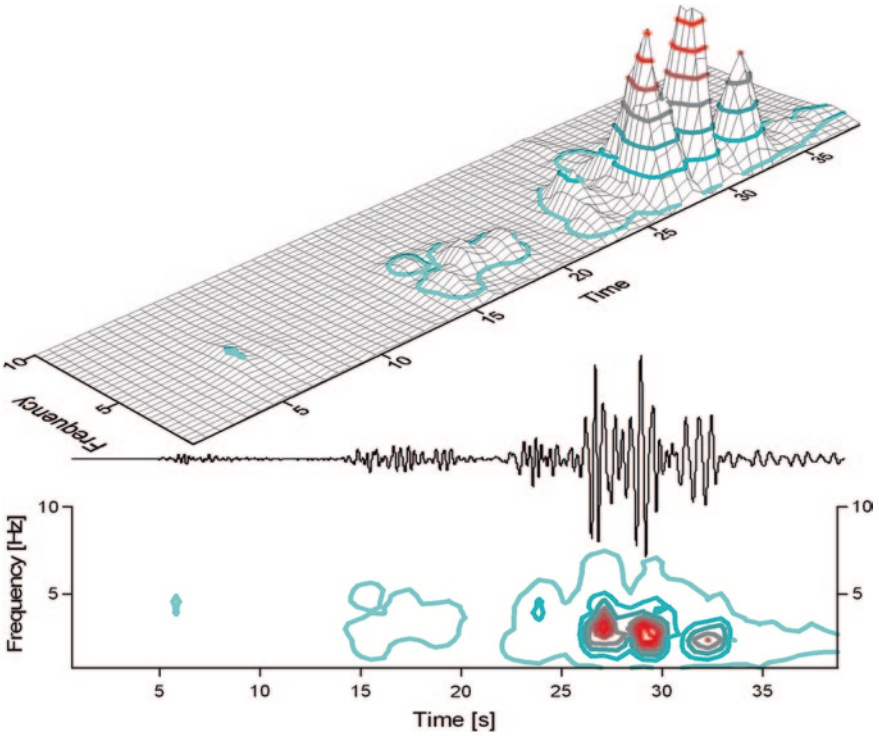


**Fig. 7.15** The icevibration event recorded on the Huron Glacier on January 15, 1991. The main phase, of maximum amplitude, is preceded by precursors of gradually growing amplitudes

The maximum observed in Fig. 7.14 corresponds to a frequency of 2 Hz. This frequency is comparable to those recorded at the Hans Glacier. Huron is a glacier whose ablation zone is similar in size to that of the Hans Glacier (Fig. 7.16). The icevibration effects recorded at Pasterze and Huron are more compact in character than those recorded at the Hans Glacier.

In the other example from the Huron Glacier, shown in Fig. 7.15, the frequency of vibrations at the maximum amplitude is similar to that in the event of Fig. 7.14. Here the group of maximum-amplitude waves is preceded by weaker precursors, as in the case of icevibrations recorded at the Hans Glacier.

It is also worth noticing that in icevibrations at the Pasterze Glacier and the Huron Glacier, the preliminary phase of vibrations, often encountered at the Hans Glacier (phase *b* in Figs. 7.8 and 7.9) has not been recorded. This phase has slightly higher frequency than the main phase *a.* It is very clearly visible in the event of Fig. 3.4 in Chap. 3. The higher frequency of vibrations occurring in the preliminary (precursory) part of the event is most probably related to a somewhat smaller area in which these vibrations are generated. Nevertheless, these vibrations are associated with large-scale dynamic processes within the glacier, not with

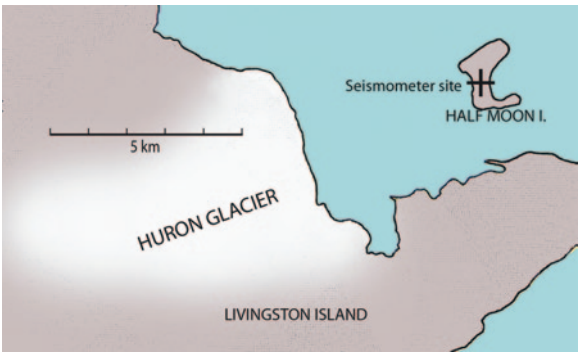


**Fig. 7.16** The Huron Glacier in Livingston Island, the Antarctic Peninsula region; the cross marks the position of a seismometer that recorded the icevibration events in the glacier. The seismometer was located on the Half Moon island, few kilometers away from the vibration-generating region

the vibrations generated in the release of relatively small stresses in numerous points in the area of future icevibration prior to the event (see sites 5, 6, and 1 in Fig. 7.1).

The velocity of the recorded waves was estimated (for both wave packets, *a* and *b,* in Figs. 7.8 and 7.9) at about 2,000 m/s. The P-wave velocity generated by icequakes is 3,620 m/s, the ratio of P- over S-wave velocity is 2 (see Chap. 4). This velocity is related to the type of waves generated by icevibrations and the manner of their propagation in a complex medium between the glacier and the seismometer.

## References

Czuba W (2013) Seismic view on the Svalbard passive continental margin. Acta Geophys. doi:10.2478/s11600-013-0126-0

Czuba W, Grad M, Guterch A (1999) Crustal structure of north-western Spitsbergen from DSS measurements. Pol Polar Res 20:131–148

Górski M (1997) Seismicity of the Hornsund region, Spitsbergen: icequakes and earthquakes, Publs Inst Geophys Pol Acad Sci B-20 (308), 1–77

Górski M (2004) Predominant frequencies in the spectrum of ice-vibration events. Acta Geoph Pol 52(4):457–464

Górski M, Teisseyre R (1991) Seismic events in Hornsund. Spitsbergen, Polish Polar Res 12:345–352

Grad M, Shiobara H, Janik T, Guterch A, Shimamura H (1997) Crustal model of the Bransfield Rift, West Antarctica, from detailed refraction experiments. Geophys J Int 130:506–518

Guterch A, Grad M, Janik T, Środa P (1998) Polish geodynamic expeditions—seismic structure of West Antarctica. Pol Polar Res 19:113–123

Lewandowska H, Teisseyre R (1964) Investigations of the ice microtremors on Spitsbergen in 1962. Biul Inf Komisji Wypraw Geof PAN 37:1–5

Majdański M, Środa P, Malinowski M, Czuba W, Grad M, Guterch A, Hegedus E (2008) 3D seismic model of the uppermost crust of the Admiraly Bay area, King George Island. West Antarctica, Polish Polar Res 29(4):303–319

Sellevoll MA, Duda JS, Guterch A, Pajchel J, Perchuć E, Thyssen F (1991) Crustal structure in the Svalbard region from seismic measurements. Tectonophysics 189:55–71

Środa P (2001) Three-dimensional modelling of the crustal structure in the contact zone between Antarctic Peninsula and South Pacific from seismic data. Pol Polar Res 22(2):129–146

Yegorova T, Bakhmutov V, Janik T, Grad M (2011) Joint geophysical and petrological models for the lithosphere structure of Antarctic Peninsula continental margin, Geophysical J Int vol 184(1), pp 90–110

# Chapter 8
# Application of the Shear-Band Model to the Determination of Focal Parameters

## 8.1 Focus Thickness

The considerations described up to this point, based on Brune's model, have not dealt with the problem of focus thickness of the examined shocks. Below we make an attempt to estimate the thickness of foci on the basis of shear-band model (Teisseyre 1996; see also Górski 2002). An analysis was made for icequakes recorded on the Hans Glacier (Chap. 6) and earthquakes occurring in the direct vicinity of the Hornsund station.

The shear-band model is based on the thermodynamics of line defects and assumes that in the source there exists a superlattice. The superlattice is described by parameter $\Lambda$; its geometrical meaning is illustrated by Fig. 8.1. Parameter $\Lambda$ is greater than the interatomic distance in a regular lattice (parameter $\lambda$). The previously calculated parameters of seismic foci: seismic moment, focus radius and radiated energy (Chap. 6) are the basis for estimating the source thickness $D$, seismic efficiency $\eta$ and entropy increase $\Delta\psi$.

Taking into account simple geometrical relations (Fig. 8.1), we can estimate the focus thickness $D$ from the formula (Teisseyre 1996)

$$D = \frac{\Lambda M_0}{\mu\lambda\pi n_{\mathrm{A}} r_0^2} \tag{8.1}$$

where $M_0$ is the seismic moment, $r_0$ is the focus radius, $\mu$ is the rigidity modulus of the material, and $n_{\mathrm{A}}$ is the number of atomic lattice defects that are active in the process of stress release in one of the superlattice planes.

The focus thicknesses calculated for the studied icequake series are displayed in Fig. 8.2. The thickness $D$ is less than 2 m for half of the events, and generally does not exceed 4 m, except for a few cases in excess of 10 m. The thicknesses of the order of 1 m well correspond to the observed forms of crackings of the glacier and we may expect that these foci are the source of crevasses to be formed on the glacier or occur in the place of old, closed crevasses. The stress release zones that are

M. Górski, *Seismic Events in Glaciers*, GeoPlanet: Earth and Planetary Sciences,
DOI: 10.1007/978-3-642-31851-1_8, © Springer-Verlag Berlin Heidelberg 2014

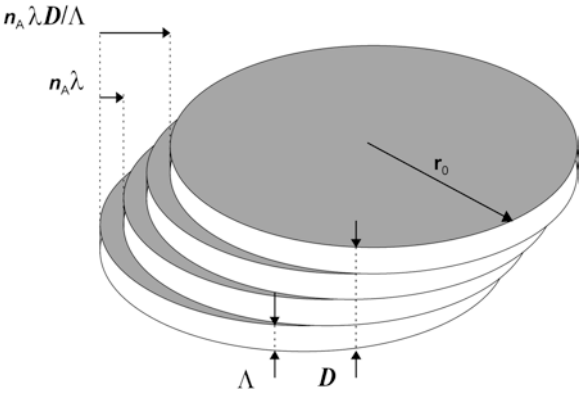


**Fig. 8.1** Geometrical parameters of the shear-band model of the earthquake focus (Teisseyre 1977); $r_0$ is the earthquake focus, $D$ is the thickness of the focus, $\lambda$ is the lattice constant, $\Lambda$ is the superlattice constant

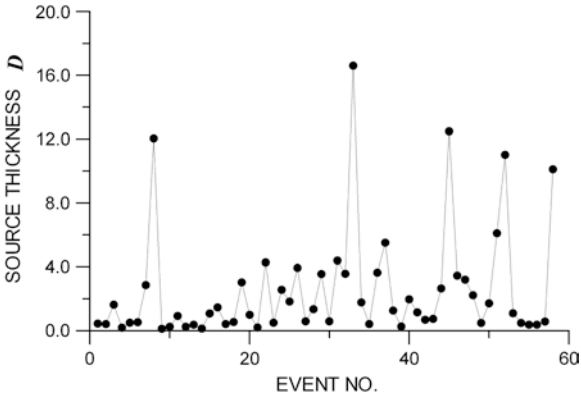


**Fig. 8.2** Focus thicknesses $D$ [m] corresponding to consecutive events of the studied icequake series (*horizontal axis*). The focus thickness was determined assuming the shear-band model

over few meters thick may occur in areas of large accumulation of stresses associated with the downgoing motion of the glacier, in its marginal zone for instance. The studied events are located exactly in such an area (see Chap. 3, Fig. 3.7); the velocity variation of glacier in its annual course (Jania 1992) showed that in this area there is a considerable gradient of velocity on the profile perpendicular to the motion direction. The velocity vectors of the glacier in its annual motion, drawn by arrows in Fig. 3.7, give evidence for a threefold increase of the glacier's velocity.

The focus thickness for events of the same seismic moment level is a sort of characteristic of the medium in the focus (durability, degree of metamorphism and cracking).

## 8.2 The Energy Released and Seismic Efficiency of the Source

The seismic efficiency of the source, $\eta$, was calculated from the definition

$$\eta = \frac{E_0}{E_T} \tag{8.2}$$

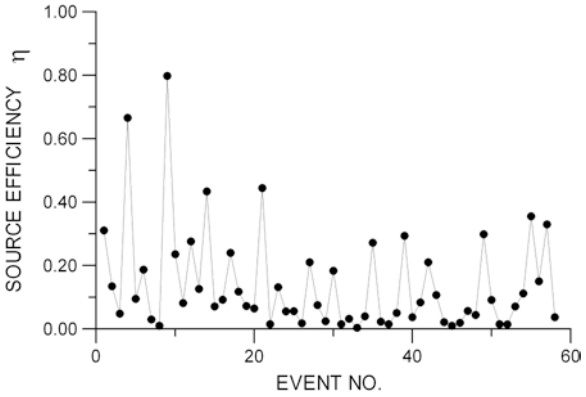


**Fig. 8.3** Behaviour of seismic efficiency $\eta = E_0/E_T$

The seismic energy $E_0$ radiated from the source was calculated on the basis of spectrum of the event (see Chap. 6, Table 6.1). The total energy $E_T$ was calculated from the relation (Teisseyre 1996)

$$E_T = \frac{1}{4\mu*}\sigma\Delta\sigma\pi r_0^2 D \tag{8.3}$$

The total energy produced in the source is related to stresses σ accumulated prior to the event and the stress drop Δσ. Energy $E_T$ takes also into account the plastic energy, μ*, which plays here a role that is similar to the shear modulus μ, but it may have a value different from μ, depending on the character of medium in the focus.

In further considerations we assumed, following Teisseyre (1996), that the stress drop is directly proportional to the stress value σ prior to the event: $\sigma = S_0\Delta\sigma$. Introducing

$$\Delta\sigma = \frac{7}{16}\frac{M_0}{r_0^3} \tag{8.4}$$

we obtain

$$E_T = 0.05\frac{S_0\Lambda}{\mu^*\mu\lambda n_A}\left(\frac{M_0}{r_0^2}\right)^3 \tag{8.5}$$

The obtained seismic efficiency values are shown in Fig. 8.3. Relatively large values of this quantity may be related to the seismic energy radiation in the process of open crevasses formation. During the energy release, the ice cracking needs much less energy than the permanent deformation without rupture. If the radiated seismic energy is the same, the events associated with the formation of cracks will have a greater seismic efficiency than the events accompanying the deformation of medium within the focus. Thus, an event of large seismic efficiency may produce one large crack or an area densely populated with small open cracks.

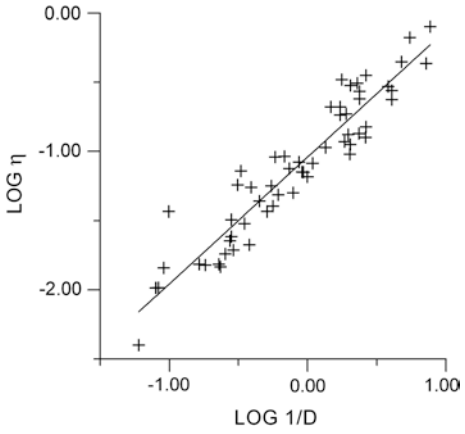


**Fig. 8.4** Logarithm of seismic efficiency η as a function of logarithm of $1/D$ ($m^{-1}$)

In Fig. 8.4 we show the diagram of the logarithms of seismic efficiency η and the reciprocal of focus thickness 1/D. The slope of the regression line is 0.92, in accordance with the equation: $\log \eta = 0.92 \log (1/D) - 1.04$.

The dependence of seismic efficiency on focus depth is most probably related to the fact that the radiation of seismic waves takes place mainly in the top and bottom surfaces of the cylinder that describes the sources. The radiation on the side surface of the cylinder is most probably attenuated by the interference of seismic waves (Teisseyre 1996).

In Fig. 8.5 we show the stress values σ and their drops Δσ (drawn with heavy lines). The stresses were calculated under the assumptions: $\sigma = S_0 \Delta\sigma$ (after Teisseyre 1996) and $S_0 = 3$.

## 8.3 The Fulfilment Coefficient and Entropy Increase

Analyzing thermodynamical processes in the source, Teisseyre (1996) obtained the following relation between the total energy density in the focus, $E_T/\pi r_0^2 D$, and the fulfillment coefficient $\Delta n^0$, defined as the number of broken atomic bonds

$$E_T = \Delta n^0 \frac{kT}{\Lambda\lambda^2} \pi r_0^2 D. \tag{8.6}$$

Taking into account (8.3) and (8.5) we obtain

$$\Delta n^0 = 0.05 \frac{S_0 \Lambda \lambda^2}{\mu^* kT} \left( \frac{M_0}{r_0^3} \right)^2. \tag{8.7}$$

The entropy increase corresponding to the energy $E_T$ released in the focus is

$$\Delta\Psi = \frac{E_T}{T}. \tag{8.8}$$

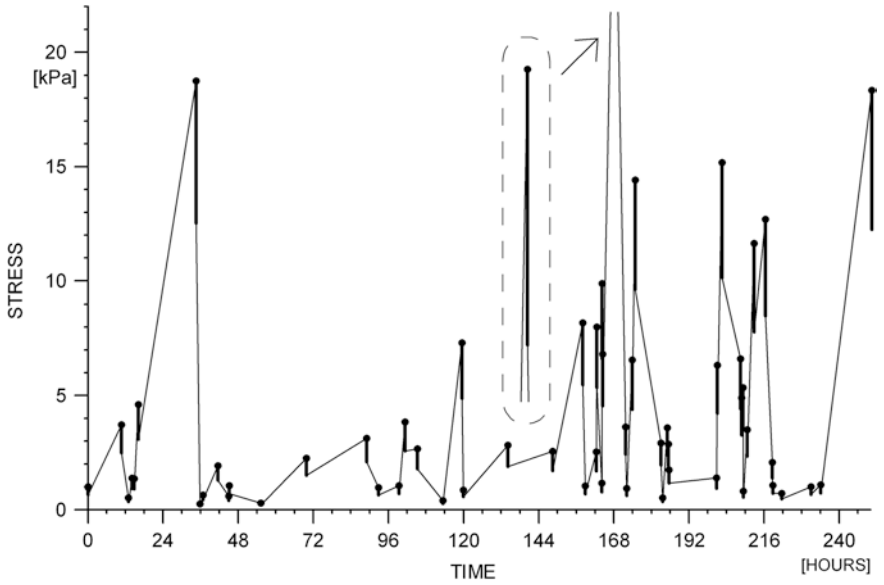


**Fig. 8.5** Stresses accumulated in the medium prior to the event, $\sigma = S_0\Delta\sigma$ (Teisseyre 1996); $S_0 = 3$. The stresses $\sigma$ are shown by *points*, stress drops $\Delta\sigma$ by *thickened vertical lines*. The *thin line* connects consecutive events (weak shocks with undetermined focal parameters have been neglected)

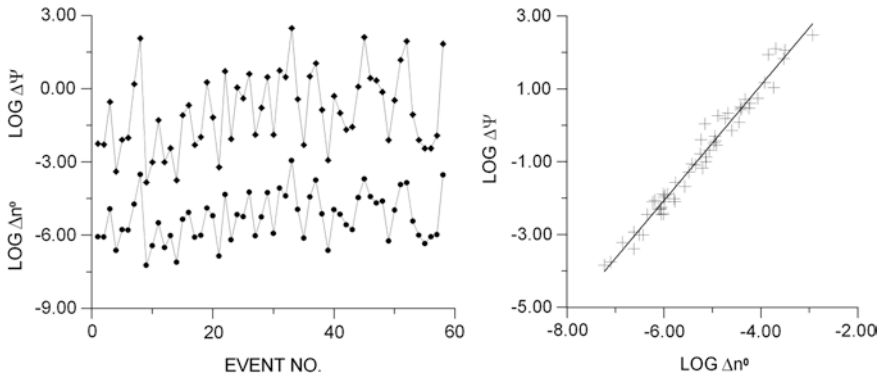


**Fig. 8.6** *Left-hand side*: behaviour of logarithm of entropy increment $\Delta\Psi$ (J/K) (*top*) and fulfillment coefficient $\Delta n^0$ (*bottom*). *Right-hand side*: logarithm of entropy increment $\Delta\Psi$ (J/K) versus logarithm of fulfilment coefficient $\Delta n^0$ (series of icequakes)

On the left-hand side of Fig. 8.6 we show the plot of entropy growth logarithms (upper curve) and fulfilment coefficient (lower curve) calculated for the analysed icequake series. The plot of entropy growth $\Delta\Psi$ as a function of fulfilment coefficient $\Delta n^0$ is shown on the right-hand diagram.

In the calculations we used the following values of constants and coefficients:

$$\Lambda/n_{\mathrm{A}} = 10^{-5}\,\mathrm{m},$$
$$\Lambda = 10^{-4}\,\mathrm{m},$$
$$\lambda = 2 \times 10^{-10}\,\mathrm{m},$$
$$\mu^* = 10^8\,\mathrm{N/m^2},$$
$$S_0 = 3.$$

Observing the focus dimensions and the rest of physical parameters calculated on the basis of the above-mentioned values we come to the conclusion that within the glacier the media in the foci are filled with a material that is weak, of small strength, and most probably densely cracked. Relatively small stress drops (large values of coefficient $S_0$) and a small value of coefficient $\mu^*$ are characteristic of such a medium. This conclusion is in agreement with direct observations of the glacier. The factors that make the ice weaker act mainly in the following areas: the interfaces between annual increments of the glacier, surfaces in the areas of its large velocity gradient, areas of old, closed and crystallized cracks and large crystalline forms.

## 8.4 Comparison of Parameters Calculated in Terms of the Shear-Band Model for Icequakes and Tectonic Earthquakes

We compared the parameters of icequakes to those of weak earthquakes, as calculated on the basis of the shear-band model.

The application of shear-band model made it possible to estimate the thicknesses of foci for the series of earthquakes localized in the direct vicinity of Polish Polar Station Hornsund (epicentral distances of less than 20 km). The series consists of 50 events and does not contain those localized nearby the east coast of Spitsbergen at the latitude of the Hornsund fiord. Subsequently, we calculated the seismic efficiency $\eta$, entropy growth $\Delta\Psi$ and the fulfilment coefficient $\Delta n^0$ in the focus of earthquake. The calculations were based on focal parameters determined from the spectra; they are listed in Table 8.1. The focus radius $r_0$, energy $E_0$ radiated from the source and stress drop $\Delta\sigma$ were determined with the method described in Chap. 6. We used the equations given above (Sects. 8.1, 8.2 and 8.3), introducing the appropriate values of constants and coefficients listed below:

$$\Lambda/n_{\mathrm{A}} = 6 \times 10^{-7}\,\mathrm{m}, \quad \Lambda = 6 \times 10^{-5}\,\mathrm{m}, \quad \lambda = 2 \times 10^{-10}\,\mathrm{m}, \quad \mu^* = 3 \times 10^8\,\mathrm{N/m^2}.$$

We made the following assumption as to the stresses $\sigma$ accumulated prior to the event: $\sigma = S_0\Delta\sigma$, $S_0 = 1.2$ (Teisseyre 1996).

**Table 8.1** Focus parameters of selected tectonic earthquakes calculated from the P and S wave spectra. The earthquakes are localized nearby Homsund station (epicentral distances <20 km)

| Event No | Magnitude $M$ | Seismic moment $M_0$ ($10^{12}$ N) | Total seismic energy $E_0$ ($10^6$ J) | $P$-wave energy $E_P$ ($10^6$ J) | $S$-wave energy $E_S$ ($10^6$ J) | Ratio $E_S/E_P$ | Source radius $r_0$ (m) | Stress drop $\Delta\sigma$ (MPa) | Apparent stress $\sigma_a$ (MPa) | $P$-wave corner frequency $f_P$ (Hz) | $S$-wave corner frequency $f_S$ (Hz) |
|---|---|---|---|---|---|---|---|---|---|---|---|
| 1 | 2.5 | 6.43 | 7.752 | 0.949 | 6.803 | 7.2 | 168.5 | 0.588 | 0.033 | 5.8 | 4.4 |
| 2 | 2.0 | 1.23 | 0.361 | 0.208 | 0.153 | 0.7 | 116.3 | 0.342 | 0.008 | 8.3 | 6.7 |
| 3 | 2.1 | 1.64 | 0.682 | 0.405 | 0.277 | 0.7 | 114.0 | 0.484 | 0.012 | 8.3 | 6.9 |
| 4 | 2.7 | 11.6] | 53.021 | 4.269 | 48.752 | 11.4 | 134.0 | 2.111 | 0.127 | 7.8 | 5.2 |
| 5 | 2.3 | 2.69 | 15.366 | 0.189 | 15.177 | 80.4 | 103.7 | 1.054 | 0.158 | 8.8 | 8.0 |
| 6 | 1.6 | 0.24 | 0.040 | 0.001 | 0.039 | 46.5 | 133.9 | 0.043 | 0.005 | 8.8 | 5.1 |
| 7 | 1.6 | 0.28 | 0.210 | 0.002 | 0.208 | 113.4 | 99.3 | 0.125 | 0.021 | 9.8 | 7.5 |
| 8 | 1.6 | 0.33 | 0.124 | 0.008 | 0.116 | 14.5 | 104.3 | 0.126 | 0.011 | 9.1 | 7.7 |
| 9 | 1.2 | 0.09 | 0.008 | 0.002 | 0.006 | 2.8 | 87.9 | 0.060 | 0.002 | 12.0 | 8.0 |
| 10 | 1.8 | 0.50 | 0.065 | 0.033 | 0.032 | 1.0 | 1183 | 0.131 | 0.004 | 8.8 | 5.9 |
| 11 | 2.0 | 1.09 | 0.549 | 0.055 | 0.494 | 8.9 | 125.0 | 0.245 | 0.014 | 8.4 | 5.4 |
| 12 | 2.7 | 13.51 | 98.145 | 43.395 | 54.751 | 1.3 | 88.5 | 8.532 | 0.201 | 10.0 | 9.3 |
| 13 | 1.6 | 0.24 | 0.021 | 0.011 | 0.010 | 0.9 | 114.6 | 0.070 | 0.002 | 9.4 | 5.8 |
| 14 | 1.6 | 0.28 | 0.057 | 0.010 | 0.046 | 4.4 | 102.3 | 0.114 | 0.006 | 10.5 | 7.0 |
| 15 | 1.7 | 0.41 | 0.101 | 0.029 | 0.072 | 2.5 | 103.6 | 0.160 | 0.007 | 10.5 | 7.0 |
| 16 | 1.3 | 0.11 | 0.009 | 0.002 | 0.006 | 2.7 | 968 | 0.054 | 0.002 | 11.6 | 7.0 |
| 17 | 1.4 | 0.13 | 0.015 | 0.004 | 0.011 | 2.8 | 90.2 | 0.077 | 0.003 | 12.0 | 7.6 |
| 18 | 1.8 | 0.54 | 0.372 | 0.061 | 0.311 | 5.1 | 82.2 | 0.421 | 0.019 | 11.7 | 9.2 |
| 19 | 2.9 | 27.31 | 96.182 | 20.405 | 75.778 | 3.7 | 162.1 | 2.807 | 0.098 | 5.2 | 5.6 |
| 20 | 1.8 | 0.53 | 0.143 | 0.049 | 0.094 | 1.9 | 106.9 | 0.191 | 0.007 | 11.1 | 6.0 |
| 21 | 3.0 | 38.12 | 101.219 | 14.910 | 86.308 | 5.8 | 219.7 | 1.572 | 0.074 | 5.2 | 3.1 |
| 22 | 2.7 | 12.91 | 37.282 | 21.797 | 15.485 | 0.7 | 130.7 | 2.531 | 0.080 | 8.2 | 5.1 |
| 23 | 1.9 | 0.94 | 0.234 | 0.108 | 0.126 | 1.2 | 128.2 | 0.195 | 0.007 | 9.2 | 4.9 |
| 24 | 2.9 | 22.10 | 86.514 | 30.896 | 55.618 | 1.8 | 147.5 | 3.013 | 0.109 | 7.1 | 4.7 |

(continued)

**Table 8.1** (continued)

| Event No | Magnitude $M$ | Seismic moment $M_0$ ($10^{12}$ N) | Total seismic energy $E_0$ ($10^6$ J) | $P$-wave energy $E_P$ ($10^6$ J) | $S$-wave energy $E_S$ ($10^6$ J) | Ratio $E_S/E_P$ | Source radius $r_0$ (m) | Stress drop $\Delta\sigma$ (MPa) | Apparent stress $\sigma_a$ (MPa) | $P$-wave corner frequency $f_P$ (Hz) | $S$-wave corner frequency $f_S$ (Hz) |
|---|---|---|---|---|---|---|---|---|---|---|---|
| 25 | 2.1 | 1.88 | 0.991 | 0.339 | 0.652 | 1.9 | 131.1 | 0.365 | 0.015 | 8.8 | 5.4 |
| 26 | 2.4 | 5.10 | 4.494 | 3.271 | 1.223 | 0.4 | 139.9 | 0.815 | 0.024 | 7.6 | 5.3 |
| 27 | 2.5 | 5.98 | 19.044 | 3.596 | 15.448 | 4.3 | 114.0 | 1.766 | 0.088 | 10.2 | 5.8 |
| 28 | 2.8 | 15.80 | 62.582 | 20.006 | 42.577 | 2.1 | 137.1 | 2.683 | 0.110 | 7.3 | 5.2 |
| 29 | 2.7 | 12.28 | 29.336 | 12936 | 16.400 | 1.3 | 145.5 | 1.744 | 0.066 | 7.2 | 4.8 |
| 30 | 2.5 | 7.94 | 12.299 | 8.562 | 3.738 | 0.4 | 134.9 | 1.416 | 0.043 | 7.8 | 5.3 |
| 31 | 3.0 | 35.61 | 184.391 | 91.527 | 92.864 | 1.0 | 141.6 | 5.484 | 0.144 | 7.4 | 5.2 |
| 32 | 3.0 | 32.51 | 146.143 | 89.333 | 56.810 | 0.6 | 145.7 | 4.602 | 0.125 | 7.5 | 4.5 |
| 33 | 2.3 | 3.55 | 4.577 | 1.377 | 3.200 | 2.3 | 122.9 | 0.836 | 0.036 | 8.7 | 5.7 |
| 34 | 2.4 | 5.74 | 11.341 | 5.520 | 5.821 | 1.1 | 124.4 | 1.306 | 0.055 | 8.7 | 5.4 |
| 35 | 1.8 | 0.67 | 0.158 | 0.091 | 0.067 | 0.7 | 112.8 | 0.204 | 0.007 | 8.6 | 6.4 |
| 36 | 2.5 | 5.07 | 5.382 | 3.87) | 1.511 | 0.4 | 140.1 | 0.808 | 0.029 | 7.8 | 5.3 |
| 37 | 1.9 | 0.82 | 0.172 | 0.097 | 0.075 | 0.8 | 127.3 | 0.173 | 0.006 | 7.9 | 5.8 |
| 38 | 1.9 | 0.96 | 0.259 | 0.124 | 0.135 | 1.1 | 129.7 | 0.193 | 0.007 | 8.9 | 5.1 |
| 39 | 2.7 | 11.55 | 18.448 | 10.114 | 8.334 | 0.8 | 160.4 | 1.225 | 0.044 | 6.6 | 4.4 |
| 40 | 1.8 | 0.51 | 0.071 | 0.037 | 0.035 | 0.9 | 126.2 | 0.112 | 0.004 | 8.5 | 5.4 |
| 41 | 2.2 | 2.01 | 0.646 | 0.480 | 0.166 | 0.3 | 147.2 | 0.275 | 0.009 | 7.6 | 4.7 |
| 42 | 2.0 | 1.03 | 0.208 | 0.081 | 0.127 | 1.6 | 138.0 | 0.171 | 0.006 | 6.9 | 5.5 |
| 43 | 1.6 | 0.34 | 0.036 | 0.012 | 0.024 | 1.9 | 117.9 | 0.090 | 0.003 | 8.0 | 6.5 |
| 44 | 2.2 | 2.14 | 0.728 | 0.293 | 0.435 | 1.5 | 148.6 | 0.286 | 0.009 | 6.6 | 5.3 |
| 45 | 2.0 | 1.13 | 0.692 | 0.079 | 0.612 | 7.7 | 123.2 | 0.266 | 0.017 | 8.7 | 5.4 |
| 46 | 2.8 | 20.90 | 50.074 | 23.473 | 26.601 | 11 | 172.0 | 1.796 | 0.066 | 6.9 | 3.7 |
| 47 | 1.9 | 0.71 | 0.085 | 0.055 | 0.030 | 0.5 | 165.5 | 0.069 | 0.003 | 10.4 | 3.5 |
| 48 | 1.2 | 0.08 | 0.003 | 0.001 | 0.003 | 3.9 | 103.7 | 0.031 | 0.001 | 11.1 | 6.8 |
| 49 | 1.6 | 0.25 | 0.022 | 0.007 | 0.015 | 2.0 | 125.7 | 0.056 | 0.002 | 8.1 | 5.9 |
| 50 | 2.4 | 5.68 | 5.178 | 2.770 | 2.409 | 0.9 | 135.4 | 1.001 | 0.025 | 7.0 | 6.3 |

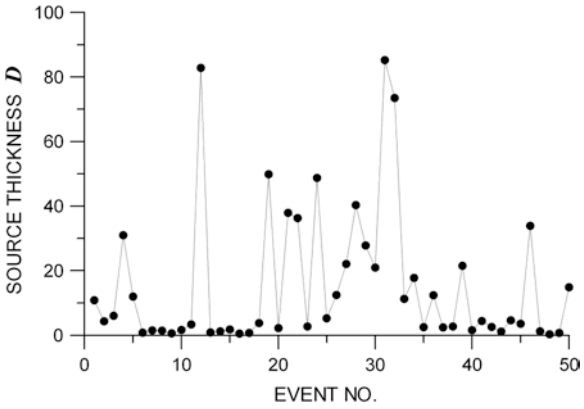


**Fig. 8.7** Focus thicknesses $D$ (m) corresponding to consecutive events of tectonic earthquakes series (*horizontal axis*). The focal thicknesses were determined assuming the shear-band model

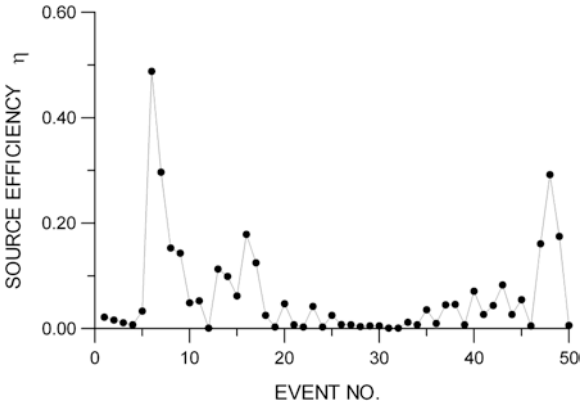


**Fig. 8.8** Seismic efficiency corresponding to consecutive tectonic events from the studied series. $E_T$ is the total energy released in the focus, calculated according to Eq. (8.3), $E_0$ is the energy emitted from the source according to Table 8.1

The focus thicknesses $D$ were calculated according to Eq. (8.1). In Fig. 8.7 we show on a vertical axis the focus thicknesses (in meters) corresponding to consecutive events indicated on the horizontal axis. For half of the events the focus thickness has not exceeded 2 m. For the rest, except of three events, the focus thickness ranges from 2 to 50 m. The maximum thicknesses of foci for this series of earthquakes are about 70 m.

The seismic efficiency of the source ($\eta = E_0/E_T$) for consecutive events is illustrated in Fig. 8.8. The values of seismic energy $E_0$ listed in Table 8.1 were used. The total energy produced in the source $E_T$ was calculated according to Eq. (8.3). For 70 % of the analyzed events the seismic efficiency $\eta$ ranges from 0.001 to 0.055. Twenty percent of the events has the efficiency less than 0.01. Large values of the efficiency may give evidence to a relatively weak structure of the medium.

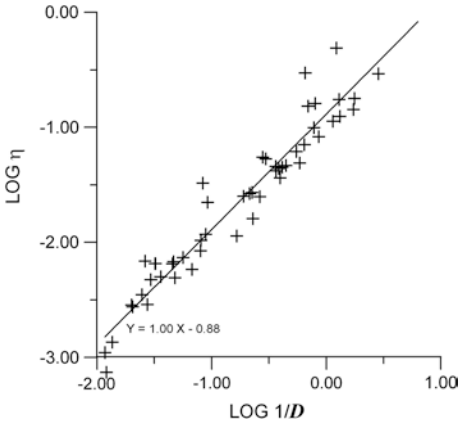


**Fig. 8.9** Logarithm of seismic efficiency η as a function of logarithm of 1/D (series of earthquakes localized nearby the Hornsund station)

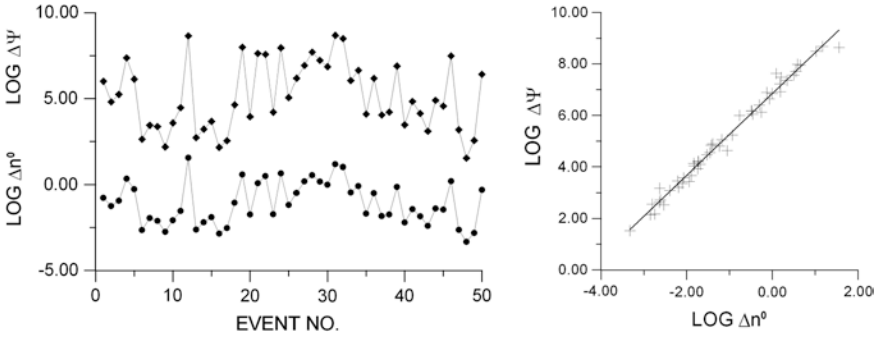


**Fig. 8.10** *Left-hand side*: behaviour of logarithm of entropy increment $\Delta\Psi$ (J/K) (*upper curve*) and fulfilment coefficient $\Delta n^0$ (*lower curve*). *Right-hand side*: entropy increment logarithm $\Delta\Psi$ (J/K) versus fulfilment coefficient $\Delta n^0$ (series of earthquakes localized nearby the Hornsund station)

The dependence between seismic efficiency and focus thickness (Teisseyre 1996) is shown in Fig. 8.9. Logarithms of seismic efficiency η were drawn as a function of logarithm of the reciprocal of focus thickness 1/D. The slope of regression curve is equal to unity (the equation of the straight line is: $\log \eta = 1.00 \log (1/D) - 0.88$).

The fulfillment coefficient $\Delta n^0$ (the number of broken atomic bonds) was calculated for the examined earthquake series from formula (8.7). The entropy growth was determined as the ratio of total energy $E_T$ produced in the focus to the absolute temperature $T$ in the focus ($\Delta\Psi = E_T/T$).

Diagrams of the logarithm of fulfillment coefficient and entropy are shown on the left-hand side of Fig. 8.10. On the right-hand side we show the dependence

between the entropy growth $\Delta\Psi$ and fulfillment coefficient $\Delta n^0$. The regression line is described by the equation $\log \Delta\Psi = 1.58 \log \Delta n^0 + 6.85$. The correlation coefficient is 0.98.

The focal parameters calculated above, under the assumption of shear-band model, are of approximate character, since the calculations are based on the previously determined spectral parameters assuming the flat Brune's model.

## References

Górski M (2002) Application of the fracture-band model to glacier seismic event series. Acta Geophys Pol 50:373–379

Jania J (1992) Some results of glaciological research—Hansbreen. In: Field workshop on glaciological research in Svalbard, University of Silesia, V/19-V/34

Teisseyre R (1977) Dislocation processes and formation of tensile cracks in glaciers. Acta Geophys Pol 25:111–118

Teisseyre R (1996) Shear band thermodynamical earthquake model. Acta Geophys Pol 44:219–236

# Appendix
# Seismological Bulletins Relating to Polar Regions, published by the Institute of Geophysics, Polish Academy of Sciences

The seismological bulletins containing data from the seismological stations in the Arctic and Antarctic regions have been published in the series ***Publications of the Institute of Geophysics, Polish Academy of Sciences***. The bulletins, covering the period from 1978 through 1995, are listed below; they can be obtained on request.

Seismological Bulletin, Arctowski Antarctic Station 1978–1982, Hornsund Polish Station 1979–1985, prepared by T. Kowalski and M. Górski. Publs. Inst. Geoph. Pol. Acad. Sc., B-9(193), 1986, 83pp.

Seismological Bulletin, Arctowski Antarctic Station 1983–1985, Hornsund Polish Station 1985–1986, prepared by T. Kowalski and M. Górski. Publs. Inst. Geoph. Pol. Acad. Sc., B-11(208), 1987, 52pp.

Seismological Bulletin, Arctowski Antarctic Station, Hornsund Polish Station 1986–1987, prepared by T. Kowalski and M. Górski. Publs. Inst. Geoph. Pol. Acad. Sc., B-12(222), 1989, 52pp.

Seismological Bulletin, Arctowski Antarctic Station, Hornsund Polish Station 1988–1991, prepared by T. Kowalski and M. Górski. Publs. Inst. Geoph. Pol. Acad. Sc., B-15(258), 1993, 74pp.

B-18 (284) Seismological Bulletin, Arctowski Antarctic Station, Hornsund Polish Station 1992–1995, prepared by M. Górski, Publs. Inst. Geoph. Pol. Acad. Sc., B-18 (284), 2000, 70pp.

M. Górski, *Seismic Events in Glaciers*, GeoPlanet: Earth and Planetary Sciences,
DOI: 10.1007/978-3-642-31851-1, © Springer-Verlag Berlin Heidelberg 2014